PART I: AN ANALYTICAL STUDY OF TRANSPORT, MIXING AND CHAOS IN AN UNSTEADY VORTICAL FLOW. PART II: TRANSPORT IN TWO DIMENSIONAL MAPS.

Thesis by

Vered Rom-Kedar

In Partial Fulfillment of the Requirements

for the degree of

Doctor of Philosophy

California Institute of Technology

Pasadena, California

1989

Submitted June 24, 1988

Acknowledgements

I would like to thank my advisor Dr. S. Wiggins whose knowledge, advice and encouragement made this work possible. I would also like to thank Dr. A. Leonard for his contributions to this work and his helpful suggestions and discussions, and to Dr. P.G. Saffman for his encouragement and support throughout my stay in Caltech.

Financial support has been generously provided by Caltech Institute fellowships, Teaching Assistantship and Research Assistantships financed by the Office of Naval Research under contract N000-14-85-k-0205 and by Caltech's Program in Advanced Technologies sponsored by Aerojet General, General Motors and TRW. In my last year at Caltech I was also supported by a Zonta Amelia Earhart Fellowship and by a P.E.O. International Peace Scholarship.

My friends at Caltech made the stay here enriching and pleasant. I would like to thank especially to Dana Hobson for stimulating discussions and even more important, for his friendship.

I will always be grateful to my parents and my brother and sister who supported me throughout the years in all my deeds.

Finally, to Shiko, who came all the way from Israel for my studies, thanks for his endless love and caring which made these years so happy for both of us.

Abstract

PART I:

We examine the transport properties of a particular two dimensional, inviscid incompressible flow using dynamical systems techniques. The velocity field is time periodic and consists of the velocity field induced by a vortex pair plus an oscillating strain-rate field. In the absence of the strain-rate field the vortex pair moves with a constant velocity and carries with it a constant body of fluid. When the strain-rate field is added the picture changes dramatically; fluid is entrained and detrained from the neighborhood of the vortices and chaotic particle motion occurs. We investigate the mechanism for this phenomena and study the transport and mixing of fluid in this flow. Our work consists of both numerical and analytical studies. The analytical study includes the interpretation of the invariant manifolds as the underlying structure which govern the transport. Then we use Melnikov's technique to investigate the behavior of the manifolds as the parameters of the problem change and to prove the existence of a horseshoe map and thus the existence of chaotic particle paths in the flows. Using the Melnikov technique once more we develop an analytical estimate of the flux rate into and out of the vortex neighborhood. We develop a technique for determining the residence time distribution for fluid particles near the vortices. The technique involves an understanding of the geometry of the tangling of the stable and unstable manifolds and results in a dramatic reduction in computational effort for the residence time distributions. Additionally, we develop a finite time analog of the Liapunov exponent which measures the effect of the horseshoes on trajectories passing through the mixing region. The numerical work verifies the analytical predictions regarding the structure of the invariant manifolds, the mechanism for entrainment and detrainment, and the flux rate.

PART II :

We study transport in the two dimensional phase space of C^r diffeomorphisms ($r \geq 1$) of two manifolds between regions of the phase space bounded by pieces of

the stable and unstable manifolds of hyperbolic fixed points. The mechanism for the transport is associated with the dynamics of homoclinic and heteroclinic tangles and the study of this dynamics leads to a general formulation for the transport rates in terms of distributions of small regions in phase space ("lobes"). It is shown how the method applies to three geometrical configurations, one of which corresponds to the geometry associated with the Kelvin-Stuart Cat's eye flow undergoing a time periodic perturbation. In this case the formulae imply, for example, that the evolution of only two lobes determines the mass transport from the upper to the lower half plane of the fluid flow. As opposed to previous studies this formulation takes into account the effect of re-entrainment of the lobes, i.e. the implications of the lobes leaving and re-entering the specified regions on the transport rates. The formulation is developed for both area preserving and non area preserving two dimensional diffeomorphisms and does *not* require the map to be near integrable. The techniques involved in applying this formulation are discussed including the possible use of the generating function for computing the distributions of the lobes in phase space, and the use of Poincaré maps which enables one to study the transport in continuous time systems via the above formalism. In particular, we demonstrate how the right choice of the Poincaré section can reduce the calculations of the transport rates.

Table Of Contents

List Of Figures

PART I:

List Of Tables

PART II:

PART I: AN ANALYTICAL STUDY OF TRANSPORT, MIXING AND CHAOS IN AN UNSTEADY VORTICAL FLOW

1. Introduction

In most fluid flows of interest, transport and mixing are dominated by convective processes so that the relative motions of fluid particles are all important. Unfortunately particle motion is generally more complex than the underlying fluid dynamics. For example, while the motion of three point vortices in an unbounded domain is integrable, particle motion in this flow can be chaotic (Aref [1983]) and certain simple steady, spatially periodic solutions to the Euler equations in three dimensions, known as ABC (Arnold, Beltrami and Childress) flows yield chaotic particle motion (Dombre et al. [1986]).

Of course, if the fluid dynamics is sufficiently simple then particle motions are integrable and a direct analytical attack on the problem may be fruitful. An example in this class is the analysis of a diffusion flame by Marble [1985], involving the rolling of an initially plane interface in the flow of a viscous line vortex in two dimensions. At the other end of the scale, when the flow is turbulent, direct numerical integration of the Navier-Stokes equations plus convective equation for passive scalars (Kerr [1985], Pope [1987]) is a computational approach to mixing problems, where as a theoretical approach might consist of constructing reasonable physical models for mixing processes (Broadwell [1987], Dimotakis [1987], Kerstein and Ashurst [1984]). In this paper we consider an intermediate case, one in which the flow is relatively simple but the particle motion is chaotic. We show that the recent rapid development in the theory of nonlinear dynamical systems and chaotic phenomena gives much hope for a rather extensive analysis of particle motion in flows. Indeed, the dynamical systems approach to the study of fluid flows is very similar in spirit to the flow visualization techniques utilized in the experimental study of coherent structures in the sense that dynamical systems theory is concerned with the global topology of the flow from a Lagrangian point of view. Since to good approximation temperature and mass move with the fluid velocity, understanding the structures governing particles motion in fluid flows is necessary for interpretations of flow visualizations (the visualization of motion of mass particles) and predictions of mass and heat transfer in technological applications.

The application of dynamical systems theory to the study of the global topology of fluid particle motions is not new. The first work appears to be that of Henón who, acting on a suggestion of Arnold [1965], numerically studies the fluid particle motions of a certain steady solution of the Euler equations which has come to be known as the ABC flow (for Arnold, Beltrami, and Childress). Henón showed that the flow contained KAM tori as well as chaotic motions of the Smale horseshoe type. This flow has recently been the subject of more extensive study by Dombre et al. [1986]. Chaotic particle motions in the ABC flows also have relevance to the kinematic dynamo problem, see Arnold and Korkine [1983], Galloway and Frisch [1986], and Moffat and Proctor [1985].

At the opposite end of the Reynolds number spectrum Aref [1984] showed that an unsteady stokes flow consisting of the flow between eccentric rotating cylinders where the rotation rate is modulated periodically in time can exhibit chaotic particle motions of the Smale horseshoe type. Thus this particular stokes flow is effectively nonreversible. This same flow has also been studied experimentally as well as theoretically by Chaiken et al. [1986]. Ottino and coworkers [1985], [1986], [1987] have studies chaotic fluid particle motions in a variety of flows with particular emphasis on using dynamical systems techniques as a theoretical basis for the discussion of mixing processes. Broomhead and Ryrie [1987] study fluid particle motions in the velocity field of Taylor vortices close to the onset of the wavy instability and demonstrate the chaotic transference of fluid between neighboring vortices. Feingold et al. [1988] study models for particle motion in three dimensional time dependent flows. Additional references applying dynamical systems techniques to the study of fluid particle trajectories are Suresh [1985] and Arter [1983].

In this paper we study fluid particle motions in the velocity field induced by two counter-rotating point vortices of equal strength subject to a time periodic strain field. This is a fundamental type of flow which is relevant to a wide variety of applications. For example, in the study of oscillatory flows in wavy walled tubes (see Ralph [1986], Sobey [1985], and Appendix 1), in the study of trailing vortices, and in the study of the vortex ring (Shariff [1987]).

The main difference in our analysis of the topology of a fluid flow via dynamical systems techniques as opposed to previous analyses is that rather than just using the framework of dynamical systems theory to give a description of the topology and indicate the presence of chaotic fluid particle trajectories we use the framework in order to calculate physically measurable quantities such as fluxes and the distribution of volumes via residence times. We do this by first identifying the structures in the flow responsible for these physical processes and then using the dynamics of these structures in order to predict these physical quantities. Thus in some sense we realized the goal of the study of coherent structures for our problem.

This paper is organized as follows: in section 2 we derive the velocity field, in section 3 we begin our discussion of the analysis of the velocity field by discussing the idea of a Poincaré map, in section 4 we discuss three qualitatively distinct regions which arise in our flow which we call the free flow region, the core, and the mixing region, in section 5 we discuss tangledynamics which turns out to be the mechanism for mass transport in the flow, in section 6 we discuss mass transport in detail and give precise definitions to the concepts of entrainment and detrainment in terms of tangle dynamics, in section 6 we give a detailed discussion of our results and predictions concerning mass transport and show how they agree with extensive numerical computations, in section 7 we discuss the concept of chaos and show how it arises in our flow, in section 8 we discuss the concept of mixing and the role of the Liapunov exponent and we conclude with several appendices describing various techniques from dynamical systems theory which are probably somewhat unfamiliar to most members of the fluid mechanics community as well as giving the proofs of certain theorems which we state in the main body of the paper.

2. Oscillating Vortex Pair

We examine the flow governed by a vortex pair in the presence of an oscillating external strain-rate field. The vortices have circulations $\pm\Gamma$ and are separated by a nominal distance 2d in the y-direction. The stream function for the flow in a frame moving with the average velocity of the vortices is

$$\Psi = -\frac{\Gamma}{4\pi}\log\left[\frac{(x-x_v)^2+(y-y_v)^2}{(x-x_v)^2+(y+y_v)^2}\right] - V_v y + \varepsilon x y \sin(\omega t) \tag{2.1}$$

where $(x_v(t), \pm y_v(t))$ are the vortex positions, ε is the strain rate and V_v is the average velocity of the vortex pair. If $\varepsilon = 0$ then $(x_v, y_v) = (0, d)$ and $V_v = \frac{\Gamma}{4\pi d}$. The equations of particle motion are

$$\frac{dx}{dt} = \frac{\partial\Psi}{\partial y} \qquad \frac{dy}{dt} = -\frac{\partial\Psi}{\partial x} \tag{2.2}$$

We show, as an example, in Appendix 1 that this flow approximates the flow induced by a vortex pair in a wavy-wall channel. We obtain dimensionless variables as follows:

$$x/d \to x,\ y/d \to y,\ \frac{\Gamma t}{2\pi d^2} \to t,\ \frac{\varepsilon}{\omega} \to \varepsilon,\ \frac{2\pi d V_v}{\Gamma} \to v_v,\ \frac{\Gamma}{2\pi\omega d^2} \to \gamma,\ \frac{2\pi\Psi}{\Gamma} \to \Psi$$

Then (2.1) and (2.2) become

$$\begin{aligned}
\frac{dx}{dt} &= -\left[\frac{(y-y_v)}{(x-x_v)^2+(y-y_v)^2} - \frac{y+y_v}{(x-x_v)^2+(y+y_v)^2}\right] - v_v + \frac{\varepsilon x}{\gamma}\sin(t/\gamma) \\
\frac{dy}{dt} &= (x-x_v)\left[\frac{1}{(x-x_v)^2+(y-y_v)^2} - \frac{1}{(x-x_v)^2+(y+y_v)^2}\right] - \frac{\varepsilon y}{\gamma}\sin(t/\gamma)
\end{aligned} \tag{2.3}$$

Using the fact that a point vortex is convected with the flow but does not induce self velocity we obtain the following equations for the vortex position locations:

$$\begin{aligned}
\frac{dx_v}{dt} &= \frac{1}{2y_v} - v_v + \frac{\varepsilon x_v}{\gamma}\sin(t/\gamma) \\
\frac{dy_v}{dt} &= -\frac{\varepsilon y_v}{\gamma}\sin(t/\gamma)
\end{aligned} \tag{2.4}$$

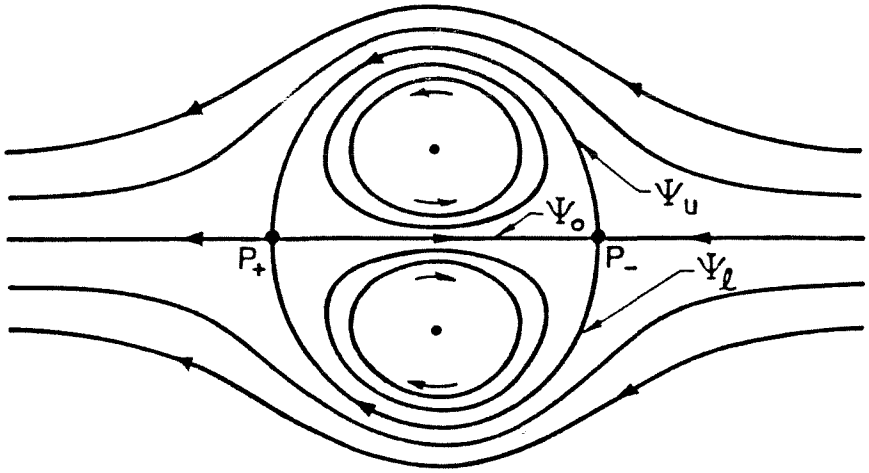

Figure 2.1 Streamlines of the Unperturbed Flow.

The resulting motion of the vortices is relatively simple. Equation (2.4) with the initial conditions $x_v(0) = 0,\ y_v(0) = 1$, are easily integrated to give

$$\begin{aligned} x_v(t) &= \frac{\gamma}{2} e^{-\varepsilon(\cos(t/\gamma)-1)} \int_0^{t/\gamma} \left[1 - 2v_v e^{\varepsilon(\cos(s)-1)}\right] ds \\ y_v(t) &= e^{\varepsilon(\cos(t/\gamma)-1)} \end{aligned} \tag{2.5}$$

The requirement that the mean velocity of the vortex pair be zero in the moving frame yields $v_v = \frac{e^\varepsilon}{2I_0(\varepsilon)}$, where I_0 is the modified Bessel function of order zero. From (2.5) it is clear that the vortices oscillate in orbits near the points $(0, \pm 1)$. Thus we term the resulting flow given by (2.3) the Oscillating Vortex Pair (OVP) flow.

Equations (2.3) together with (2.5) give the equations of particle motion as a function of two dimensionless parameters γ and ε, proportional to vortex strength and strain rate, respectively. For part of the analysis that follows we shall assume that ε is small and will require an expansion of the right hand side of (2.3) in powers of ε. This expansion yields equations of motion for fluid particles which are of the form of a periodically perturbed integrable Hamiltonian system:

$$\begin{aligned} \frac{dx}{dt} &= f_1(x,y) + \varepsilon g_1(x,y,t/\gamma;\gamma) + O(\varepsilon^2) \\ \frac{dy}{dt} &= f_2(x,y) + \varepsilon g_2(x,y,t/\gamma;\gamma) + O(\varepsilon^2) \end{aligned} \tag{2.6}$$

The functions f_i, g_i are given in Appendix 2.

For $\varepsilon = 0$ the phase portrait of the integrable Hamiltonian system, or equivalently the streamlines of the flow induced by a vortex pair in the frame moving with the vortices, appears in Figure 2.1. Note that for this case, there are two hyperbolic stagnation points p_-, p_+ connected by three limiting streamlines Ψ_u, Ψ_0 and Ψ_l defined by $\Psi(x,y)|_{\varepsilon=0} = 0$ and $|x| \leq \sqrt{3}$, with $y > 0$, $y = 0$, and $y < 0$ respectively. Note also that for any ε, the flow is symmetric about the x axis and thus we need only study the flow in the upper half plane.

3. Analysis: The Poincaré Map

We are interested in the structure of the flow generated by the velocity field (2.3) and how the structure varies as the parameter γ is varied. A brute force method for achieving this goal would be to numerically integrate (2.3) for a large number of initial conditions for the range of γ values of interest. Although this would be an efficient means for generating a large list of numbers, it is not at all clear how one would extract information concerning the structure of the flow from this list of numbers. One might try plotting the trajectories of a large number of fluid particles in space, however, since the velocity field is unsteady, these trajectories may intersect themselves as well as others many times leading to a complicated topological structure which might obscure relatively simple structures whose dynamics essentially govern the flow. In order to better understand the dynamics of the unsteady flow generated by (2.3) we will study the associated *Poincaré map.*

Roughly speaking, the Poincaré map of the flow is constructed by associating to a fluid particle at a fixed phase of the external strain-rate field its location under evolution by the flow after one period of the strain-rate field. More mathematically, we rewrite the unsteady two dimensional velocity field (2.3) as a steady three dimensional velocity field by introducing the phase of the strain-rate field as a new dependent variable. We do this by defining the function

$$\theta(t) = t/\gamma \mod 2\pi$$

in which case (2.3) can be written as:

$$\begin{aligned} \dot{x} &= f_1(x,y) + \varepsilon g_1(x,y,\theta;\gamma) + O(\varepsilon^2) \\ \dot{y} &= f_2(x,y) + \varepsilon g_2(x,y,\theta;\gamma) + O(\varepsilon^2) \\ \dot{\theta} &= 1/\gamma. \end{aligned} \tag{3.1}$$

A two dimensional *cross-section* of the three dimensional phase space of (3.1) is given by:

$$\Sigma^{\overline{\theta}} = \{(x,y,\theta) | \theta = \overline{\theta} \in (0, 2\pi]\}$$

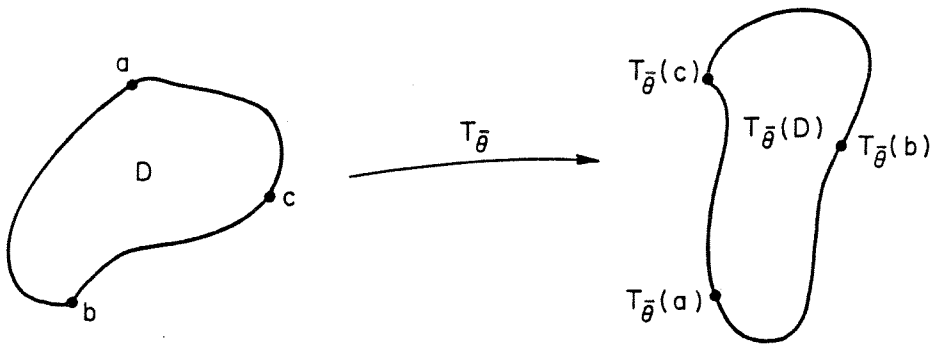

Figure 3.1. Orientation Preservation of $T_{\overline{\theta}}$.

and the Poincaré map of $\Sigma^{\overline{\theta}}$ into $\Sigma^{\overline{\theta}}$ is defined as:

$$\begin{aligned} T_{\overline{\theta}} &: \Sigma^{\overline{\theta}} \to \Sigma^{\overline{\theta}} \\ (x(\overline{\theta}), y(\overline{\theta})) &\mapsto (x(\overline{\theta} + 2\pi), y(\overline{\theta} + 2\pi)). \end{aligned} \tag{3.2}$$

So studying the flow via the Poincaré map is equivalent to sampling fluid particle trajectories at time intervals equal to the period of the strain-rate field. In spirit this procedure bears some similarities to the technique of conditional sampling used in the search for persistent structures in turbulent flows (Blackwelder and Kaplan [1976]).

The main advantage obtained from using the Poincaré map to study unsteady, time-periodic velocity fields is that the technique tends to filter out redundant dynamical phenomena and reveal the underlying structures which govern various properties of the flow such as mixing and transport. For example, a periodic particle trajectory in the flow which may have a very complicated topological structure is manifested as a finite, discrete set of points for the Poincaré map. Many more examples will follow throughout the rest of the paper.

Before embarking on our study of (2.3) via the Poincaré map, we want to make some final remarks of a general nature concerning the Poincaré map.

Area Preservation. A consequence of the conservation of mass is that the Poincaré map preserves area.

Orientation Preservation. Poincaré maps obtained by discretely sampling trajectories of ordinary differential equations have the property of preserving the orientation of area elements. Analytically, this means that the determinant of the Jacobian of the map is strictly positive over its domain of definition (note: by area preservation the determinant of the Jacobian is identically one). Geometrically, orientation preservation can be described as follows. Consider a simply connected area element D with three points denoted a, b, and c on the boundary of D. Suppose that as one walks along the boundary of D in a counterclockwise sense (i.e. with the left arm point toward the interior of D) beginning at a that next b and then c is encountered. Now let $T_{\overline{\theta}}(D) = D'$ with $T_{\overline{\theta}}(a) = a'$, $T_{\overline{\theta}}(b) = b'$, and $T_{\overline{\theta}}(c) = c'$. $T_{\overline{\theta}}$ is orientation preserving if as one walks along the boundary of D' in a counterclockwise sense starting at a' then next b' and then c' is encountered. This implies that the interior of a closed curve is mapped to the interior of its image. See Figure 3.1 for an illustration of the geometry of orientation preservation.

Variation of the Cross-section $\Sigma^{\overline{\theta}}$. Notice from (3.2) that the Poincaré map depends on the phase of the strain-rate field. The question then arises as to how the Poincaré map changes as the phase of the field is varied? Fortunately, there is no qualitative difference in any of these maps. The technical term is that the different maps are *differentiably equivalent* (see Irwin [1980]) which means that given any two Poincaré maps obtained by fixing two different phases of the strain-rate field there exists a differentiable change of coordinates which transforms one map into the other. In particular, the nature of the stability of a fluid particle trajectory is the same for each Poincaré map. Since there is no qualitative difference in the Poincaré maps we will take $\overline{\theta} = 0$. This choice has the advantage that the Poincaré map on this cross-section is symmetric about the y-axis with time reversed. We refer to the associated Poincaré map as T.

Flow Dynamics via the Poincaré Map. In studying the motion of fluid particles the concepts of streamlines, pathlines, and streaklines are very natural. However, as mentioned earlier, their use in the study of unsteady flows is limited since their relationship to such dynamical phenomena as mixing and transport properties is

unclear (Ottino [1987]). In fact these concepts may be misleading. For example, Hama[1962] showed that streaklines and pathlines in a time-dependent laminar flow may look turbulent. In the context of the Poincaré map, the dynamical evolution of fluid particles is expressed in terms of the *orbits* of the Poincaré map. The orbit of a fluid particle is defined as follows: Let p be a fluid particle, then the orbit of p under T is the bi-infinite sequence of points given by:

$$\{\ldots,\ T^{-n}(p),\ldots,\ T^{-1}(p),\ p,\ T(p),\ldots,\ T^{n}(p),\ldots\}$$

where

$$T^n(p) = \overbrace{T(T(\cdots(T(p))\cdots))}^{n \text{ factors}}.$$

Our goal will be to study properties of the orbit structure of the Poincaré map in order to discover the structures necessary to predict mixing and transport properties of the flow.

For more information concerning Poincaré maps, see Guckenheimer and Holmes [1983] or Wiggins [1988].

4. The Three Qualitatively Distinct Flow Regions

Let us recall the structure of the unperturbed velocity field now in the context of the Poincaré map. In this case the velocity field is steady and fluid particles follow the streamlines defined by the level curves of the stream function. Thus orbits of the Poincaré map are sequences of discrete points lying on the streamlines. The streamlines are examples of *invariant curves or manifolds* of the Poincaré map meaning that particles which start on such a curve must thereafter remain on that curve under all iterations of the Poincaré map. The stagnation points p_- and p_+ are fixed points of the Poincaré map. Orbits of fluid particles on Ψ_u, and Ψ_l approach p_+ asymptotically in positive time and p_- asymptotically in negative time. In the terminology of dynamical systems theory, Ψ_u and Ψ_l are referred to as the stable manifold of p_+, denoted W^s_+, and Ψ_0 is the unstable manifold of p_+, denoted W^u_+. Similarly, Ψ_u and Ψ_l are referred to as the unstable manifold of p_-, denoted W^u_-, and Ψ_0 is the stable manifold of p_-, denoted W^s_-. Orbits of fluid particles starting on Ψ_u, Ψ_0, and Ψ_l are referred to as *heteroclinic* orbits and $\Psi_u \cup \Psi_0 \cup \{p_+\} \cup \{p_-\}$ and $\Psi_l \cup \Psi_0 \cup \{p_+\} \cup \{p_-\}$ are said to form *heteroclinic* cycles. The importance of these ideas and this terminology will become evident later on.

Notice that fluid particle motions outside the region bounded by Ψ_u, Ψ_l, p_+, and p_- are qualitatively different than those inside this region. We now want to discuss more fully the different possible fluid particle motions and how they are constrained by structures in the flow.

The Free Flow Region. Under the influence of the unperturbed velocity field fluid particles outside the region bounded by $\Psi_u \cup \Psi_l \cup \{p_+\} \cup \{p_-\}$ move from right to left along the unbounded streamlines. We refer to this as the *free flow region.*

Under the influence of the externally strained velocity field fluid particles which are sufficiently far from $\Psi_u \cup \Psi_l \cup \{p_+\} \cup \{p_-\}$ behave in the same manner as those in the unperturbed velocity field. The implications of the phrase "sufficiently far" from $\Psi_u \cup \Psi_l \cup \{p_+\} \cup \{p_-\}$ will become clear shortly when we describe how the curve $\Psi_u \cup \Psi_l \cup \{p_+\} \cup \{p_-\}$ "breaks up" under the influence of external strain and becomes a chaotic mixing region.

The Core. For the unperturbed velocity field, we refer to the region of fluid which is bounded by $\Psi_u \cup \Psi_l \cup \{p_+\} \cup \{p_-\}$ as the *core.* It contains fluid which is trapped by the streamlines connecting p_+ and p_-. The core contains two separate cells with boundaries $C_u = \Psi_u \cup \Psi_0 \cup \{p_+\} \cup \{p_-\}$ and $C_l = \Psi_l \cup \Psi_0 \cup \{p_+\} \cup \{p_-\}$. Fluid particles in the interior of C_u and C_l move in closed paths along the streamlines of the unperturbed velocity field. We can uniquely label each closed streamline in C_u and C_l by the area which it encloses. We label this area by I (note: in the context of Hamiltonian mechanics I is called the *action*, see Arnold [1978]). Associated with each closed streamline is a period T(I) which is the time needed for a particle starting on the streamline to make one complete circuit along the streamline. The period goes to zero as the point vortices are approached and to ∞ as $\Psi_u \cup \Psi_0 \cup \{p_+\} \cup \{p_-\}$ or $\Psi_l \cup \Psi_0 \cup \{p_+\} \cup \{p_-\}$ are approached.

We would now like to interpret this extremely simple motion of fluid particles in the unperturbed case inside C_u and C_l in terms of orbits of the Poincaré map. The ultimate benefit of this point of view will shortly become apparent. The streamlines in this case are examples of *invariant curves* of the Poincaré map. That is, orbits of fluid particles which start on the streamlines must always stay on the streamlines. There are two types of orbits depending on whether or not the number $\frac{T(I)}{2\pi\gamma}$ is rational or irrational (note: in the context of dynamical systems theory the number $\frac{T(I)}{2\pi\gamma}$ is referred to as a *rotation number*). These two types of orbits behave very differently under the influence of the time periodic strain-rate field.

$T(I)/2\pi\gamma = p/q$: p, q, *integers.* In this case, *every* fluid particle on the invariant circle in the Poincaré map in the unperturbed case returns to its original position after q cycles of the Poincaré map. However, in the process it makes p complete revolutions around the invariant circle. Thus all fluid particles on the invariant circle move periodically with period q.

In general, this situation can be expected to change dramatically under the influence of the time periodic strain-rate field. The invariant circle is destroyed and a finite even number of periodic orbits of alternating stability type will be preserved in the externally strained case. Half of the periodic orbits will be stable and half

will be unstable of saddle type. The stable and unstable manifolds of the saddle type motions may intersect transversely yielding chaotic fluid particle motions. The resulting structure is known as a *p/q resonance band* or *stochastic layer*, see Arnold and Avez [1968] for more details.

$T(I)/2\pi\gamma = \omega : \omega$ *irrational.* In the unperturbed velocity field every fluid particle starting on an invariant circle of the Poincaré map rotates around the circle never returning to its initial position. Two possibilities for the behavior of these orbits under external strain are as follows:

KAM tori. If ω is sufficiently poorly approximated by rational numbers, i.e. it satisfies a diophantine condition (see Arnold and Avez [1968] or Moser [1973]), then, for sufficiently small amplitude strain-rates ε, the invariant circle is preserved in the perturbed Poincaré map. This invariant circle is referred to as a *KAM torus* after Kolmogorov, Arnold, and Moser who first proved the result (known as the KAM theorem). KAM tori are extremely important since they represent total barriers to fluid motion and hence strongly influence transport.

Cantori. If ω fails to satisfy the number theoretic hypotheses of the KAM theorem then the work of Percival [1980], Aubry and LeDaeron [1983], and Mather [1984] implies that the invariant circle may break down under the time periodic strain-rate field into an invariant cantor set or *cantorus.* The dynamics on the cantorus are similar to the dynamics on the KAM torus. However, the cantorus contains gaps which permit the (possibly very slow) passage of fluid.

We refer the reader to Figure 4.1 for an illustration of resonance bands, KAM tori, and cantori in the core. We remark that these three structures govern the fluid transport in the core. However, we will be concerned mainly with the fluid dynamics in the mixing region. In the parameter range we are studying there exists the largest KAM torus which serves as a complete barrier to the flow, and therefore will prevent the mixing of outer fluid with the fluid in the core. An interesting question is whether the core region is composed of a single region bounded by a KAM torus or if there islands outside the largest KAM torus in which the motion is bounded. Numerically, we observe that for $\gamma = 0.5$ there is only one observable

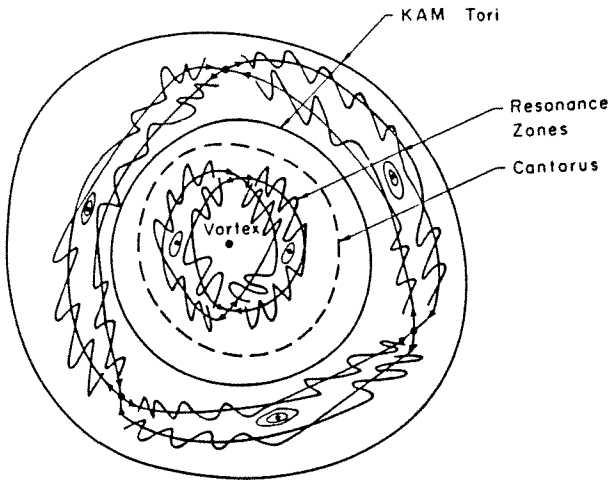

Figure 4.1. Resonance Bands and KAM Tori.

core region while for $\gamma = 1.38$ there are at least two (see Figure 6.10).

The Mixing Region. We now want to focus our attention on p_+ and p_- and their stable and unstable manifolds. In the unperturbed flow W^s_+ and W^u_- coincide along the streamlines Ψ_u and Ψ_l to create a boundary separating the core from the free flow region. With the addition of external strain we can make the following assertions:

1. For sufficiently small amplitude strain fields (i.e. for ε sufficiently small) p_+ and p_- persist as fixed points of the Poincaré map. We shall denote them by $p_{+,\varepsilon}$ and $p_{-,\varepsilon}$, respectively.
2. The stable and unstable manifolds of p_+ and p_- persist. We denote them by $W^s_{+,\varepsilon}$, $W^u_{+,\varepsilon}$, $W^s_{-,\varepsilon}$, and $W^u_{-,\varepsilon}$, respectively.

These two results follow from general theorems regarding the persistence of invariant manifolds which can be found in Fenichel [1971] or Hirsch, Pugh, and Shub [1977] and they are independent of the specific analytical form of the time periodic strain-rate field (note: these results would also apply to quasiperiodic strain rates, See Wiggins [1987], [1988]).

We will see in section 6 that particle transport is governed by the invariant manifolds and that the unstable manifold is the observable structure in a broad class of flow visualizations.

From our discussion of the symmetry of the velocity field in section 3, it follows

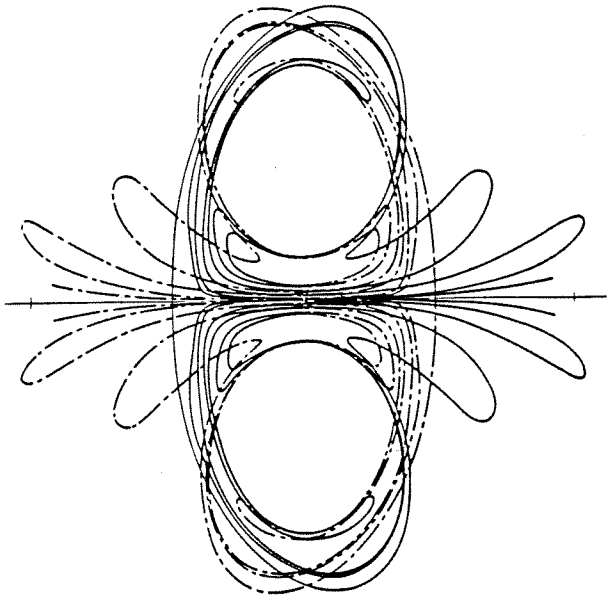

Figure 4.2. The Homoclinic Tangle in the Mixing Region.

that y = 0 is always an invariant manifold for both the perturbed and unperturbed velocity field. This implies that $\Psi_0 = W^u_+ \cup W^s_- = W^u_{+,\epsilon} \cup W^s_{-,\epsilon}$ persists as an invariant streamline. However, the interpretation of $W^s_{+,\epsilon}$ and $W^u_{-,\epsilon}$ is more subtle since they need not coincide as in the unperturbed case. Now $W^s_{+,\epsilon}$ and $W^u_{-,\epsilon}$ are smooth invariant curves and a fluid particle path starting on these curves in the continuous time flow is represented as an infinite set of discrete points on these curves in the Poincaré section. As such it is possible for $W^u_{-,\epsilon}$ and $W^s_{+,\epsilon}$ to intersect in an isolated point as shown in Figure 4.2. Note that Figure 4.2 could not hold in the unperturbed case because, for steady flows, particle paths must coincide with streamlines and streamlines cannot intersect in isolated points without violating uniqueness of solutions of ordinary differential equations. If we consider the orbit of this point of intersection under the Poincaré map, then by invariance of $W^u_{-,\epsilon}$ and $W^s_{+,\epsilon}$ it must forever remain on both $W^u_{-,\epsilon}$ and $W^s_{+,\epsilon}$ resulting in a geometrical shape similar to that shown in Figure 4.2. This splitting of the stable manifold of p_+ and the unstable manifold of p_- results in a mechanism for the transference of fluid between the core and the free flow region. It also provides the mechanism for chaotic particle motion. For this reason, we refer to this region as the *mixing region.*

We will shortly describe this mechanism for the transport of fluid between the core and free flow zone and also define what we mean by the term "chaos". However, first we need to describe a method for rigorously justifying Figure 4.2 which will allow us to get a quantitative handle on the dynamics in the mixing region.

The Melnikov Technique

We will see that much of the fluid mechanics of this system is governed by the behavior of $W^s_{+,\varepsilon}$ and $W^u_{-,\varepsilon}$. An analytical technique which allows us to predict the behavior of $W^s_{+,\varepsilon}$ and $W^u_{-,\varepsilon}$ was developed by Melnikov [1963] and consists of a measurement of the distance between $W^s_{+,\varepsilon}$ and $W^u_{-,\varepsilon}$. Up to a known normalization factor, the first order term of the Taylor series expansion about $\varepsilon = 0$ of the distance between $W^s_{+,\varepsilon}$ and $W^u_{-,\varepsilon}$ can be computed without solving (2.3). This first order term is known as the *Melnikov function.* In Appendix 3, we discuss the geometry of the Melnikov function as well as some of the relevant technical points behind its derivation. In this section, we state the results of the calculations for our problem.

The distance between $W^s_{+,\varepsilon}$ and $W^u_{-,\varepsilon}$ is given by

$$d(t_0,\varepsilon) = \varepsilon \frac{M(t_0)}{||f(q_u(-t_0))||} + O(\varepsilon^2) \tag{4.1}$$

where $q_u(t)$ is a heteroclinic fluid particle trajectory of the unperturbed velocity field lying in Ψ_u, t_0 parametrizes distance along Ψ_u, and

$$||f(q_u(-t_0))|| = \sqrt{(f_1(q_u(-t_0)))^2 + (f_2(q_u(-t_0)))^2}.$$

The Melnikov function $M(t_0)$ is defined to be

$$M(t_0) = \int_{-\infty}^{\infty} [f_1(q_u(t))g_2(q_u(t), t+t_0) - f_2(q_u(t))g_1(q_u(t), t+t_0)]\, dt. \tag{4.2}$$

and Melnikov's theorem (see Appendix 3) shows us that simple zeros of $M(t_0)$ (i.e. $M(t_0) = 0$, $\frac{\partial M}{\partial t_0} \neq 0$) imply simple zeros of $d(t_0,\varepsilon)$ for ε sufficiently small. We remark that $d(t_0,\varepsilon)$ may be either positive or negative which is slightly contrary to the notion of "distance". However, $d(t_0,\varepsilon)$ is a signed measure of the distance between $W^s_{+,\varepsilon}$ and $W^u_{-,\varepsilon}$ and in Appendix 3, we show that the sign of $d(t_0,\varepsilon)$ gives

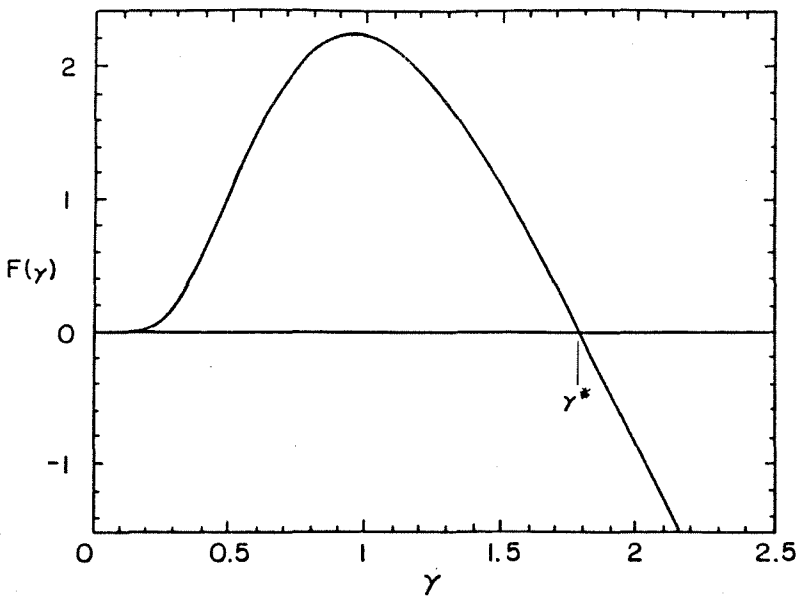

Figure 4.3 Graph of $F(\gamma)$.

us information concerning the relative orientation of $W^s_{+,\varepsilon}$ and $W^u_{-,\varepsilon}$. Also note that $||f(q_u(-t_0))|| \to 0$ exponentially fast as $t_0 \to \pm\infty$ which implies that $|d(t_0,\varepsilon)| \to \infty$ as $t_0 \to \pm\infty$. This just reflects the fact that $W^s_{+,\varepsilon}$ and $W^u_{-,\varepsilon}$ oscillate unboundedly near $p_{-,\varepsilon}$ and $p_{+,\varepsilon}$, respectively.

We numerically calculate the Melnikov function for the velocity field (2.3) and obtain

$$M(t_0) = \frac{F(\gamma)}{\gamma}\sin(t_0/\gamma) \tag{4.3}$$

where $F(\gamma)$ is plotted in Figure 4.3. Note that for fixed γ, $M(t_0)$ has an infinite number of isolated zeros at which $\frac{\partial M}{\partial t_0} \neq 0$. By Theorem A3.1 these correspond to transverse intersections of $W^s_{+,\varepsilon}$ and $W^u_{-,\varepsilon}$ and therefore we obtain a direct analytical confirmation of Figure 4.2. At $\gamma \cong 1.78$, $F(\gamma)$ changes sign, which corresponds to a change in the orientation of the intersection of $W^s_{+,\varepsilon}$ and $W^u_{-,\varepsilon}$. For $\gamma \cong 1.78$, $M(t_0) = 0$ implying that $d(t_0,\varepsilon) = 0(\varepsilon^2)$. In Figure 4.4 we present the manifolds for several values of γ confirming the change of orientation of the intersection.

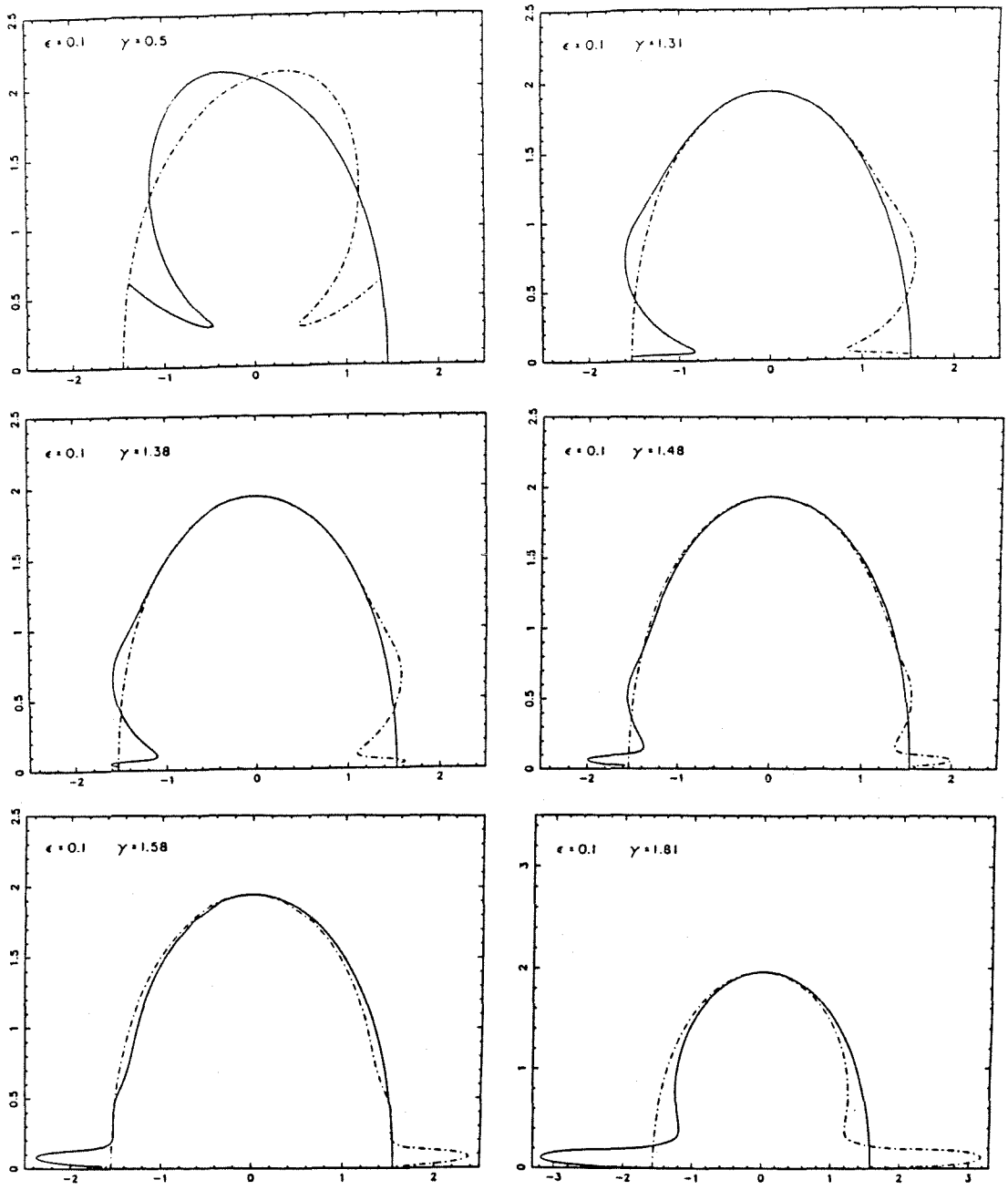

Figure 4.4 Numerical Computations of the Invariant Manifolds for Various Parameter Values.

——— Unstable Manifold – · – · – Stable Manifold

5. Tangle Dynamics

We now want to describe the dynamics associated with the tangling of the stable and unstable manifolds of $p_{+,\varepsilon}$ and $p_{-,\varepsilon}$. Specifically, we want to describe the essential dynamical mechanisms for fluid transport between the free flow region and the core. We will see that the properties of invariance of the stable and unstable manifolds as well as the orientation preserving property of the Poincaré map render a temporal simplicity to the geometrically complex structure associated with the tangling of the manifolds which allows us to obtain a quantitative hold on the dynamics in the mixing region.

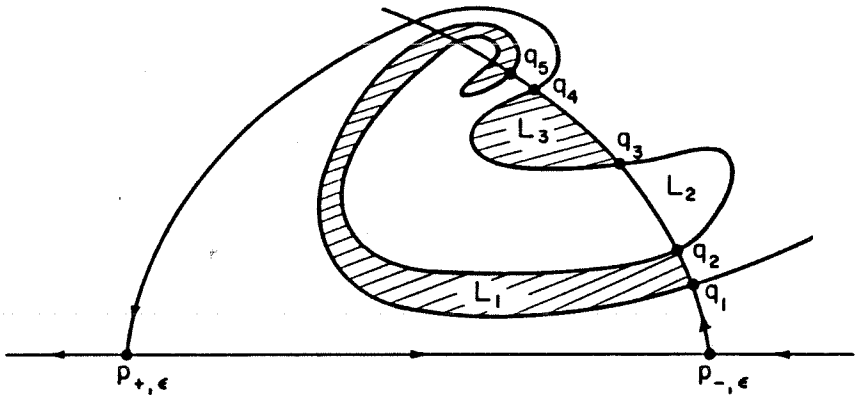

Figure 5.1. The Pip and Lobe definition

q_1, q_2, q_3, q_4 are pip's, q_5 is not a pip. L_1, L_2, L_3 are lobes with $L_1 < L_2 < L_3$.

Lobe Motion. We begin with two definitions:

Definition 5.1. Consider a point $q \in W^s_{+,\varepsilon} \cap W^u_{-,\varepsilon}$ and let $p_{+,\varepsilon}q$ denote the segment of $W^s_{+,\varepsilon}$ from $p_{+,\varepsilon}$ to q and let $p_{-,\varepsilon}q$ denote the segment of $W^u_{-,\varepsilon}$ from $p_{-,\varepsilon}$ to q. Then q is called a *primary intersection point* (pip) if $p_{+,\varepsilon}q$ and $p_{-,\varepsilon}q$ intersect only in q, i.e. $p_{+,\varepsilon}q \cap p_{-,\varepsilon}q = \{q\}$. See Figure 5.1.

Definition 5.2. Let q_1 and q_2 be two adjacent pip, i.e. there are no pip on the segments of $W^s_{+,\varepsilon}$ and $W^u_{-,\varepsilon}$ which connect q_1 and q_2. We refer to the region bounded by the segments of $W^s_{+,\varepsilon}$ and $W^u_{-,\varepsilon}$ which connect q_1 and q_2 as a *lobe*. See Figure 5.1.

The spatial structure of the manifolds provides a natural ordering by time which is useful when we discuss the flux as well as entrainment and detrainment. To describe this ordering we need the following definitions:

Definition 5.3.. Let q_1 and q_2 be pip's. Then we say that $q_1 < q_2$ if q_1 is closer than q_2 to $p_{-,\varepsilon}$ in terms of distance along $W^u_{-,\varepsilon}$.

Definition 5.4.. Suppose that L_1 and L_2 are lobes. Then we say that $L_1 < L_2$ if each of the pip's defining L_1 are less than or equal to each of the pip's defining L_2.

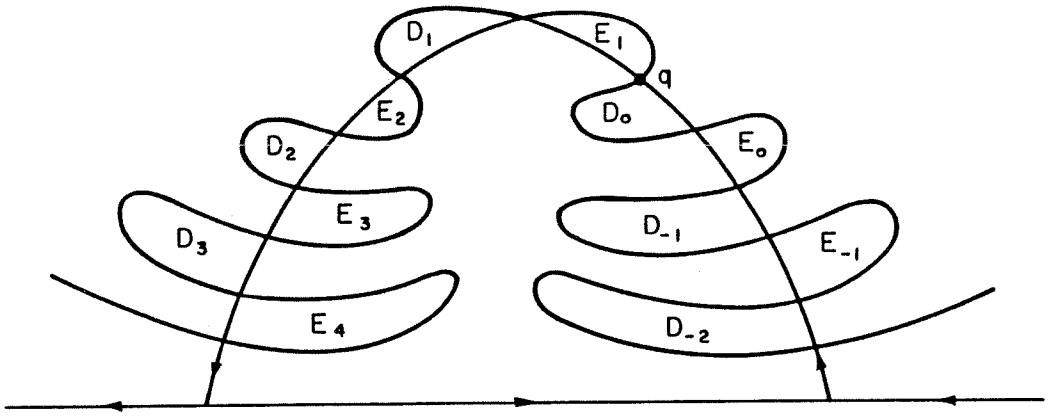

Figure 5.2. The E_i and D_i.

Let q be a pip and consider the region bounded by $p_{+,\varepsilon}q \cup p_{-,\varepsilon}q \cup [W^u_{+,\varepsilon} \cap W^s_{-,\varepsilon}]$. We refer to this as region A. We want to describe the motion of fluid across the boundary of A.

Definition 5.5. A lobe is called an *exterior lobe* if no part of its interior is contained in A. A lobe that is not an exterior lobe is called an *interior lobe.*

Now consider Figure 5.2. The lobes E_i are exterior lobes for $i \leq 0$ and interior lobes for $i > 0$. Similarly, the lobes D_i are exterior lobes for $i > 0$ and interior lobes for $i \leq 0$. The following theorem is our main result concerning the dynamics of the lobes.

Theorem 5.1. Suppose $M(t_0)$ has 2n simple zeros in one period $\tau = 2pi\gamma$. Then:

1. $T(E_i) = E_{i+n}$

2. $T(D_i) = D_{i+n}$

Proof. See Appendix 4.

The concise statement of Theorem 5.1 belies its many underlying implications which we now want to point out.

After one cycle of the time periodic strain-rate field (i.e. one iterate of the Poincaré map) $E_0, \ldots, E_{-n+1}$ enter region A. Similarly, after one cycle $D_0, \ldots, D_{-n+1}$ leave region A.

The lobes E_i, D_i maintain their ordering throughout their evolution in time under the action of the Poincaré map, i.e.

$$E_i < E_j \text{ implies } T^k(E_i) < T^k(E_j)$$

$$D_i < D_j \text{ implies } T^k(D_i) < T^k(D_j)$$

$$E_i < D_j \text{ implies } T^k(E_i) < T^k(D_j)$$

for all k. This is a consequence of the fact that the Poincaré map preserves orientation and therefore the relative ordering of points along $W^u_{-,\epsilon}$ is preserved.

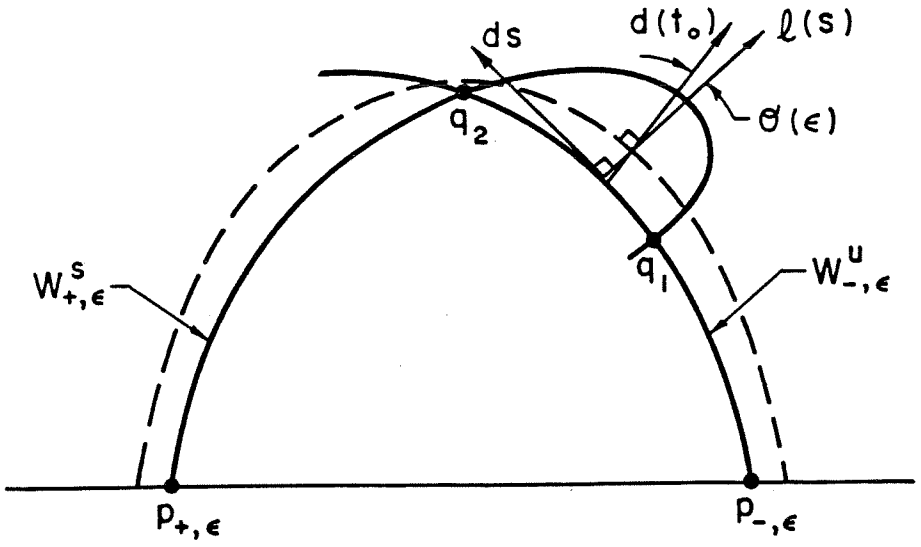

Figure 5.3 Geometry of the Area of the Lobes.

Lobe Area. From Theorem 5.1, the periodicity properties of the Melnikov function tell us how many lobes enter A per cycle. Thus knowledge of the area of the lobes

would tell us the amount of fluid entering A per cycle. We show that the Melnikov function gives this information.

Consider Figure 5.3 and the lobe L defined by the pip's q_1 and q_2. Let us denote the infinitesimal element of arclength along $W^u_{-,\varepsilon}$ by ds and let $l(s)$ denote the perpendicular distance between $W^s_{+,\varepsilon}$ and $W^u_{-,\varepsilon}$. Then the area of L, denoted $\mu(L)$, is given by

$$\mu(L) = \int_{q_1}^{q_2} l(s)ds. \tag{5.1}$$

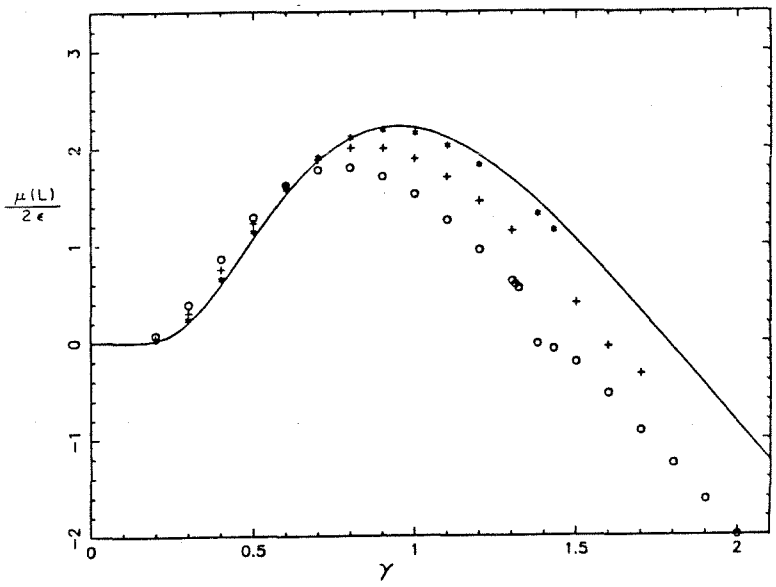

Figure 5.4 Comparison Between Theoretical and Numerical Calculations of Lobe Areas

—— F (γ), $*$, $\varepsilon = 0.01$, $+$, $\varepsilon = 0.05$, $\circ$, $\varepsilon = 0.1$.

Now $W^s_{+,\varepsilon}$ and $W^u_{-,\varepsilon}$ can be approximated uniformly on semi-infinite time intervals (see Guckenheimer and Holmes [1983]) and because these manifolds move only an $O(\varepsilon)$ amount from the unperturbed manifolds on these time intervals the angle between the line along which $d(t_0, \varepsilon)$ is measured (see appendix 3) and the line along which $l(s)$ is measured is $O(\varepsilon)$. Thus we can write

$$l(s) = |d(t_0, \varepsilon)| + O(\varepsilon^2) = \frac{\varepsilon |M(t_0)|}{||f(q_u(-t_0))||} + O(\varepsilon^2) \tag{5.2}$$

and

$$ds = \frac{ds}{dt_0} dt_0 = (||f(q_u(-t_0))|| + O(\varepsilon))\, dt_0. \tag{5.3}$$

substituting (5.2) and (5.3) into (5.1) gives

$$\begin{aligned} \mu(L) &= \int_{t_{01}}^{t_{02}} \left[\frac{\varepsilon |M(t_0)|}{||f(q_u(-t_0))||} + O(\varepsilon^2) \right] (||f(q_u(-t_0))|| + O(\varepsilon))\, dt_0 \\ &= \varepsilon \int_{t_{01}}^{t_{02}} |M(t_0)| dt_0 + O(\varepsilon^2) \end{aligned} \tag{5.4}$$

where $q_u(-t_{01}) = q_1$ and $q_u(-t_{02}) = q_2$. Thus we see that the integral of the Melnikov function between two adjacent pip's gives an $O(\varepsilon)$ approximation to the area of the lobe defined by the pip's. Several comments are now in order.

1. The validity of (5.4) relies heavily on the validity of the approximation of the perturbed manifolds via regular perturbation theory which is rigorous only on semi-infinite time intervals. Thus (5.4) is only valid for lobes defined by pip's which are outside of sufficiently small neighborhoods of $p_{+,\varepsilon}$ and $p_{-,\varepsilon}$. However, in our case, the Poincaré map preserves area, so knowing the area of one lobe implies that we know the area of all the images of that lobe under the Poincaré map.
2. For our problem, substituting (4.3) into (5.4) gives the following expression for the area of the lobes

$$\mu(L) = 2\varepsilon |F(\gamma)| + O(\varepsilon^2). \tag{5.5}$$

   This gives us the explicit dependence of the area of the lobes on the parameter γ. A comparison between the numerical calculation of lobe area and the analytical result gives good agreement as seen in Figure 5.4.

Now let us return to our specific problem. In general, the region A can be defined by an arbitrary pip. However, in our problem we choose the region A to be defined by the pip which lies on the y axis. This is because the resulting shape of the region is very similar to the region of trapped fluid in the unperturbed velocity field, see Figure 5.5.

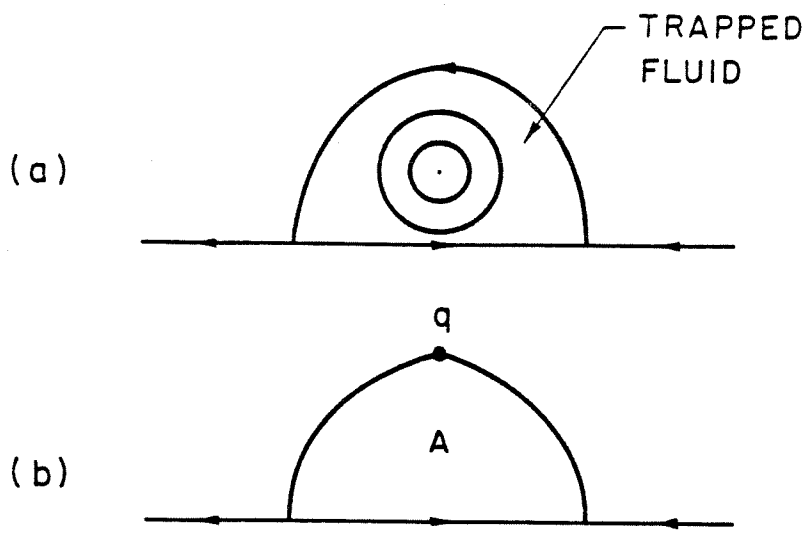

Figure 5.5. The Geometry of Region A.
a) unperturbed flow. b) perturbed flow.

From (4.3), $M(t_0) = (F(\gamma)/\gamma)\sin t_0/\gamma$ and, therefore, one lobe enters and one lobe leaves the region A during each cycle with the area of the lobes equal to $2\varepsilon|F(\gamma)| + O(\varepsilon^2)$. Notice that for $\gamma \cong 0.93$, $F(\gamma)$ obtains its maximum, thus the volume of fluid entrained per cycle is maximal at this γ. The volume entrained per unit time is maximum at $\gamma \cong 0.7$ when $F(\gamma)/\gamma$ is maximum. Notice that for $\gamma = 1.78$ the Melnikov function vanishes identically. Hence the $O(\varepsilon^2)$ terms in the formula for the distance between the manifolds become important. Numerically, we observe that, near this γ value, two lobes enter and leave the region A per cycle (see Figure 4.4c, d, e.).

6. Particle Transport

In this section we discuss particle transport - the flow into and out of the core A. We saw that in the unperturbed flow fluid particles either flow past region A or stay in A forever, while in the perturbed flow the behavior is more interesting, fluid particles can move from the free flow region into A and vice versa. The time spent in A depends on the particle's initial conditions and we define this time as the *residence time.* A volume of fluid therefore has an associated *residence time distribution.*

The notion of a residence time distribution is an important concept in mixing systems. For example, if fluid is injected into a catalytic reactor, the amount of product will be mostly influenced by the time spent by the fluid in the reactor. Other processes such as chemical reaction and heat or mass transfer have similar dependencies on the residence time distribution. Danckwerts [1953] discussed the importance and the application of this notion for steady flows through vessels (such as a pipe or tank) and the work presented here is similar to his in spirit. Both works rely on the simple observation that in order to determine the residence time distribution of the fluid initially in the vessel or in A, one needs to know the future of entering fluid only. Though developed separately, the method described here can be thought of as a discretization of Danckwerts' work to maps, where again the advantage of working with the Poincaré map instead of the time dependent flow is apparent.

We refer to the motion of fluid from the free flow region into the core as *entrainment* and the motion of fluid from the core into the free flow region as *detrainment.* Theorem 5.1 tells us that if the Melnikov function has 2n simple zeros per period then n lobes are entrained and n lobes are detrained per cycle. For our problem the Melnikov function has 2 simple zeros per period and therefore (at least for sufficiently small ε) one lobe is entrained and one lobe is detrained per cycle. We denote these lobes by E and D, respectively, see Figure 6.1. This implies that the volume of fluid entrained into region A during each cycle is the area of lobe E or $\mu(E)$. Also, the amount detrained from region A during each cycle is the area of

lobe D or $\mu(D)$ and by incompressibility it must be equal to $\mu(E)$ and, in general,

$$\mu(T^l D) = \mu(T^k E) \qquad \text{for all} l, k = 0, \pm 1, \pm 2, \ldots \tag{6.1}$$

In this section we discuss more detailed questions of particle transport which can be answered by applying the following rules:

R1. Fluid entering region A on cycle k must be in E on cycle k-1.

R2. Fluid leaving region A on cycle k must be in D on cycle k-1.

R3. $T^l(E)$ cannot intersect $T^k(E)$ and $T^l(D)$ cannot intersect $T^k(D)$ for any k, $l = 0, \pm 1, \pm 2, \ldots$

Regarding R3, we note that it is possible for $T^l(E)$ to intersect $T^k(D)$ for some integers l and k.

The questions we wish to address are:

1. How long does it take fluid to escape A given that it started in A?

Remarkably, it will turn out that answering this question is equivalent to answering the following question:

2. How long does it take fluid to escape from A given that it is in lobe E initially?

More specifically we wish to determine the residence time distributions for the two initial conditions mentioned above. The answer to question 1 may be obtained by brute force calculations, where a large number of initial conditions in A are integrated and the number escaping each cycle are counted. The results of such calculations for two γ values are presented in Figure 6.10a,b. The similarity to the manifolds shape as seen in Figure 4.2 and demonstrated in Figure 6.10c is not accidental, it is a manifestation of the lobe dynamics as described in Section 5. Using the lobe dynamics enables us to reduce the problem to the computation of the residence time distribution for lobe E only.

Escape Rates We consider first fluid that is in lobe E initially (at cycle 0). As discussed previously, after one cycle the fluid in E enters A. However, it may not remain in A since at some later time, say cycle k-1, a portion of the original fluid

may be found in lobe D and therefore will escape A on the next cycle. We define e_k to be that portion, i.e.,

$$e_k = \textit{volume of fluid in lobe } E \textit{ at cycle } 0 \textit{ that escapes } A \textit{ on the } k^{th} \textit{ cycle.}$$

clearly,

$$e_k = \mu(T^{k-1}E \cap D) \qquad k = 1, 2, \ldots \tag{6.2a}$$

and

$$e_k = 0 \qquad k \leq 0 \tag{6.2b}$$

Note that the corresponding distribution of escape times is given by $e_k/\mu(E)$. Using incompressibility (6.2a) can alternatively be written

$$e_k = \mu(E \cap T^{-k+1}D) \qquad k = 1, 2, \ldots \tag{6.3}$$

Figure 6.1 illustrates the geometry associated with (6.2a) and (6.3).

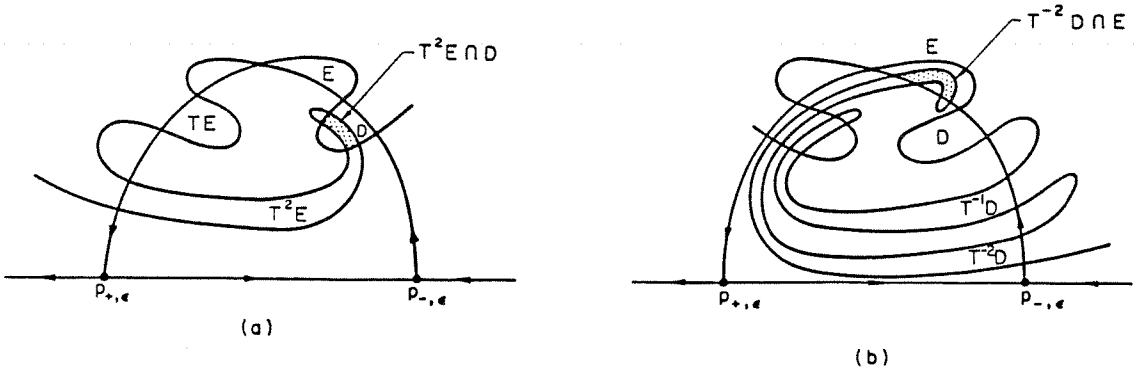

Figure 6.1 The Lobe Intersections

a) $e_3 = \mu(T^2E \cap D)$ b) $e_3 = \mu(E \cap T^{-2}D)$.

Note that replacing E with $T^{-l}E$ in (6.2a) and (6.3) gives the volume of fluid in lobe $T^{-l}E$ at cycle 0 that escapes A on the k^{th} cycle. This is clearly equal to e_{k-l}. In fact, the e_k's contain information concerning all possible intersections of any E_i lobe with any D_j because

$$e_k = \mu(T^{k+m-1}E \cap T^m D) \qquad m = 0, \pm 1, \pm 2, \ldots$$

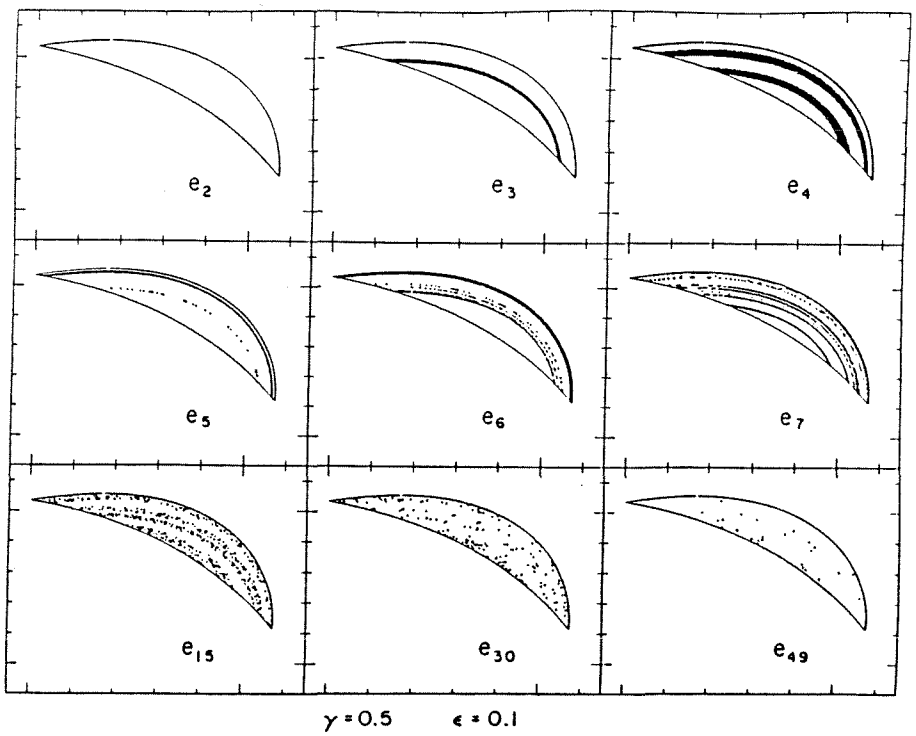

Figure 6.2a. Geometry of $E \cap T^{-k+1}D$ for Various Values of k, $\gamma = 0.5$.

In Figure 6.2 we illustrate the case $m = -k+1$ by displaying the sets $E \cap T^{-k+1}D$ for several values of k and $\gamma = 0.5, 0.9$.

Now we consider the escape distribution for region A and define escape volumes as follows:

$$a_k = \textit{ volume of fluid in region A on cycle 0 that escapes on cycle k.}$$

From previous discussions it follows that fluid leaving A on the k^{th} cycle must be in the lobe $T^{-k+1}D$ at cycle 0. However not all of $T^{-k+1}D$ was in A at cycle 0 since portions of $T^{-k+1}D$ may intersect $T^{-l}E$, $0 \leq l \leq k$, and should not be counted. So it follows that

$$a_k = \mu(T^{-k+1}D) - \sum_{l=0}^{k} \mu(T^{-k+1}D \cap T^{-l}E). \tag{6.4}$$

where the sum in (6.4) represents the volume of $T^{-k+1}D$ that is also in some $T^{-l}E$ for $0 \leq l \leq k$. By incompressibility we have

$$\mu(T^{-k+1}D) = \mu(D) = \mu(E) \tag{6.5}$$

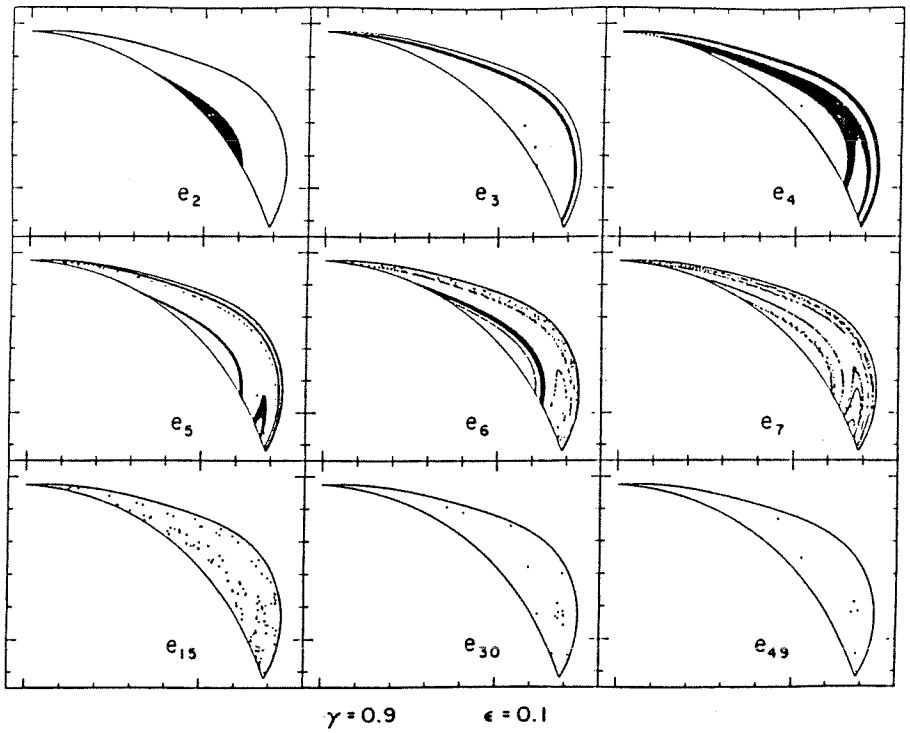

Figure 6.2b. Geometry of $E \cap T^{-k+1}D$ for Various Values of k, $\gamma = 0.9$.

and from (6.3) we have

$$e_{k-l} = \mu(T^{-k+1}D \cap T^{-l}E) \tag{6.6}$$

Using (6.6) and (6.5) allows us to simplify (6.4) as follows

$$a_k = \mu(E) - \sum_{l=0}^{k} e_{k-l}$$

or

$$a_k = \mu(E) - \sum_{l=1}^{k} e_l \tag{6.8}$$

Thus, to compute a_k, we need only information concerning the dynamics of lobe E, namely the e_k. We find e_k numerically by computing the escape cycle for each member of a regular array of grid points in lobe E. To verify the relation between the e_k and the a_k given by (6.8), we have also computed the a_k for one particular choice of the parameters ε and γ by a "brute force" calculation using an array of grid points in region A. The results are shown in Figure 6.3 and confirm (6.8).

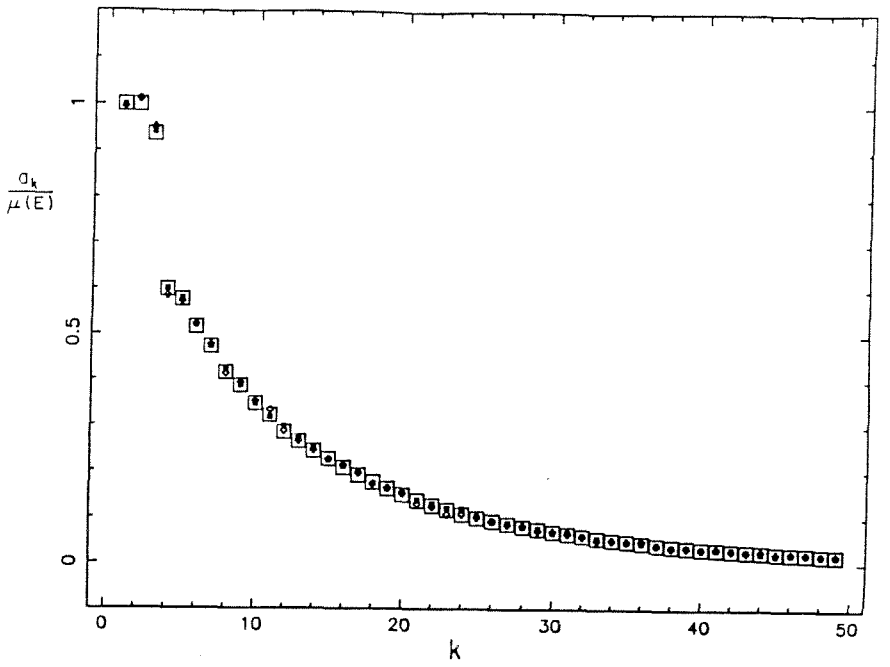

Figure 6.3 Comparison of the Brute Force and the Reduced Calculation for $\gamma = 0.5$. ▪ brute force calculation with mesh=0.005, ▫ reduced calculation with mesh=0.005, ◇ brute force calculation with mesh=0.0075.

We note that with little effort we can obtain other quantities, which are of physical interest, in terms of the e_k such as:

$$r_k = \textit{volume of fluid initially in } A \textit{ that remains in } A \textit{ after } k \textit{ cycles.}$$

clearly,

$$r_k = r_{k-1} - a_k \tag{6.9}$$

or

$$r_k = \mu(A) - \sum_{i=1}^{k} a_i \tag{6.10}$$

Using (6.8) we obtain:

$$r_k = \mu(A) - k\mu(E) + \sum_{i=1}^{k}(k - i + 1)e_i \tag{6.11}$$

Since e_k and r_k are finite and positive and $\sum_{i=1}^{k} e_i \leq \mu(E)$, we deduce that

$$\sum_{i=1}^{\infty} e_i = \mu(E) \tag{6.12}$$

$$\sum_{i=1}^{\infty}(i-1)e_i = \mu(A) - \mu(C) \tag{6.13}$$

where $r_\infty = \mu(C) \leq \mu(A)$ and $\mu(C)$ is the volume of fluid initially in A that never escapes, i.e. the core of A. The relation (6.12) is also evident from incompressibility.

We note also the inversion formula

$$e_k = r_k - 2r_{k-1} + r_{k-2}. \tag{6.14}$$

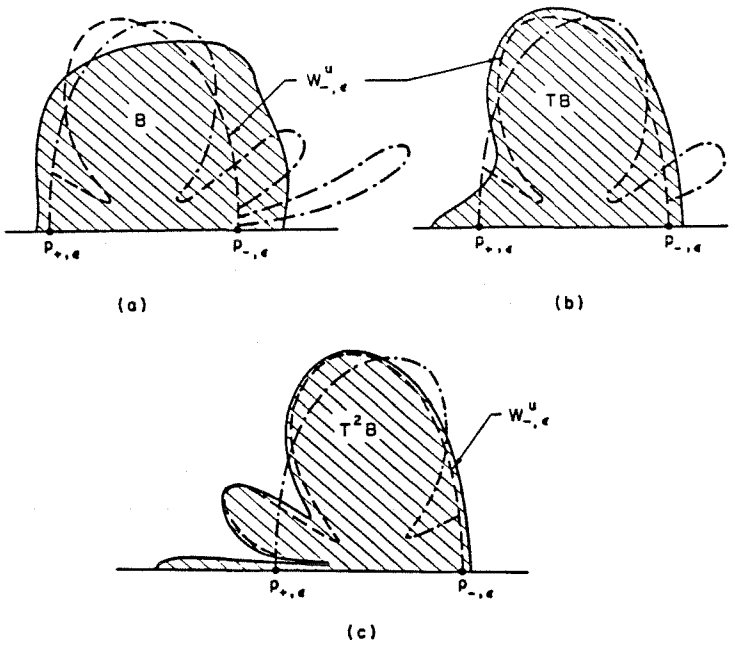

Figure 6.4 The Motion of a General Initial Shape B.

a) $t = 0$ b)$t = 2\pi\gamma$ c) $t = 4\pi\gamma$.

In general one would like to know the residence time distribution associated with any initial shape B of finite area. This seems at the moment too hard a question. Qualitatively, one expects to have similar behavior as obtained for A. Specifically, for any initial shape B which can be regarded as distortion of A (B includes non-trivial parts of the mixing region, namely it is not contained in one D lobe), the dominant structure which will be visualized and which will control the transport is $W^u_{-,\varepsilon}$. This is a result of the motion of the E lobes which accumulate on $W^u_{-,\varepsilon}$ as $t \to \infty$, and the assumption that B has finite area. Therefore for large enough k^*, $T^{-k}E$ contains a very small portion of B for all $k > k^*$, which implies that for $k > k^*$, T^kB will have a

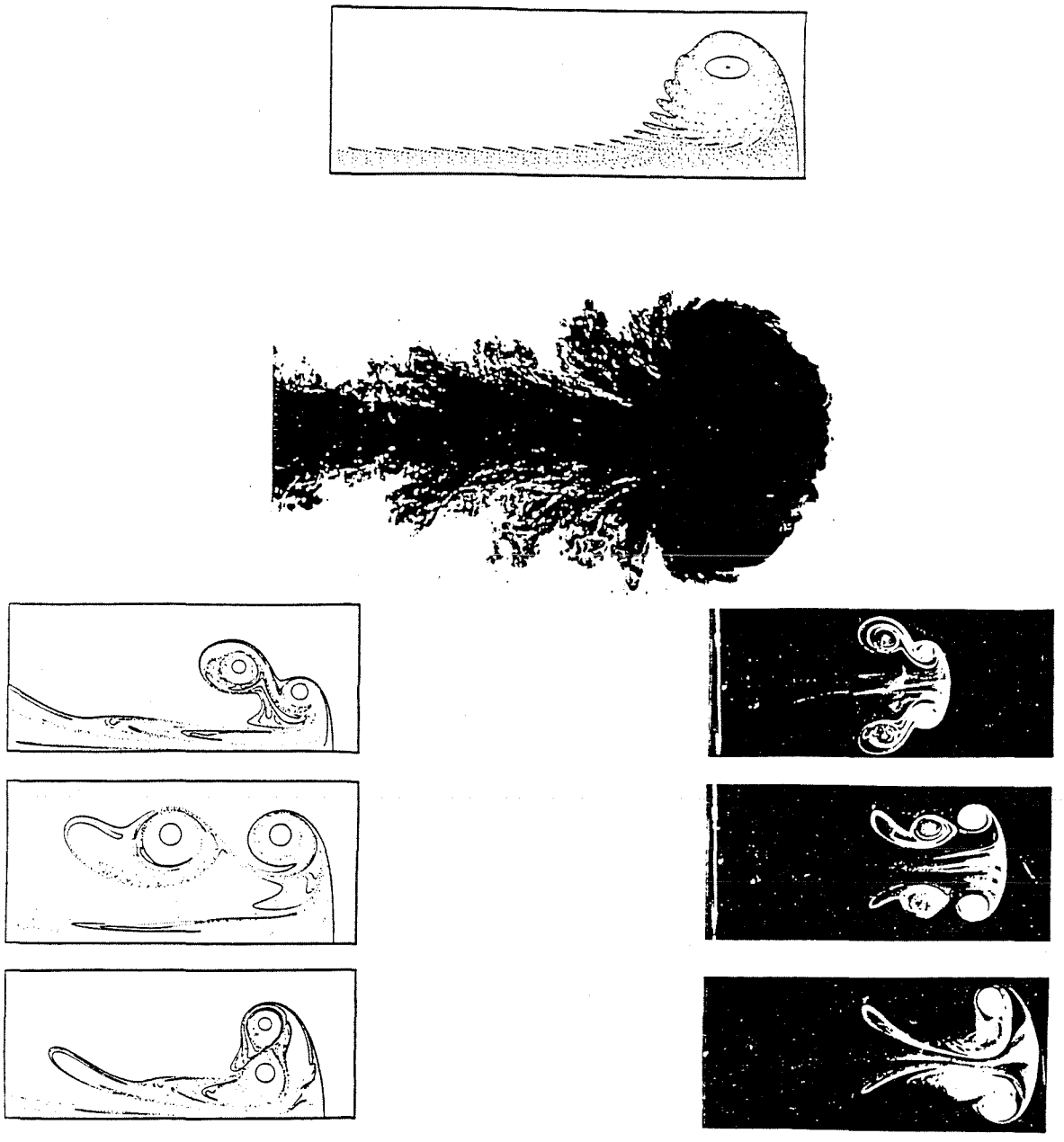

Figure 6.5 Comparison between Flow Visualizations and
the Unstable Manifold Calculations.

a) A computation of the unstable manifold of an axisymmetric vortex ring with an elliptical core, where only the upper half of the ring cross-section is plotted.

b) Flow visualization of a cross-section of a turbulent vortex ring.

c) A computation of the unstable manifold of leapfrogging of two axisymmetric vortex rings, where only the upper half of the cross-section is plotted.

d) Flow visualization of leapfrogging of two vortex rings.

very narrow layer upstream of $W^u_{-,\epsilon}$, see Figure 6.4. The above argument applies to a broad class of flows having similar structure, namely hyperbolic stagnation points with cyclic motion near them, implying that the unstable manifold is the observed structure in many flow visualizations. We demonstrate this point in Figure 6.5 by comparing numerical computations of the unstable manifold for two axisymmetric flows by Shariff [1987] and Shariff et al. [1987], and two flow visualizations of similar flow configurations by Glezer and Coles [1987] and Yamada and Matsui [1978].

Numerical Results and Discussion

We now present numerical results for the residence time distributions, (e_k, a_k, and r_k properly normalized) and discuss their dependence on k and the parameter γ. In particular, some characteristics of the numerical results can be readily understood from the manifold structure.

The $e_k = \mu(E \cap T^{-k}D)$ can be computed in one of two ways:

1. Compute the boundaries of the lobes E and $T^{-k}D$ and find the area of their intersection.
2. Track area elements of the interior of lobe E to determine the area that escapes A at each cycle.

Although the first method is theoretically more satisfying, there are two substantial difficulties: (1) the problem of the exponential stretch of the manifolds and thus of the lobe boundary and (2) the determination of the interior of a tangled boundary for large k. We therefore use the second method where the grid mesh on E was chosen to be sufficiently small. In Figure 6.2, for large k, it appears as if the escape area is composed of a number of isolated area elements, but this is merely the result of using a finite number of nondeforming area elements. The actual areas in $E \cap T^{-k}D$ must be composed of a finite number of shapes that connect to each other or the boundary of E since $T^{-k}D$ is simply connected. The appearance of isolated computational points for a relatively fine mesh (dx = dy = 0.005) shows that the widths of the interior regions of $E \cap T^{-k}D$ become extremely narrow and demonstrates the difficulties one would encounter when using a scheme that tracks the boundary of E or D.

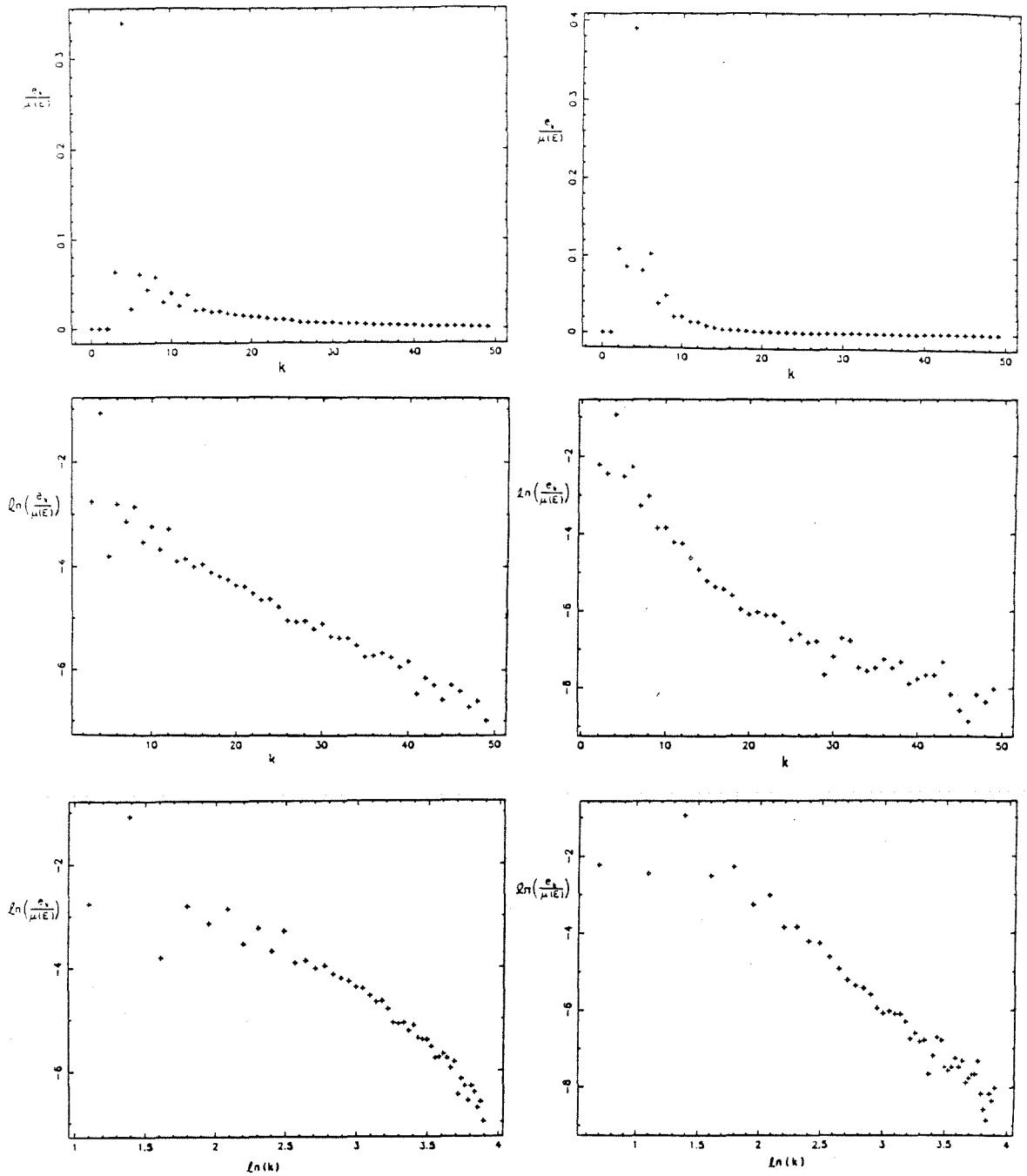

Figure 6.6 The e_k's.

a) $\gamma = 0.5$ b) $\gamma = 0.9$ c) γ=0.5, log-linear plot d) γ=0.9, log linear plot

e) γ=0.5, log-log plot f) γ=0.9, log-log plot.

It is interesting to note how the quantities vary according to qualitative features of the manifolds. Figure 6.6 contains plots of e_k for two γ values. The rapid oscillations of e_k with k are typical for all values of γ and are discussed below.

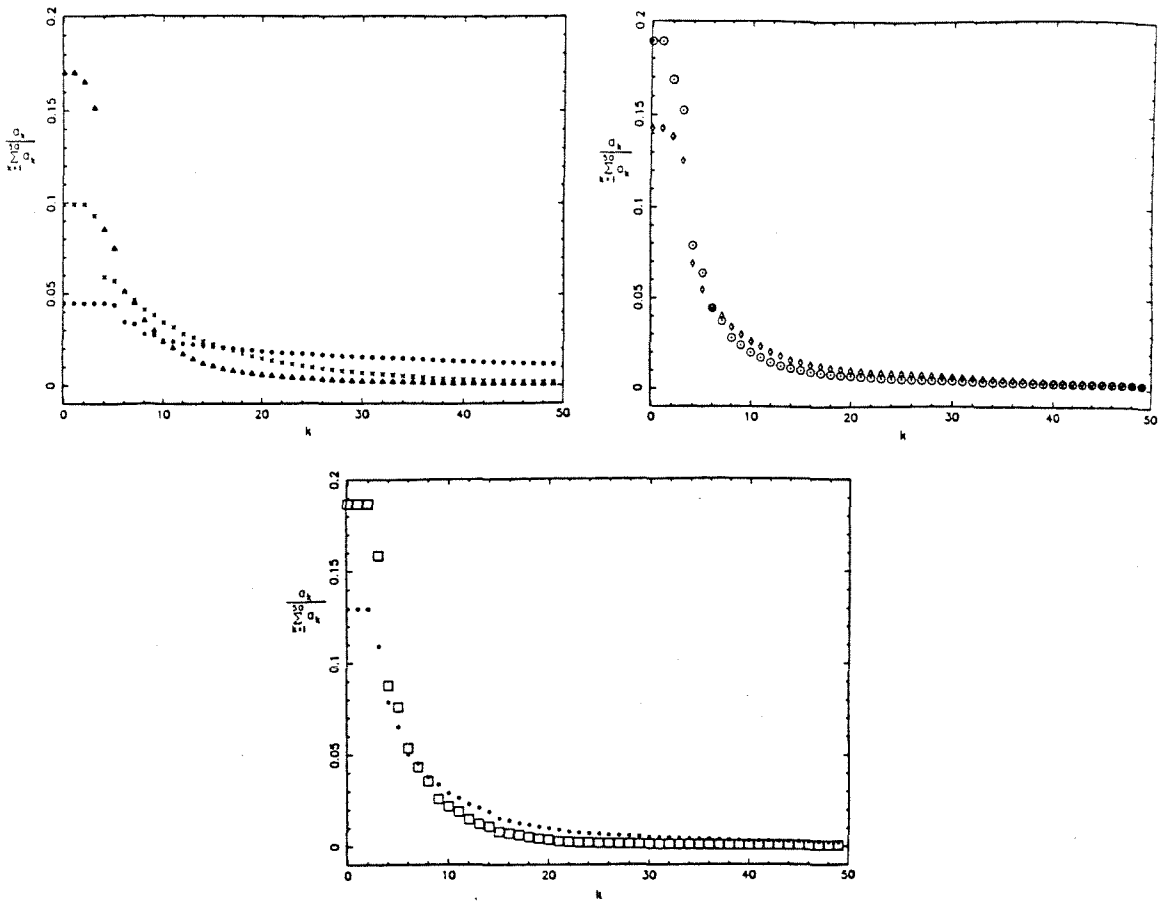

Figure 6.7 The a_k's.

a) γ=0.3, 0.5, 0.7 b) γ=0.9, 1.1 c) γ=1.7, 1.9.

We include log-linear and log-log plots as an aid to identifying possible exponential or power law behavior but, because of the fluctuations of the e_k for small and large k, we will defer the discussion of these possibilities until the a_k are presented. The small k fluctuations consist of two-cycle oscillations with even k maxima and odd k minima. We explain this phenomenon as follows. Note that the invariance of the manifolds gives $e_2 k = \mu(T^{2k}E \cap D) = \mu(T^k E \cap T^{-k}D)$ and $e_{2k-1} = \mu(T^{k-1}E \cap T^{-k}D)$. Now, in the symmetric Poincaré map $T^k E$ and $T^{-k}D$ are mirror images of each other. Since near the x axis both lobes are flat, we will obtain, in general, a larger volume of intersection than is obtained in a "transversal" intersection which occurs in the asymmetric intersection of $T^{k-1}E \cap T^{-k}D$. However, secondary intersections far from the neighborhood of the stagnation point will relax this difference as k increases. Thus the two-cycle oscillation of the e_k decays.

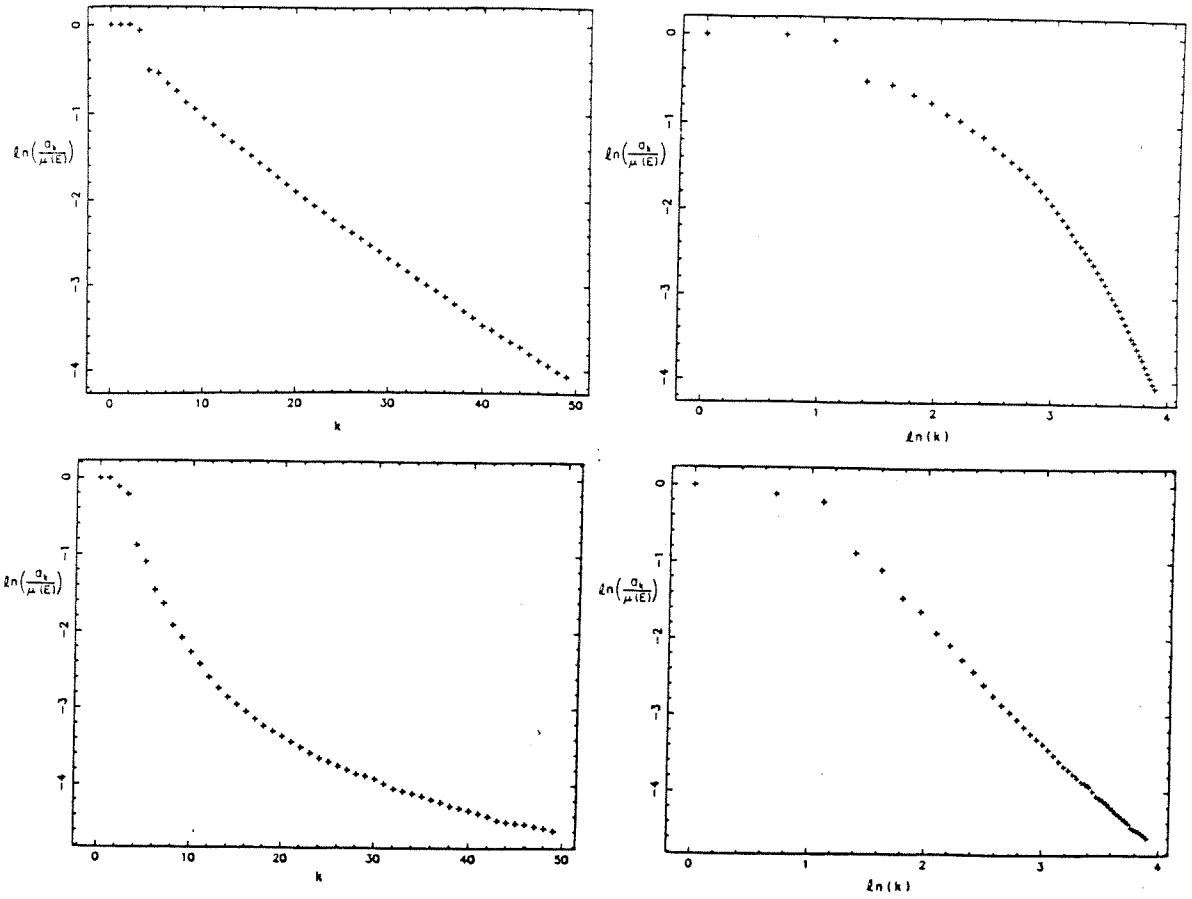

Figure 6.7 The a_k.

d)γ=0.5, log-linear plot. e)γ=0.5, log-log plot.

f)γ=0.9, log-linear plot. g)γ=0.9, log-log plot.

For larger k ($k > 20$) the fluctuations observed in Figure. 6.6c-6.6f are due to the statistics of the computation. We have verified that a finer mesh will decrease these fluctuations.

The a_k are shown in Figure. 6.7. Note that for small k the a_k, as a function of γ, increase with γ up to $\gamma \cong 0.8$ then decrease until $\gamma \cong 1.3$ then increase again. This behavior is directly related entrainment rate or lobe area given by $2\varepsilon|F(\gamma)| + O(\varepsilon^2)$. (see Figure 5.4). Using Figures 6.7d-6.7g we can make tentative conclusions regarding the asymptotic behavior of the a_k for large k for $\gamma = 0.5$ and 0.9. Figure 6.7d strongly indicates exponential behavior for $\gamma = 0.5$ or

$$a_k \sim \beta(r_k - r_\infty) \qquad \text{as} \quad k \to \infty$$

i.e. a constant probability of escape from A-C for large k. For $\gamma < 0.5$, similar

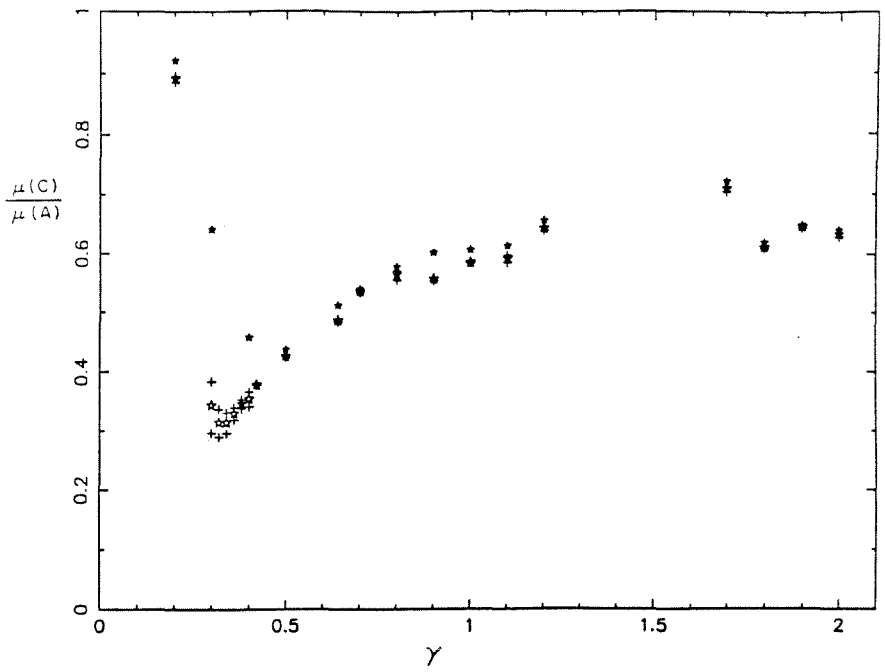

Figure 6.8 The Core Area.

$\star$ $r_{50}/\mu(A)$, $\bigstar$ $r_\infty/\mu(A)$, + upper and lower bounds on $r_\infty/\mu(A)$

exponential behavior is indicated. For $\gamma > 0.5$ there are no strong indications for either exponential or power law behavior with the possible exception of $\gamma \cong 0.9$. For $\gamma = 0.9$, Figure 6.7g suggests a power law behavior for a_k or

$$a_k \sim \frac{\lambda}{k}(r_k - r_\infty)$$

i.e. a decreasing probability of escape as $k \to \infty$.

Fitting an exponential for the a_k by using a least square method for the log-linear plots, we can compute r_∞ using 6.10:

$$r_\infty = r_{k_0-1} - \sum_{i=k_0}^{\infty} a_i = r_{k_0-1} - \frac{ce^{-\alpha k_0}}{1-e^{-\alpha}}$$

where c and α are related to the best linear fit coefficients. The results are presented in Figure (6.8) where r_{50}, r_∞, and the bounds on r_∞ computed via the least square method are presented. The exponents we get are relatively small and therefore the linear fit to the log-linear plots, as well as the results for r_∞, should be taken with caution.

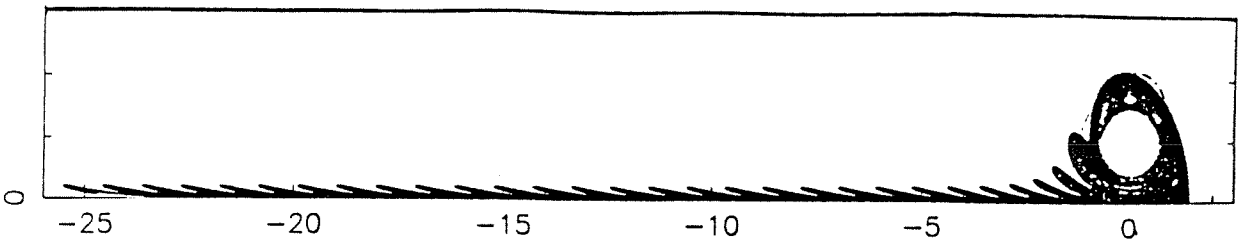

Figure 6.9 The Unstable Manifold for $\gamma = 0.3$.

The core C is not necessarily composed of only one region. In fact, we find that the core splits into at least two separate domains for $\gamma = 1.38$ for example. This is indicated from the photographs of the escape map (Figure 6.10a,b), in which the red regions can be approximately identified with the core.

The appearance of a different number of regions with bounded motion for different γ's is the result of the distinctive resonances associated with each γ value. Recall from Section 4 that the streamline associated with a p/q resonance is determined via the relation $T(I)/2\pi\gamma = p/q$. Therefore, as γ increases, the streamline corresponding to the above relation has larger period and hence must be closer to the mixing region. Therefore, assuming that the largest KAM torus position is approximately independent of γ, we expect that as γ increases more resonance bands are present outside the largest KAM torus and with further increase in γ, they approach the manifolds and become unobservable. The scenario which is shown in Figures 6.9 and 6.10 fits the above description as follows:

For $\gamma = 0.3$ the $p = 4$ $q = 1$ resonance band outside the largest KAM torus is manifested as four white spots outside the large white region - the main core. (In Figure 6.9 the unstable manifold is plotted, and the white regions are the regions which the manifold cannot penetrate). In Figure 6.10a, where the escape map for $\gamma = 0.5$ is plotted we observe only one core region - the $q = 1$ $p = 4$ resonant disappeared in the vicinity of the manifolds and no other resonance bands appear. As γ increases to $\gamma = 1.38$ the $p = 1$ $q = 1$ resonance band appears outside the largest KAM torus and two core regions are revealed in Figure 6.10b.

Figure 6.10 The Escape Map. (next page)

a) $\gamma = 0.5$ b) $\gamma = 1.38$ c) γ=0.5 With the Unstable Manifold Plotted in White. The initial conditions are colored according to their residence time: the color is graded from blue via green to red with residence time from 0 to 50 cycles.

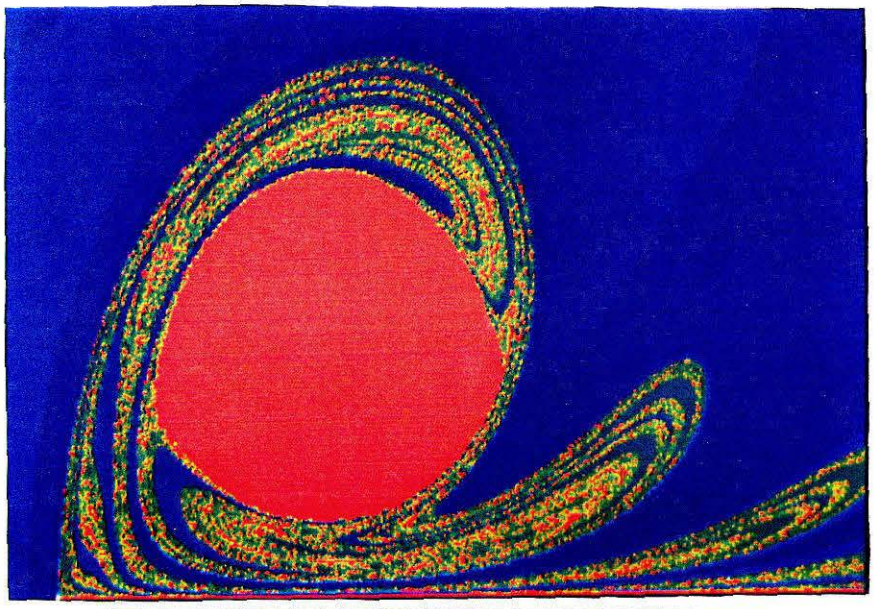

$\epsilon = 0.1$

$\gamma = 0.5$

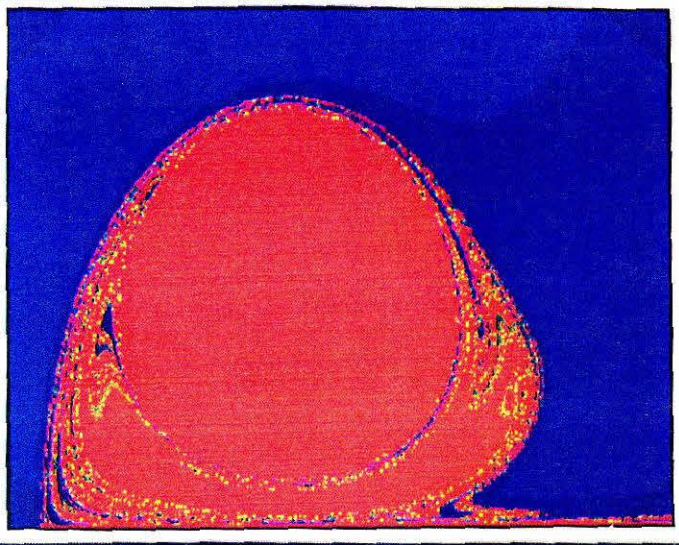

$\epsilon = 0.1$

$\gamma = 1.38$

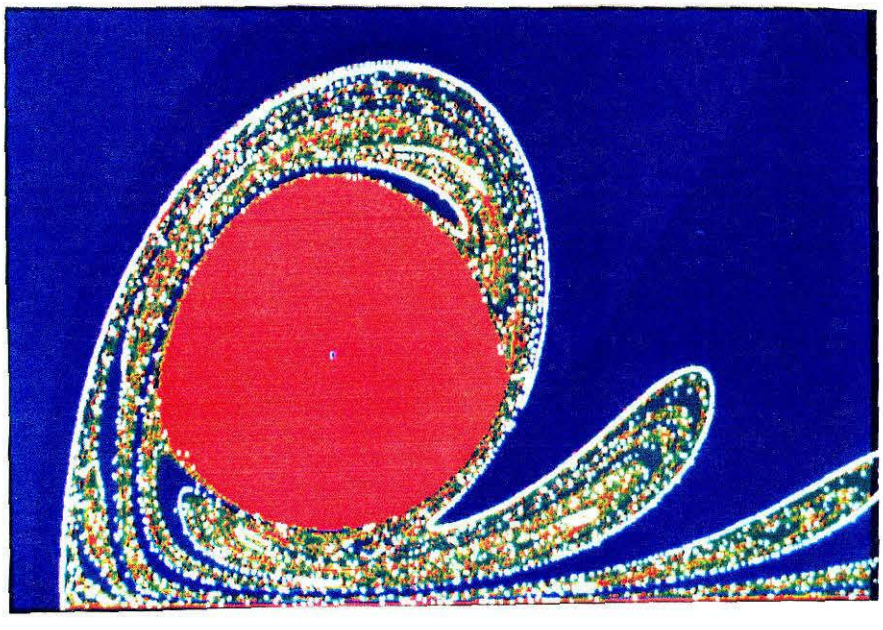

$\epsilon = 0.1$

$\gamma = 0.5$

7. "Chaos"

We have seen that transport between the core and the free flow region can be understood by studying the interaction between the stable and unstable manifolds of $p_{+,\varepsilon}$ and $p_{-,\varepsilon}$, respectively. Now we want to show that this interaction gives rise to another important dynamical effect, namely chaotic fluid particle motion.

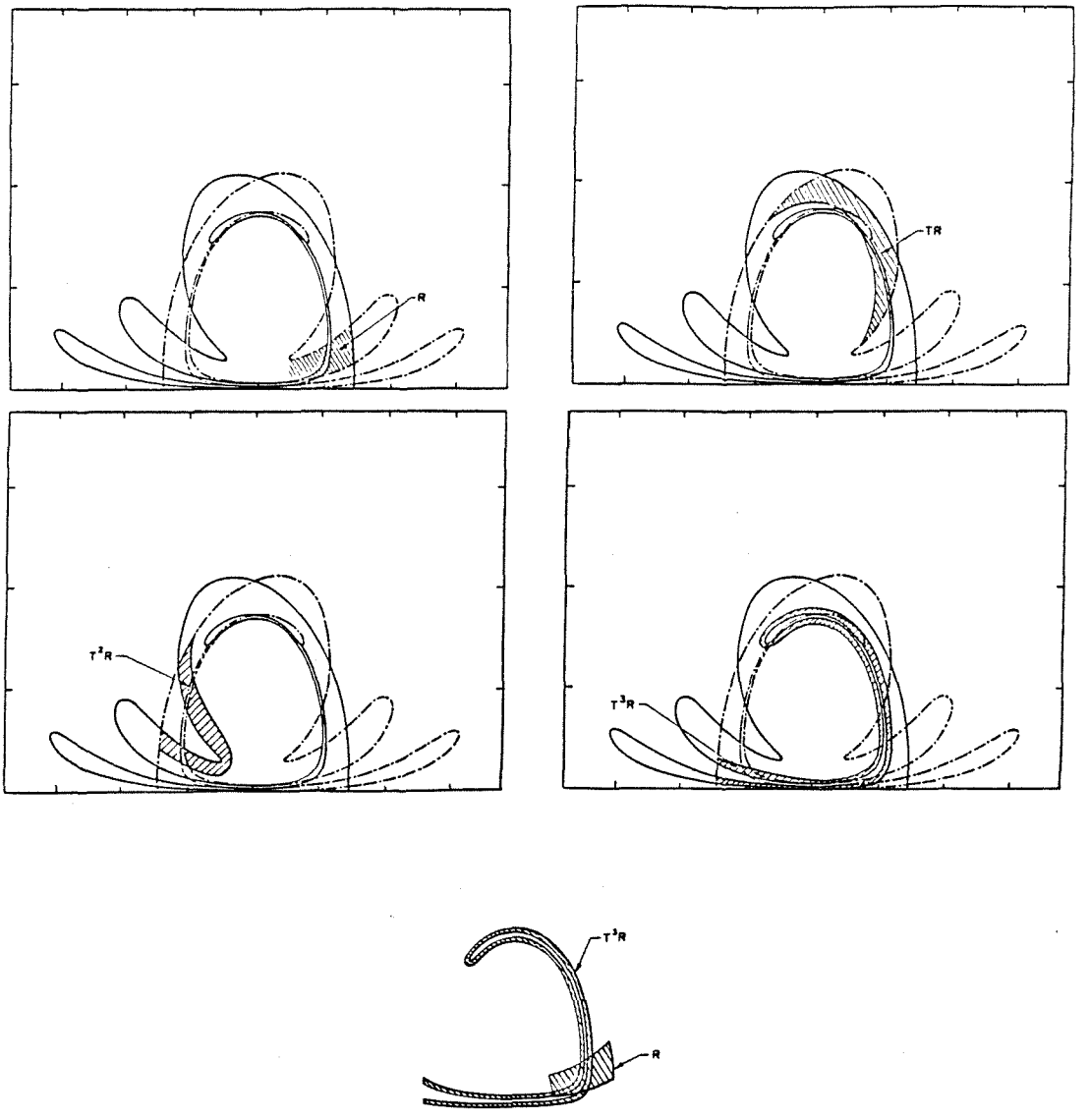

Figure 7.1. The Geometry of the Horseshoe Map.

Roughly speaking, chaotic fluid particle motion may result when structures in the flow conspire to strongly stretch, contract and fold a region of fluid. In our flow the tangling of the manifolds provides the folding mechanism and the fixed points

$p_{+,\varepsilon}$ and $p_{-,\varepsilon}$ provide the stretching and contraction mechanism. The notion of chaos is made unambiguous when we show that this scenario enables us to prove that the Poincaré map possesses *Smale horseshoes* using the Smale-Birkhoff homoclinic theorem, see Guckenheimer and Holmes [1983] or Wiggins [1988]. Consider Figure 7.1 and the "rectangular" region of fluid denoted R. Following the evolution of this region under iteration by the Poincaré map T we see that it is folded, stretched, and contracted and eventually mapped back over itself in the shape of a horseshoe.

We leave out the details but using techniques which can be found in Moser [1973] or Wiggins [1988] one can show that "R" contains an invariant cantor set Λ such that $T^n|_\Lambda$, for some $n \geq 1$, has

1. A countable infinity of unstable periodic fluid particle motions of all possible periods.

2. An uncountable infinity of unstable nonperiodic fluid particle motions.

3. A fluid particle whose orbit under T^n eventually approaches every other point in Λ arbitrarily closely.

Λ is called a chaotic invariant set for T^n. We remark that in Moser [1973] and Wiggins [1988] it is shown that by a continuous change of coordinates $T^n|_\Lambda$ can be transformed into a Bernoulli process hence making precise the notion of deterministic chaos. The construction shown in Figure 7.1 could be repeated near any transverse heteroclinic point hence Smale horseshoes and their associated chaotic dynamics exist throughout the part of the mixing region in A.

So the existence of transverse heteroclinic orbits in a heteroclinic cycle give rise to Smale horseshoes and are therefore the underlying mechanism for chaos. The Melnikov function allows us to determine if transverse heteroclinic orbits are present in the flow and hence give a specific criteria for the presence of Smale horseshoes in terms of the system parameters.

It should be apparent that the presence of horseshoes in a fluid flow may have a significant effect on neighboring fluid particle motions. However, it is difficult to quantify this effect. Two things can be said:

1. The unperturbed velocity field is integrable therefore fluid particles may separate at a linear rate at best. However, in the perturbed velocity field fluid particles may separate at an exponential rate and moreover the presence of horseshoes may cause fluid particle motions in the mixing region to become rapidly uncorrelated. Intuitively, one would believe that horseshoes are desirable in order to enhance mixing. We discuss these issues in the next section.

2. In order to quantify the mixing of fluid between the core and the free flow region one must understand the dynamics of the interface, i.e. the stable manifold of $p_{+,\varepsilon}$ and the unstable manifold of $p_{-,\varepsilon}$. This is a topic which we are currently investigating in more detail. However, from our previous description a significant observation can be made. That is, in the unperturbed velocity field the interface separating the core and the free flow region has finite length but in the perturbed velocity field this interface has infinite length.

Liapunov Characteristics Exponent and Residence Time Distribution

We investigate the rate of stretching of material lines in the Oscillating Vortex Pair (OVP) flow and its relation to the time spent in the mixing region. The classical measure for quantifying the local stretching of material lines on the average is the largest Liapunov Characteristic Exponents (LCE), see for example Khakhar, Rising and Ottino [1986]. The motivation for computing the LCE's is that they quantify the chaos in the system; when a positive LCE exists nearby trajectories diverge from each other exponentially. This notion is particularly useful when dealing with dissipative systems with attractors, since then all initial conditions will eventually diverge as much as trajectories on the attractor diverge. In the OVP flow we have proven the existence of an uncountable infinity of orbits in the mixing region which are chaotic and therefore have a positive LCE. This set of chaotic orbits is of measure zero. Nevertheless, these orbits are responsible for the expansion and contraction in the mixing region: particles passing through this region will experience the exponential stretching and contraction associated with the chaotic orbits, though only for a finite time, which implies that their LCE's vanish. To quantify this phenomenon we define time dependent LCE's, which measure the local stretching of material lines averaged over finite time, and the total stretch, which measures the elongation of a material element due to its motion through the chaotic region. As motivated in section 4, we concentrate on analyzing the behavior in the mixing region.

We start by defining the stretching rate and its relation to the LCE following the formulation of Khakhar, Rising, and Ottino [1986]. Next, we prove that the LCE's are identically zero for all particles which escape the mixing region and define related quantities such as time-dependent stretching rate and the total stretch. We then describe the algorithm used to find these quantities and present results relating the total stretch and the residence time for a sample of initial conditions.

Since most of the discussion presented here is applicable to many other systems of the same nature (open flows which exist for all time with localized chaos), we

start with a general system of ODE's (Ordinary Differential Equation) of the form:

$$\dot{p} = F(p,t) \qquad p \in R^2 \tag{8.1}$$

where F is infinitely differentiable. Most of the following formulation can be generalized easily to $p \in R^n$, $n \geq 2$, but for simplicity of explanation we take $n = 2$. The linearized equation about an arbitrary solution of (8.1) is given by

$$\dot{m} = DF(p(t),t)m \tag{8.2}$$

where DF is the matrix of partial derivatives of F.

Following Khakhar, Rising and Ottino [1986] we define the length stretch $\lambda(p,m,t)$ of an infinitesimal material line dx emanating from p with orientation m at t=0 as:

$$\lambda(p,m,t) = \frac{|m(t)|}{|m|} \tag{8.3}$$

where $m(t)$ is a solution of (8.2), $m \neq 0$.

Physically, the length stretch measures how much the length of an infinitesimal line emanating from p with initial orientation m is amplified under the flow.

An LCE of the orbit p is defined as

$$\sigma(p,m) = \lim_{t\to\infty} \frac{1}{t} \ln \lambda(p,m,t) \tag{8.4}$$

where m is a nonzero vector in R^2.

Oseledec [1968] proved the existence of this limit for dynamical systems defined on compact domains, where the compactness is needed for solutions to exist for all time. In addition Oseledec's theorem requires that $DF(p(t),t)$ is non-singular and that the following holds:

$$\lim_{t\to\infty} \frac{1}{t} ln||DF(p(t),t)|| < \infty$$

where $||DF(p(t),t)||$ is the largest eigenvalue of $DF(p(t),t)$. Oseledec proved that given the above conditions $\sigma(p,m)$ attains exactly two values $\sigma_1(p) \geq \sigma_2(p)$, where $\sigma_2(p)$ is attained only if m is in the direction of minimal growth rate normal to the orbit of p, see Oseledec [1968] for more details. The asymptotic rate of expansion of a neighborhood of p is given by $\exp\{(\sigma_1(p) + \sigma_2(p))t\}$ which implies that in the area preserving case $\sigma_1(p) = -\sigma_2(p) = \sigma(p) \geq 0$.

Since the OVP flow is an open flow the compactness requirement in Oseledec's theorem does not hold in general, but can be applied to the core region. In this region one would expect to find positive LCE's associated with the Smale Horseshoes which should be present there by the recent result of Holmes, Marsden, and Scheurle [1987]. In contrast with the mixing region, there the KAM tori prevent the trajectories from escaping the chaotic region. However, for small perturbation, most of the core is occupied by KAM tori and therefore it is hard to detect the chaotic regions. In fact, it is still an open question whether the chaotic regions in between KAM tori are of positive measure. We performed a few numerical experiments in this region, in which we followed a few trajectories with different recurrence times (the recurrence time is approximately the natural period of an orbit). In all these cases $\lambda(p,m,t)$ appears to be of the form $\lambda(p,m,t) = t^{\beta(p,m)} + \alpha(p,m,t)$ where $\alpha(p,m,t)$ is periodic in t and $\beta(p,m) < 1$. This implies, using (8.4), that for all these initial conditions $\sigma(p,m) = 0$. The period of α is found to be related to the recurrence time of p. Note that since the flow is not ergodic and also cannot possess an attractor (since it is area preserving) the LCE does depend in general on the initial conditions.

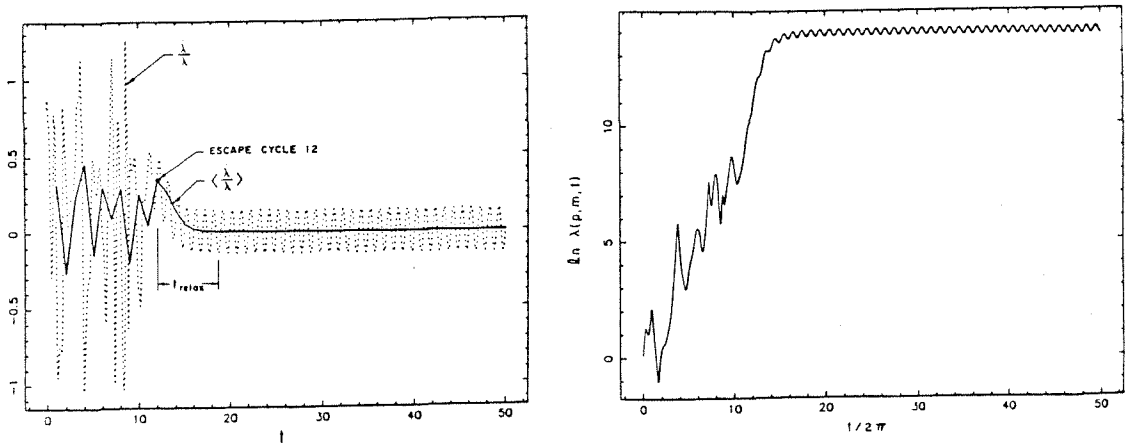

Figure 8.1 The Time Dependent LCE's.

a) $\frac{\dot{\lambda}}{\lambda}$ for an Initial Condition in A-C. b) $\ln \lambda$ for the Same Initial Condition.

We now concentrate on the region of our interest, the mixing region. This region is composed, by definition, of the lobes $E_k, D_k \quad k = 0, \pm 1, \ldots$ and the invariant sets

associated with the Smale horseshoes which are of measure zero. On an invariant set we expect to find a positive LCE but we cannot detect them numerically. In practice the important feature of the Smale horseshoes are their influence on the neighboring orbits, orbits which are contained in the lobes E_k, D_k. From equation (6.12) it follows that the lobes E_k are contained (up to measure zero) in $\cup_{k=-\infty}^{\infty} D_k$, therefore we need to investigate the orbits in the D_k lobes only. Since this region and its images under the flow are not compact Oseledec's results cannot be used. However, we prove that $\lim_{t\to\infty} \frac{1}{t} \ln \lambda(p,m,t)$ exists in the OVP case, for $p \in \cup_{k=-\infty}^{\infty} D_k$ and that it is identically zero. We prove first that λ is asymptotically periodic and then that this implies that $\sigma(p,m)$ vanishes. The proofs are in appendix 5.

Lemma 8.1: If $p = (x,y) \in \cup_{k=-\infty}^{\infty} D_k$ then for some $t_0 > (t_{esc} + t_{ent})$

1) $\quad y(t) = O(\varepsilon)$

$$\text{for} \quad t > t_0$$

2) $\quad x(t) = -0.5t + O(\varepsilon t, \ln t)$

where t_{esc} is the residence time for p, meaning the time p spends in region A, and t_{ent} is the time it takes p to enter A (if $p \in A$ initially $t_{ent} = 0$, and if $p \in D_k$, $k \geq 1 \quad t_{ent} = t_{esc} = 0$)

Lemma 8.2: If $p \in \cup_{k=-\infty}^{\infty} D_k$ then

$$\lambda(p,m,t) = \chi(p,m,t) + O(\frac{1}{t^2}) \quad \text{for} \quad t > t_0 \tag{8.5}$$

where $\chi(p,m,t)$ is a periodic function in t.

Lemmas 8.1 and 8.2 show that if $p \in \cup_{k=-\infty}^{\infty} D_k$ then $\lambda(p,m,t)$ is asymptotically periodic and as discussed below, our numerical results indicate that λ appears periodic only a few cycles after escape.

We show next that the asymptotic periodicity of λ implies that the LCE vanish. We define the time dependent LCE's to be $\frac{\dot{\lambda}}{\lambda}$ averaged over t:

$$\sigma(p,m,t) = \frac{1}{t} \int_0^t \frac{\dot{\lambda}}{\lambda} dt = \frac{1}{t} \ln \lambda(p,m,t) \tag{8.6}$$

Since λ measures the total elongation of an infinitesimal material line until time t, $\frac{\dot{\lambda}}{\lambda}$ measures the instantaneous change in the elongation rate normalized by λ. So the LCE can be thought of as the long-time average of the instantaneous change in the elongation rate, as indicated by Khakhar, Rising and Ottino [1986].

We proved in Lemmas 8.1 and 8.2 that λ (and therefore $\ln \lambda$) is asymptotically periodic in t for $t > t_0$ where $t_0 = t_{esc} + t_{ent} + t_{relax}$. The relaxation time t_{relax} is the time it takes $p(t_{esc} + t_{ent})$ to leave the neighborhood of the rear stagnation point where stretching still occurs (see Figure 8.1 and Appendix 5).

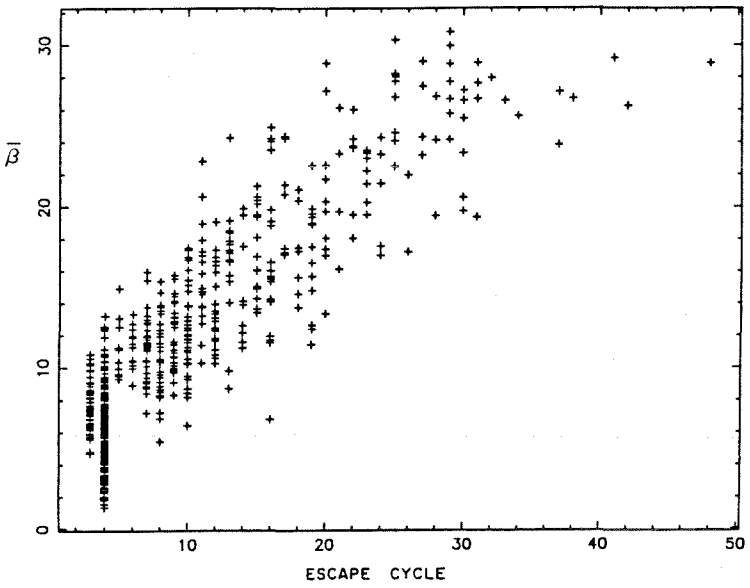

Figure 8.2 The Total Stretch $\overline{\beta}$.

Rewriting equation 8.6, using the definition of t_0 we obtain:

$$\sigma(p,m) = \lim_{t\to\infty} \frac{\beta(p,m) + \alpha(p,m,t)}{t} = 0 \tag{8.7}$$

where

$$\beta(p,m) = \int_0^{t_0} \frac{\dot{\lambda}}{\lambda} \qquad \alpha(p,m,t) = \int_{t_0}^{t} \frac{\dot{\lambda}}{\lambda} = \ln(\chi(p,m,t) + O(\frac{1}{t^2})) - \ln \lambda(p,m,t_0)$$

And $\alpha(p,m,t)$ is an asymptotically periodic function by Lemma 8.2. In Figure 8.1, we demonstrate numerically for a particular initial condition starting in A-C (so that $t_{ent} = 0$) the periodicity of $\frac{\dot{\lambda}}{\lambda}$ and the fact that $\frac{\dot{\lambda}}{\lambda}$, averaged over each period,

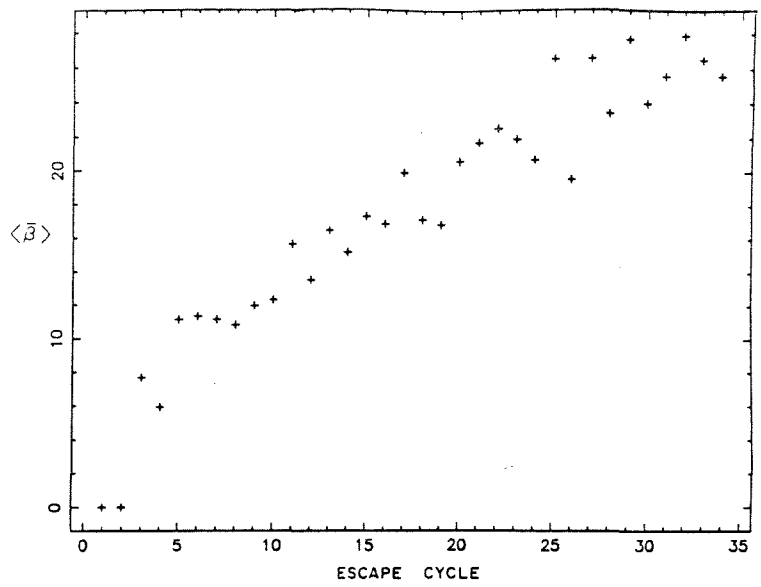

Figure 8.3 The Total Stretch Averaged over a Sample of Initial Conditions with the Same Escape Cycle.

(i.e. $\alpha(2n\pi(\gamma+1)) - \alpha(2n\pi\gamma))$ is practically zero for $t > t_0$. It is worthwhile to note that Goldhirsch et al. [1987] find similar behavior of the Liapunov exponents in five dissipative systems (for example, the system studied by Lorenz) namely they find:

$$\sigma(p,m) = \lim_{t\to\infty}(\sigma + \frac{c+d(t)}{t})$$

In their cases the systems possess an attractor hence, $\sigma \neq 0$ and is independent of p, m. They, therefore, refer to the terms $\frac{c+d(t)}{t}$ as a slowly decaying error of the standard algorithm (Benettin et al. [1980], Wolf et al. [1984]) and develop a method to achieve faster convergence. In the OVP flow only β remains as the useful physical quantity which measures the total elongation of a material element.

The maximal elongation of an infinitesimal neighborhood around p until time $t = 2n\pi\gamma$ is given by

$$\overline{\beta}(p) = \max_m \ \beta(p,m) = \max_m \ \ln\lambda(p,m,2n\pi\gamma) \tag{8.8}$$

Where t is sufficiently large so that λ is essentially periodic after time greater than $t - 2\pi\gamma$. (The additional period is taken to incorporate the mean of α into $\overline{\beta}$, though in practice we find that α has zero mean).

The total stretch $\overline{\beta}$ has an importance of the same nature as of the largest LCE in that it is the most observable elongation rate. Therefore material elements, noise and numerical errors will be most noticeably amplified by this rate. In other words, an infinitesimal blob of dye of radius $|m|$ placed at p at $t = 0$ will amplify its length by $\overline{\beta}$ at time t, and from then on its length will oscillate periodically with mean $\overline{\beta}|m|$. Note that in formula (8.8) we need to maximize β in contrast with the procedure for finding the largest LCE, where almost all vectors will stretch at the same rate eventually. This is the result of analyzing the finite time average (8.6) instead of the asymptotic result. The method to obtain $\overline{\beta}$ follows.

Let M(t) be the fundamental solution matrix of equation (8.2) so that

$$\dot{M} = DF(p(t), t)M \tag{8.9}$$

$$M(0) = I$$

Then, a general solution $m(t)$ of equation (8.2) is given by $m(t) = M(t)m$. Therefore,

$$\max_m \lambda(p, m, t) = \max_m \left(\frac{m^T M^T M m}{m^T m} \right)^{1/2} = \sqrt{\rho(M^T M)}$$

where $\rho(M^T M)$ is the maximal eigenvalue of $M^T M$.

Note that in general $\sqrt{\rho(M^T M)} \neq \rho(M)$, see Goldhirsch et al. [1987]. To compute $\rho(M^T M)$ we develop an ODE for the components of MM^T, noting that in two dimensions $\rho(M^T M) = \rho(MM^T)$.

Since the OVP flow is irrotational and incompressible the matrix $DF(p(t), t)$ is symmetric and has the form:

$$DF(p(t), t) = \begin{pmatrix} a(t) & b(t) \\ b(t) & -a(t) \end{pmatrix}$$

where $a(t) = \frac{\partial(f_1 + \varepsilon g_1)}{\partial x}(p(t), t)$ $b(t) = \frac{\partial(f_1 + \varepsilon g_1)}{\partial y}(p(t), t)$

Using equation (8.9) and this form of DF we obtain

$$\frac{d}{dt}(MM^T) = \frac{dM}{dt}M^T + M\frac{dM^T}{dt} = (MM^T)DF + DF(MM^T) \tag{8.10}$$

Now MM^T is a symmetric matrix of the form

$$MM^T = \begin{pmatrix} q & r \\ r & s \end{pmatrix}$$

And equation (8.10), written in component form, gives a system of three ODE's for the matrix elements q,r,s. Since det(MM^T)=1 we obtain the following expression for $\rho(MM^T)$:

$$\rho(MM^T) = \frac{q+s+\sqrt{(q+s)^2-4}}{2}$$

$q+s$ can be obtained either from the ODE's for q, r, s or by solving the integral equation:

$$(q+s)^2 = 4\left[\int_0^t a(t')(q+s)(t')dt'\right]^2 + 4\left[\int_0^t b(t')(q+s)(t')dt'\right]^2 + 4$$

Using the former technique we have found $\overline{\beta}$ for a sample of 530 initial conditions in region $A \cap \cup_{k=0}^{\infty} D_{-k}$. The results are presented in Figure 8.2 where we plot $\overline{\beta}$ versus the escape cycle of p. Though $\overline{\beta}$ attains different values for each escape cycle, the general tendency of $\overline{\beta}$ is to increase with the escape cycle, with increasing deviation from the mean. In Figure 8.3, we average $\overline{\beta}$ over the set of initial conditions having the same escape cycle, and the tendency of $\overline{\beta}$ to increase with the escape cycle is apparent.

To summarize, we have shown that the LCE's vanish in the OVP flow in the mixing region, and observed numerically that they are zero also in the core and in the free flow region. We have shown that for the mixing region this is a result of the flow being open with localized chaos, allowing fluid particles to be convected to infinity after a finite amount of stretching. We defined therefore the total stretch $\overline{\beta}$, to be the maximal elongation of a fluid element while in the chaotic region. We found that on the average this quantity increases with residence time which shows that interface stretching is correlated with the residence time distribution.

Appendix 1: Vortex Pair in a Wavy-Wall Channel

We show that the particle motion given by (2.3) and (2.5) approximates the motion in the vicinity of a vortex pair moving in a wavy-wall channel. Consider the following solution to the Euler equations, given by the streamfunction of a vortex pair, Ψ_v, plus the streamfunction of a potential flow:

$$\Psi = \Psi_v + \Psi_{pot} \tag{A1.1a}$$

where

$$\Psi_v = -\frac{\Gamma}{4\pi}\log\frac{(x-x_v)^2+(y-y_v)^2}{(x-x_v)^2+(y+y_v)^2} \tag{A1.1b}$$

and

$$\Psi_{pot} = (V+\varepsilon V_1(\varepsilon))y - \frac{\varepsilon}{k^2}\cos(kx)\sinh(ky) \tag{A1.1c}$$

Here $\pm\Gamma$ are the circulations of the vortices whose positions are $(x_v(t), \pm y_v(t))$, $V+\varepsilon V_1(\varepsilon)$ the average fluid velocity in the channel far away from the vortex pair and $\varepsilon V_1(\varepsilon)$ is defined such that the average velocity of the vortex pair is independent of ε (see below). The vortices move with the fluid velocity given by

$$\frac{dx}{dt} = \frac{\partial\Psi}{\partial y} \qquad \frac{dy}{dt} = -\frac{\partial\Psi}{\partial x} \tag{A1.2}$$

For $\varepsilon = 0$, we have

$$\begin{aligned} x_v(t) &= (V+\frac{\Gamma}{4\pi d})t \\ y_v(t) &= d \end{aligned} \tag{A1.3}$$

Setting $\Psi = \Psi_{wall} = const$ in (A1.1a) and assuming that $\frac{y_v}{y_{wall}} \ll 1$ we find the equation for the wall boundary,

$$\begin{aligned} y &= y_{wall}(x) \\ &= \frac{\Psi_{wall}}{V} - \frac{\varepsilon V_1(0)\Psi_{wall}}{V^2} + \frac{\varepsilon}{k^2 V}\sinh(\frac{k\Psi_{wall}}{V})\cos(kx) + O(\varepsilon^2) + O(\frac{y_v}{y_{wall}}) \end{aligned} \tag{A1.4}$$

confirming that equations (A1.1) represent flow in a wavy-wall channel where the walls are sufficiently far from the vortices.

Now we compute particle motion by (A1.2) and let $x = \tilde{x} + f(t)$, $x_v(t) = \tilde{x}_v(t) + f(t)$. If $k\tilde{x}_v \ll 1$ and we consider the flow field near the vortices with $ky \ll 1$, then we obtain the desired form:

$$\begin{aligned}
\frac{d\tilde{x}}{dt} &= -\frac{\Gamma}{2\pi}\left[\frac{y-y_v}{(\tilde{x}-\tilde{x}_v)^2+(y-y_v)^2} - \frac{y+y_v}{(\tilde{x}-\tilde{x}_v)^2+(y+y_v)^2}\right] \\
&\quad - V_v + \varepsilon\tilde{x}\sin(\omega t) + O(\varepsilon^2) \\
\frac{dy}{dt} &= \frac{\Gamma(\tilde{x}-\tilde{x}_v)}{2\pi}\left[\frac{1}{(\tilde{x}-\tilde{x}_v)^2+(y-y_v)^2} - \frac{1}{(\tilde{x}-\tilde{x}_v)^2+(y+y_v)^2}\right] \\
&\quad - \varepsilon y\sin(\omega t) + O(\varepsilon^2)
\end{aligned} \tag{A1.5}$$

if f(t) is the solution to

$$\frac{df}{dt} = -\frac{\varepsilon}{k}\cos(kf(t)) + V + \frac{\Gamma}{4\pi d} + \varepsilon V_1(\varepsilon) \tag{A1.6}$$

where $V_1(\varepsilon)$ is defined such that

$$f(t) = (V + \frac{\Gamma}{4\pi d})t + \varepsilon g(t,\varepsilon) \tag{A1.7}$$

where g is periodic in t. We also have that

$$\omega = k(V + \frac{\Gamma}{4\pi d}) \tag{A1.8}$$

and

$$V_v = \frac{\Gamma}{4\pi d} - \varepsilon V_1(\varepsilon) \tag{A1.9}$$

Appendix 2: Expansion of the Equations of Motion

The nondimensional equations of motion (2.3) have the following expansion in ε:

$$\begin{aligned} \frac{dx}{dt} &= f_1(x,y) + \varepsilon g_1(x,y,t/\gamma;\gamma) + O(\varepsilon^2) \\ \frac{dy}{dt} &= f_2(x,y) + \varepsilon g_2(x,y,t/\gamma;\gamma) + O(\varepsilon^2) \end{aligned} \tag{A2.1}$$

where the f_i are given by:

$$\begin{aligned} f_1 &= -\frac{y-1}{I_-} + \frac{y+1}{I_+} - \frac{1}{2} \\ f_2 &= x\left[\frac{1}{I_-} - \frac{1}{I_+}\right] \end{aligned} \tag{A2.2}$$

and the g_i are given by:

$$\begin{aligned} g_1 = [\cos(t/\gamma) - 1]&\left\{\frac{1}{I_-} + \frac{1}{I_+} - \frac{2(y-1)^2}{I_-^2} - \frac{2(y+1)^2}{I_+^2}\right\} + \\ &(x/\gamma)\sin(t/\gamma)\left\{\gamma^2\left[\frac{y-1}{I_-^2} - \frac{y+1}{I_+^2}\right] + 1\right\} - \frac{1}{2} \\ g_2 = 2x[\cos(t/\gamma) - 1]&\left\{\frac{y-1}{I_-^2} + \frac{y+1}{I_+^2}\right\} + \\ &(1/\gamma)sin(t/\gamma)\left\{\frac{\gamma^2}{2}\left[\frac{1}{I_-} - \frac{1}{I_+}\right] - x^2\gamma^2\left[\frac{1}{I_-^2} - \frac{1}{I_+^2}\right] - y\right\} \end{aligned} \tag{A2.3}$$

The definitions of $I_\pm$ are

$$I_\pm = x^2 + (y \pm 1)^2 \tag{A2.4}$$

Appendix 3: The Melnikov Function

In this appendix, we want to discuss some aspects of the Melnikov Function. Specifically, how it arises and what it measures. Recall that the perturbed velocity field can be written in the form

$$\begin{aligned} \dot{x} &= f_1(x,y) + \varepsilon g_1(x,y,\theta;\gamma) + O(\varepsilon^2) \\ \dot{y} &= f_2(x,y) + \varepsilon g_2(x,y,\theta,\gamma) + O(\varepsilon^2) \\ \dot{\theta} &= 1/\gamma \end{aligned} \tag{A3.1}$$

As a convenient shorthand notation we will often write (A3.1) in the following vector form

$$\begin{aligned} \dot{q} &= f(q) + \varepsilon g(q,\theta;\gamma) + O(\varepsilon^2) \\ \dot{\theta} &= 1/\gamma \end{aligned} \tag{A3.2}$$

where $q = (x,y)$, $f = (f_1, f_2)$, and $g = (g_1, g_2)$.

In each case the unperturbed velocity field is obtained by taking $\varepsilon = 0$ in (A3.1) and (A3.2). We study the two dimensional Poincaré map T obtained from the solutions of (A3.2) which is defined as follows:

$$\begin{aligned} T &: \Sigma \to \Sigma \\ (x(0), y(0)) &\mapsto (x(2\pi\gamma), y(2\pi\gamma)). \end{aligned} \tag{A3.3}$$

Recall that the Poincaré map obtained from the unperturbed velocity field has saddle points at p_+ and p_- which are connected to each other by the three heteroclinic orbits Ψ_u , Ψ_0 , and Ψ_l (see Figure 2.1). As noted earlier, by symmetry of the unperturbed flow Ψ_0 remains unbroken under the external strain. We use the Melnikov function to determine the behavior of Ψ_u and Ψ_l . Since the perturbed velocity field is symmetric about the x-axis, for definiteness, we will only draw pictures of the upper half plane in our development of the Melnikov function.

The construction of the Melnikov function consists of four steps:

1. Develop a parametrization of the unperturbed heteroclinic orbit in the Poincaré section.
2. Define a moving coordinate system along the unperturbed heteroclinic orbit in the Poincaré Section.

3. Define the distance between $W^s_{+,\varepsilon}$ and $W^u_{-,\varepsilon}$ in the moving coordinate system at points along the unperturbed heteroclinic orbit.
4. Utilize Melnikov's trick to develop a computable form for the geometrically defined distance between $W^s_{+,\varepsilon}$ and $W^u_{-,\varepsilon}$ of the points along the unperturbed heteroclinic orbit.

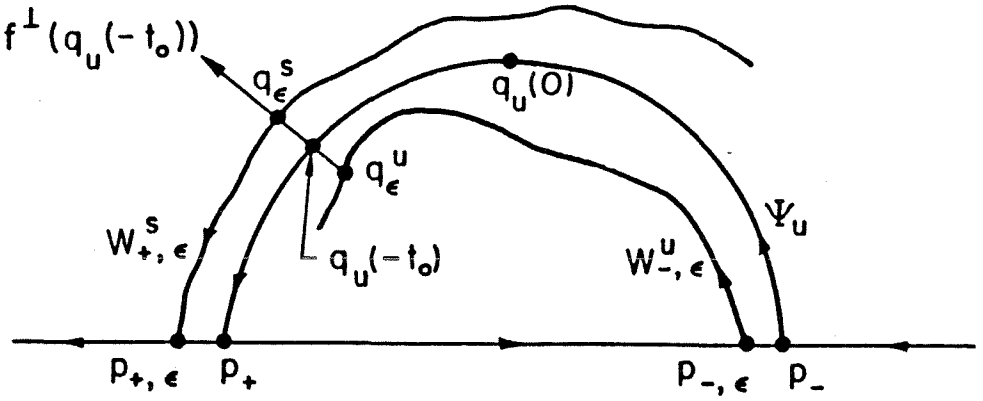

Figure A3.1. The Geometry of the Distance between $W^s_{+,\varepsilon}$ and $W^u_{-,\varepsilon}$.

We begin with Step 1.

Step 1: Let $q_u(t)$ denote a heteroclinic trajectory of the unperturbed velocity field which lies in Ψ_u. Then since the unperturbed velocity field is not time dependent (i.e., it is autonomous) $q_u(t-t_0)$ is also a heteroclinic trajectory of the unperturbed velocity field which lies in Ψ_u for any $t_0 \in R$ (see Arnold [1973] for a proof of this fact). Thus $q_u(-t_0)$, $t_0 \in R$ provides a parametrization of Ψ_u where t_0 is the unique time that it takes for a fluid particle on Ψ_u to flow to $q_u(0)$.

Step 2: The vector $f^{\perp}(q_u(-t_0)) = (-f_2(q_u(-t_0)), f_1(q_u(-t_0))$ is perpendicular to Ψ_u at each point $q_u(-t_0)$ on Ψ_u. Thus varying t_0 will serve to move $f^{\perp}(q_u(-t_0))$ along Ψ_u and the distance between the manifolds $W^s_{+,\varepsilon}$ and $W^u_{-,\varepsilon}$ will be measured along $f^{\perp}(q_u(-t_0))$.

Step 3: At $\varepsilon = 0$, W^s_+ and W^s_- intersect $f^{\perp}(q_u(-t_0))$ transversely at each $q_u(-t_0) \in \Psi_u$ (see Arnold [1982] for a definition of the transversal intersection of two manifolds). The intersections are preserved under perturbations so that for ε sufficiently

small $W^s_{+,\varepsilon}$ and $W^u_{-,\varepsilon}$ intersect $f^\perp(q_u(-t_0))$ transversely in the points q^s_ε and q^u_ε. Thus we define the *distance between* $W^s_{+,\varepsilon}$ *and* $W^u_{-,\varepsilon}$ *at the point* $q_u(-t_0)$ *to be*

$$distance = |q^u_\varepsilon - q^s_\varepsilon| \tag{A3.4}$$

see Figure A3.1.

The problem with this definition of the distance is that is does not lend itself to an expression which can easily be computed without solving explicitly for fluid particle motions of the perturbed velocity field; a task which would be quite formidable. However following Melnikov [1963], we define the following "signed" distance measurement

$$d(t_0,\varepsilon) = \frac{f^\perp(q^u(-t_0))\cdot(q^u_\varepsilon - q^s_\varepsilon)}{||f(q^u(-t_0))||} \tag{A3.5}$$

where "$\cdot$" denotes the usual vector dot product. It should be clear that by the choice of q^u_ε and q^s_ε that $d(t_0,\varepsilon) = 0$ if and only if $q^u_\varepsilon = q^s_\varepsilon$. Now were $W^s_{+,\varepsilon}$ and $W^u_{-,\varepsilon}$ vary differentiably with respect to parameters (Fenichel [1971], Hirsch, Pugh, and Shub [1977]) so we can Taylor expand (A3.5) about $\varepsilon = 0$ to obtain

$$d(t_0,\varepsilon) = \varepsilon\frac{f^\perp(q_u(-t_0))\cdot(\frac{\partial q^u}{\partial\varepsilon}\Big|_{\varepsilon=0} - \frac{\partial q^s}{\partial\varepsilon}\Big|_{\varepsilon=0})}{||f(q_u(-t_0))||} + O(\varepsilon^2) \tag{A3.6}$$

where we have used the fact that $q^u_0 = q^s_0$.

The *Melnikov function*, denoted $M(t_0)$, is defined to be:

$$M(t_0) = f^\perp(q_u(-t_0))\cdot(\frac{\partial q^u_\varepsilon}{\partial\varepsilon}\Big|_{\varepsilon=0} - \frac{\partial q^s_\varepsilon}{\partial\varepsilon}\Big|_{\varepsilon=0}) \tag{A3.7}$$

and is (up to the normalization factor $||f(q_u(-t_0))||^{-1}$) the leading order term in the Taylor series expansion for the distance between $W^s_{+,\varepsilon}$ and $W^u_{-,\varepsilon}$ at the point $q_u(-t_0)$.

Step 4. Melnikov [1963] was able to derive an expression for (A3.7) without explicitly computing particle paths of the perturbed velocity field. His procedure consisted of the following steps:

a). Prove that the particle paths of the perturbed velocity field through the points q^u_ε and q^s_ε exist on the time intervals $(-\infty, 0]$ and $[0,\infty)$, respectively.

b). Using a) along with the first variational equation for solutions through q_ε^u and q_ε^s (i.e. regular perturbation theory) derive a linear first order ordinary differential equation for the time dependent Melnikov function

$$M(t,t_0) = f^\perp(q_u(t-t_0)) \cdot \left(\frac{\partial q_\varepsilon^u(t)}{\partial \varepsilon}\Big|_{\varepsilon=0} - \frac{\partial q_\varepsilon^s(t)}{\partial \varepsilon}\Big|_{\varepsilon=0}\right) \qquad (A3.8)$$

where $q_\varepsilon^u(t)$ and $q_\varepsilon^s(t)$ are particle paths of the perturbed velocity field satisfying $q_\varepsilon^u(0) = q_\varepsilon^u$ and $q_\varepsilon^s(0) = q_\varepsilon^s$, respectively. Thus $M(0,t_0) \equiv M(t_0)$.

c). Solve the linear first order differential equation for $M(t,t_0)$ and obtain the Melnikov function by evaluating at $t = 0$. In the process boundary conditions for the solution at $\pm\infty$ are imposed which were the reason for needing the existence proof of particle paths on semi-infinite time intervals as described in a).

For the full details of these steps see Guckenheimer and Holmes [1983] or Wiggins [1988]. Finally, one obtains the following form for the Melnikov function.

$$M(t_0) = \int_{-\infty}^{\infty} [f_1(q_u(t))g_2(q_u(t), t+t_0) - f_2(q_u(t))g_1(q_u(t), t+t_0)]\, dt \qquad (A3.9)$$

and we have the following key theorem.

Theorem A3.1. Suppose there exists $t_0 = \bar{t}_0$ such that

1) $M(\bar{t}_0) = 0$

2) $\frac{\partial M}{\partial t_0}(\bar{t}_0) \neq 0$

Then $W_{+,\varepsilon}^s$ and $W_{-,\varepsilon}^u$ intersect transversely near $q_u(-\bar{t}_0)$. If $M(t_0)$ is bounded away from zero for all t_0, then $W_{+,\varepsilon}^s$ and $W_{-,\varepsilon}^u$ are bounded away from each other.

Proof. See Guckenheimer and Holmes [1983] or Wiggins [1988].

Thus we can determine whether or not $W_{+,\varepsilon}^s$ and $W_{-,\varepsilon}^u$ intersect without solving for fluid particle motions of the perturbed velocity field.

We now want to point out two properties of the Melnikov function which are important.

1. *Zero's of $M(t_0)$ Correspond to Primary Intersection Points*

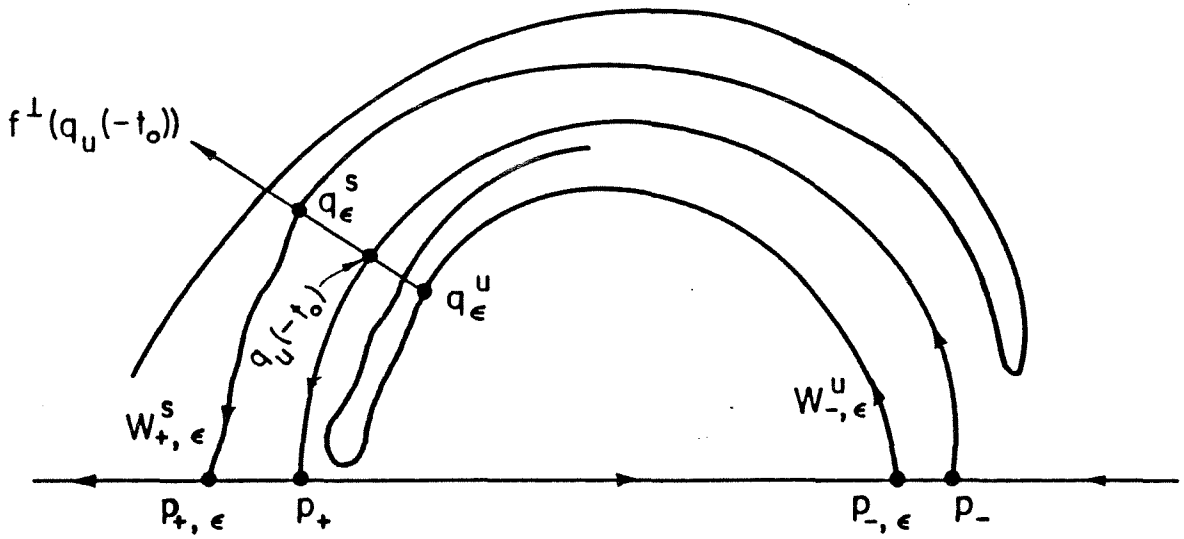

Figure A3.2. Intersection of the Manifolds with $f^{\perp}(q_u(-t_0))$.

The Melnikov function is a first order measure of the distance between $W^s_{+,\varepsilon}$ and $W^u_{-,\varepsilon}$ along the line $f^{\perp}(q_u(-t^0))$. However, it is possible that $W^s_{+,\varepsilon}$ and $W^u_{-,\varepsilon}$ may intersect $f^{\perp}(q_u(-t_0))$ many times as depicted in Figure A3.2. The question arises of which two points on $W^s_{+,\varepsilon} \cap f^{\perp}(q_u(-t_0))$ and $W^u_{-,\varepsilon} \cap f^{\perp}(q_u(-t_0))$ is the distance being measured. The answer to this question comes from the validity of the regular perturbation theory which was used to obtain a computable expression for the Melnikov function (step 4). The fact that we can approximate fluid particle motions of the perturbed velocity field uniformly only on semi-infinite time intervals coupled with the geometry of the time dependent Melnikov function implies that the Melnikov function is a measurement between points in $W^s_{+,\varepsilon}$ and $W^u_{-,\varepsilon}$ along $f^{\perp}(q_u(-t^0))$ which are "closest" to $p_{+,\varepsilon}$ and $p_{-,\varepsilon}$, respectively, in the sense of elapsed time of motion along $W^s_{+,\varepsilon}$ and $W^u_{-,\varepsilon}$. These points are denoted $\overline{q}^s_\varepsilon$ and $\overline{q}^u_\varepsilon$ in Figure A3.2. From definition 5.1, it follows that $\overline{q}^s_\varepsilon$ and $\overline{q}^u_\varepsilon$ are primary intersection points, for more details see Wiggins [1988].

2. *The Relative Displacement of $W^s_{+,\varepsilon}$ and $W^u_{-,\varepsilon}$*

Since transport in the mixing region is governed by $W^s_{+,\varepsilon}$ and $W^u_{-,\varepsilon}$ it is useful to know their relative positions and, because the Melnikov function is a signed distance measurement it contains this information. From the definition of the distance

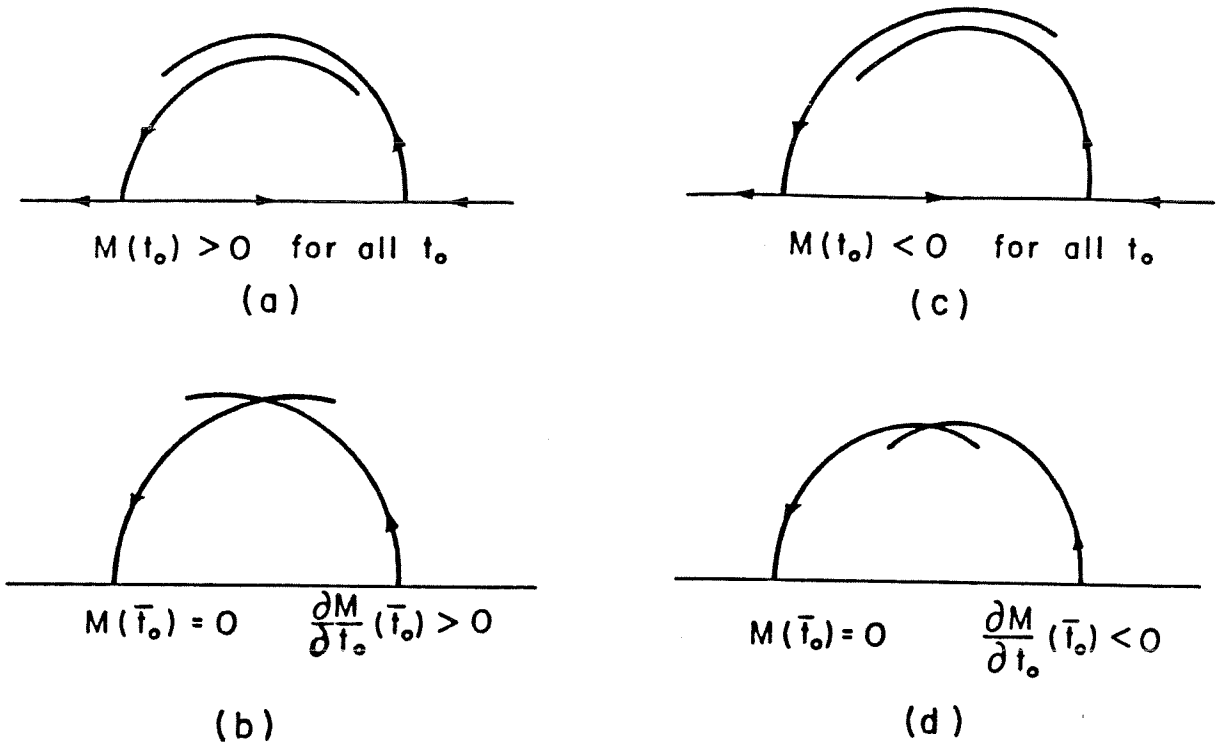

Figure A3.3. The Melnikov Function and the Relative Orientations of the Manifolds.

between $W^s_{+,\epsilon}$ and $W^u_{-,\epsilon}$ given in (A3.5), it is simple to show that the geometry of the manifolds shown in Figure A3.3 holds. For the OVP flow the Melnikov function is given by equation 4.3 and Figures 4.3 and 4.4 confirm the relation between the Melnikov function and the relative positions of the stable and unstable manifolds for this flow.

3. *Periodicity of* $M(t_0)$

The Melnikov function is a periodic function of t_0 having the same period as the external strain field (see Guckenheimer and Holmes [1983]). This is an indication that one heteroclinic point implies the existence of a countable infinity of heteroclinic points.

Appendix 4: The Melnikov Function and Lobe Motion

We now give the proof of Theorem 5.1 which is restated below:

Theorem 5.1. Suppose $M(t_0)$ has 2n simple zeros in one period τ. Then

1) $T(E_i) = E_{i+n}$

2) $T(D_i) = D_{i+n}$

Proof: From Appendix 3, simple zeros of the Melnikov function correspond to pip's. We denote the 2n zeros of $M(t_0)$ in one period as follows:

$$q_i^E < q_i^D < q_{i+1}^E < \cdots < q_{i+n-1}^E < q_{i+n-1}^D$$

where the notation and ordering (see definition 5.3) are chosen such that E_{i+k} is formed by q_{i+k}^E and q_{i+k}^D and D_{i+k} is formed by q_{i+k}^D and q_{i+k+1}^E for $k = 1, \ldots, n-1$.

Now by orientation preservation pip's maintain their relative ordering along $W_{-,\varepsilon}^u$ under iteration by T and because the velocity field (and hence the Melnikov function) is periodic in time with period τ we have:

$$T(q_i^E) = q_{i+n}^E$$

and

$$T(q_i^D) = q_{i+n}^D$$

Then by definition it follows that

$$T(E_i) = E_{i+n}$$

and

$$T(D_i) = D_{i+n}$$

□.

Appendix 5-Proofs of Lemmas 8.1 and 8.2

lemma 8.1: If $p \in \cup_{k=-\infty}^{\infty} D_k$ then for some $t_0 > (t_{esc} + t_{ent})$

1) $y(t) = O(\varepsilon)$

for $t > t_0$

2) $x(t) = -1/2t + O(\varepsilon t, \ln t)$

Proof: We begin with the proof 1). With no loss of generality, by taking an appropriate iterate T^i we can assume that $p \in D_l$, $l > 0$.

Note that for all γ, $T^i D_1 = D_{i+1}$, $i \geq 0$ is in the left upper quarter plane, meaning that $p(t_{esc}+t_{ent}) \in D_l$, $l > 0$ implies that $x(t) < 0$, $y(t) > 0$ for $t > t_{esc}+t_{ent}$, where $p = (x, y)$. This implies, by equation (A2.2b) that $f_2(p(t)) < 0$ for all $t > t_{esc}+t_{ent}$, and therefore that y is strictly decreasing as long as $|f_2| > \varepsilon|g_2|$, or in other words, as long as $f_2 = 0(1)$. From equation (A2.2b), we find that $f_2(p) = O(\varepsilon)$ in one of two cases:

1. If $y = O(\varepsilon)$ and $x = O(1)$
2. If $x = O(\varepsilon)$ and $y = O(1)$

The first case is what we wanted to demonstrate. The second case can be eliminated by the following argument. Since $p(t_{esc} + t_{ent}) \in D_l, l > 0$ and since for all γ there exists $k(\gamma)$ such that $p(t') = p(t_{esc} + t_{ent} + 2\pi k(\gamma)\gamma) \in T^{k(\gamma)} D_l$ implies $x < -\sqrt{3}$ and therefore $x(t') \neq O(\varepsilon)$ one can disregard this case by considering $p(t')$ instead of $p(t_{esc} + t_{ent})$. Thus we have proven the first part of the lemma, namely that $y = O(\varepsilon)$.

To prove part 2), we use the fact that $y = O(\varepsilon)$ for $t > t_0$, and linearize equation (A2.1) about y=0 to obtain

$$\dot{x} = -1/2 + \frac{2}{x^2 + 1} + \frac{\varepsilon x}{\gamma} \sin \frac{t}{\gamma} - \frac{\varepsilon}{2} + O(\varepsilon^2) \qquad (A5.1)$$

Let

$$x(t) = x_0(t) + \varepsilon x_1(t) + O(\varepsilon^2) \qquad (A5.2)$$

where $x_0(t)$ is the solution of (A5.1) with $\varepsilon = 0$ and the initial condition $x_0(0) = -\sqrt{3} - \tilde{x}_0$, $\tilde{x}_0 > 0$. Integrating equation A5.1 for $\varepsilon = 0$ we find:

$$x_0(t) = -1/2t - (\sqrt{3} + \tilde{x}_0) - \frac{2}{\sqrt{3}} \ln \frac{x_0(t)^2 - 3}{\tilde{x}_0(\tilde{x}_0 + 2\sqrt{3})} \qquad (A5.3)$$

Therefore, for large t the dominant balance is

$$x_0(t) = -1/2t + O(\ln t) \qquad (A5.4)$$

Substituting A5.2 in A5.1 we obtain the following equation for $x_1(t)$:

$$\dot{x}_1 = -\frac{4}{(x_0^2+1)^2} x_1 + \frac{x_0}{\gamma} \sin\frac{t}{\gamma} - \frac{1}{2}, \qquad x_1(0) = 0$$

with the solution:

$$x_1(t) = e^{-\int_0^t \frac{4}{(x_0(s)^2+1)^2} ds} \int_0^t (\frac{x_0(s)}{\gamma} \sin\frac{s}{\gamma} - \frac{1}{2}) e^{\int_0^s \frac{4}{(x_0(\xi)^2+1)^2} d\xi} ds \qquad (A5.5)$$

Substituting A5.4 in A5.5 and expanding the exponents for $t \gg 1$ we get:

$$x_1(t) = -\frac{1}{2} t(1 - \cos\frac{t}{\gamma}) + O(\ln t, S_i(t)) \qquad (A5.6)$$

where $S_i(t)$ is the the sine integral $S_i(t) = \int_0^t \frac{\sin s}{s} ds$.

Substituting A5.4 and A5.5 in A5.2 we get

$$x(t) = -\frac{1}{2}t - \frac{\varepsilon}{2}\gamma t(1 - \cos\frac{t}{\gamma}) + O(\ln t) = -\frac{1}{2}t + O(\varepsilon t, \ln t) \qquad (A5.7)$$

□.

We now discuss the dependence of the time t_0, described in Lemma 8.1, on the initial condition p. Schematically t_0 can be decomposed to four parts $t_0 = t_{ent} + t_{esc} + t_y + t_x$.

(1) $t_{ent} + t_{esc}$ is the time it takes p to enter and escape region A and is determined by the lobe which p belongs to at $t = 0$:

if $p \in D_{-k}$, $k > 0$ then $t_{ent} + t_{esc} = 2k\pi\gamma$.

(2) t_y is the time it takes the y component of $p(t_{esc}+t_{ent})$ to become $O(\varepsilon)$. This motion is governed by the unperturbed velocity field and happens on a relative rapid time - typically $t_y \sim 10$ (the number of cycles, N_y, depend on γ according to $N_y = t_y/2\pi\gamma$)

(3) t_x is the time it takes the x component of $p(t_{esc}+t_{ent}+t_y)$ to leave the fix point neighborhood so that the relation (A5.4) holds. Taking $x(t_{esc}+t_{ent}+t_y) = x_0(0)$ in A5.3 we see that t_y depends on how close p is to the stable manifold. Specifically, if $\tilde{x}_0 \ll 1$ so that for some $T \gg 1$, $x(t_{esc}+t_{ent}+t_y) = -\sqrt{3} - e^{-\frac{\sqrt{3}}{4}T}$, ($\frac{\sqrt{3}}{4}$ is the eigenvalue of the fixed point), the relation A5.4 is valid only when

$$\frac{1}{2}t_x \gg \frac{2}{\sqrt{3}}\ln(\frac{t_x^2}{y}-3) - \frac{2}{\sqrt{3}}\ln(e^{-\frac{\sqrt{3}}{4}T})(2\sqrt{3}+e^{-\frac{\sqrt{3}}{4}T})$$

which implies

$$t_x(1-\frac{8}{\sqrt{3}}\frac{\ln t_x}{t_x}) \gg T \qquad \text{if } t_x^2 \gg 12, \quad T \gg 1$$

therefore if $T \gg 1$, t_x must satisfy the following conditions:

$$t_x \gg T, \quad t_x \gg \sqrt{12}, \quad t_x \gg 1 \quad s.t. \quad \ln t_x \ll t_x$$

Note however that the region for which $p(t) \in T^k D_1$ and $x(t)+\sqrt{3} \ll 1$ (i.e. $T \gg 1$) is very small since the height of $T^k D_1$ decays exponentially.

lemma 8.2: If $p \in \cup_{k=-\infty}^{\infty} D_k$ then:

$$\lambda(p,m,t) = \chi(p,m,t) + O(\frac{1}{t^2}) \quad \text{for } t > t_0.$$

Proof:

We use the approximations found in lemma 8.1 for the above initial conditions to estimate the matrix $DF(p(t),t)$ from equation (8.2), resulting in an asymptotic solution for this equation and therefore for λ.

Examining the equations of motion we get the following estimates for $DF(x(t),t) = Df + \varepsilon Dg$; using $|x| \gg 1, |y| \ll 1$ it follows from equations (A2.1-4) that:

$$Df = \begin{pmatrix} a & b \\ b & -a \end{pmatrix}$$

where

$$a = \frac{\partial f_1}{\partial x} = 2x\left[\frac{y-1}{I_-^2} - \frac{y+1}{I_+^2}\right] = \frac{2}{x^3}\left\{\frac{y-1}{(1+(\frac{y-1}{x})^2)^2} - \frac{y+1}{(1+(\frac{y+1}{x})^2)^2}\right\}$$

$$= \frac{2}{x^3}\Bigg\{(y-1)\left(1-2(\frac{y-1}{x})^2 + O((\frac{y-1}{x})^4)\right) -$$

$$(y+1)\left(1-2(\frac{y+1}{x})^2 + O((\frac{y+1}{x})^4)\right)\Bigg\}$$

$$= -\frac{4}{x^3} + O(\frac{1}{x^5})$$

$$b = \frac{\partial f_1}{\partial y} = \frac{\partial f_2}{\partial x} = \frac{1}{I_-} - \frac{1}{I_+} + 2x^2(-\frac{1}{I_-^2} + \frac{1}{I_+^2})$$

$$= \frac{1}{x^2}\left(-(\frac{y-1}{x})^2 + (\frac{y+1}{x})^2 + O(\frac{1}{x^4})\right)$$

$$+ \frac{2}{x^2}\left(-(1-2(\frac{y-1}{x})^2 + O(\frac{1}{x^4})) + (1-2(\frac{y+1}{x})^2 + O(\frac{1}{x^4})\right)$$

$$= -\frac{12y}{x^4} + O(\frac{1}{x^6})$$

and that

$$Dg = \begin{pmatrix} \frac{1}{\gamma}\sin\frac{t}{\gamma} + O(\frac{1}{x^3}) & O(\frac{1}{x^3}) \\ O(\frac{1}{x^3}) & -\frac{1}{\gamma}\sin\frac{t}{\gamma} + O(\frac{1}{x^3}) \end{pmatrix}$$

and therefore

$$DF(x(t),t) = \begin{pmatrix} \frac{\varepsilon}{\gamma}\sin\frac{t}{\gamma} - \frac{4}{x^3} & 0 \\ 0 & -\frac{\varepsilon}{\gamma}\sin\frac{t}{\gamma} + \frac{4}{x^3} \end{pmatrix} + O(\frac{\varepsilon}{x^3}, \frac{1}{x^5}, \frac{y}{x^4})$$

Substituting the approximated solutions $x(t) \sim -1/2t$, $y(t) \sim 0$ we obtain that for large t

$$DF(x(t),t) = \begin{pmatrix} \varepsilon\sin\frac{t}{\gamma} + \frac{32}{t^3} & 0 \\ 0 & -\varepsilon\sin\frac{t}{\gamma} - \frac{32}{t^3} \end{pmatrix} + O(\frac{\ln t}{t^4}, \frac{\varepsilon}{t^3}, \frac{1}{t^5})$$

which using equation(8.2) implies that

$$m(t) = \begin{pmatrix} m_0 e^{-\varepsilon\cos\frac{t}{\gamma} - \frac{16}{t^2}} \\ m_1 e^{\varepsilon\cos\frac{t}{\gamma} + \frac{16}{t^2}} \end{pmatrix} + O(\frac{\ln t}{t^3}, \frac{\varepsilon}{t^2}) = \begin{pmatrix} m_o e^{-\varepsilon\cos\frac{t}{\gamma}} \\ m_1 e^{\varepsilon\cos\frac{t}{\gamma}} \end{pmatrix} + O(\frac{\ln t}{t^3}, \frac{1}{t^2})$$

and therefore

$$\lambda(p,m,t) = \frac{|m(t)|}{|m(o)|} = \chi(p,m,t) + O(\frac{1}{t^2})$$

Where $\chi(p,m,t)$ is a periodic function of t with period $2\pi\gamma$.

References

Arnold, V. I. 1965 Sur La Topologie Des Ecoulements Stationnaires De Fluides Parfaits, *C.R. Acad. Sci. Paris*, **261**, 17.

Arnold, V. I. 1973 *Ordinary Differential Equations*, M.I.T. Press, Cambridge, MA.

Arnold, V. I. 1978 *Mathematical Methods of Classical Mechanics*, Springer-Verlag, New York.

Arnold, V. I. and Avez, A. 1968 *Ergodic Problems of Classical Mechanics*, W.A. Benjamin, New York.

Arnold, V. I. and Korkina, E. I. 1983 The Growth of a Magnetic Field in a Steady Compressible Flow, *Vestn. Mosk. Univ. Mat. Mekh.*, **3**, 43 (in Russian).

Aref, H. 1983 Integrable, Chaotic, and Turbulent Vortex Motion in Two Dimensional Flows, *Ann. Rev. Fluid Mech.*, **15**, 345.

Aref, H. 1984 Stirring by Chaotic Advection, *J. Fluid Mech.*, **143**, 1.

Aref, H. and Balachandar S. 1986 Chaotic Advection in a Stokes Flow, *Phys. Fluids*, **29**, 3515.

Arter, W. 1983 Ergodic Streamlines in Steady Convection, *Phys. Lett.*, No. 97A, 171.

Aubry, S. and Le Daeron, P. R. 1983 The Discrete Frenkel-Kontorova Model and its Extensions. 1. Exact Results for the Ground States, *Physica 8D*, 381.

Benettin, G., Galgani, L., Giorgilli, A., Strelcyn, J. M. 1980 Lyapunov Characteristic Exponents for Smooth Dynamical Systems and for Hamiltonian Systems; A Method for Computing All of Them. Part I: Theory, Part 2: Numerical Application, *Meccanica*, **15**, 9.

Blackwelder and Kaplan 1976 On the Wall Structure of the Turbulent Boundary Layer, *J. Fluid Mech.*, **76**, 89.

Broadwell, J. E. 1987 A Model For Reactions In Turbulent Jets: Effects of Reynolds, Schmidt, and Damkohler Numbers, to appear in *Turbulent Reactive Flows. Vol. I. Structure: Diagnostic and Analysis*, Springer-Verlag Lectures in engineering.

Broomhead, D. S. and Ryrie, S. C. 1987 Particle Paths in Wavy Vortices, *Submitted to Nonlinearity.*

Chaiken, J., Chevray, R., Tabor, M., and Tan, Q. M. 1986 Experimental Study of Lagrangian Turbulence in Stokes Flow, *Proc. R. Soc. Lond. A*, **408**, 105.

Chella, R. and Ottino, J. M. 1984 Conversion and Selectivity Modifications Due to Mixing in Unpremixed Reactors, *Chem. Eng. Sci.*, **39**, 551.

Chella, R. and Ottino, J. M. 1985 Stretching in Some Classes of Fluid Motions and Asymptotic Flow Efficiencies as a Measure of Flow Classification, *Arch. Rat. Mech.*, **90**, 15.

Chien, W. -L, Rising III, H., and Ottino, J. M. 1986 Laminar and Chaotic Mixing in Several Cavity Flows, *J. Fluid Mech.*, **170**, 355.

Danckwerts, P. V. 1953 Continuous Flow Systems of Residence Times, *Chem. Eng. Sci.*, **2**, 1.

Deisler, R. J. and Kaneko, K. 1987 Velocity-Dependent Lyapunov Exponents as a Measure of Chaos, *Phys. Lett. A*, **19**, No. 8, 397.

Dimotakis, P. E. 1987 Turbulent Shear Layer Mixing with Fast Chemical Reactions, to appear in *J. Fluid Mech.*.

Dombre, T., Frisch, U., Greene, J. M., Henon, M., Mehr, A., and Soward, A. 1986 Chaotic Streamlines in the ABC Flows, *J. Fluid Mech.*, **167**, 353.

Feingold, M., Kadanoff L. P., and Piro O. 1988 Passive Scalars, 3D Volume Preserving Maps and Chaos, *To appear in J. Statis. Phys.*.

Fenichel, N. 1971 Persistence and Smoothness of Invariant Manifolds for Flows, *Indiana Univ. Math. J.*, **21**, 193.

Franjione, J. G. and Ottino, J. M. 1987 Feasibility of Numerical Tracking of Material Lines and Surfaces in Chaotic Flows, *Phys. Fluids*, **30**, No. 12, 3641.

Galloway, D. and Frisch, U. 1986 Dynamo Action in a Family of Flows with Chaotic Streamlines, *Geophys. Astrophys. Fluid Dynamics*, **36**, 53.

Glezer, A. and Coles, D. 1987 Private Communication.

Goldhirsch, I., Sulem, P. L., and Orzag, S. A. 1987 Stability and Lyapunov Stability of Dynamical Systems: A Different Approach and a Numerical Method, *Physica*, **27D**, 311.

Guckenheimer, J. and Holmes, P. 1983 *Non-Linear Oscillations, Dynamical Systems and Bifurcations of Vector Fields*, Springer-Verlag, New York.

Hama, F. R. 1962 Streaklines in a Perturbed Shear Flow, *Phys. Fluids*, **5**, No. 6, 644.

Hirsch, M. W., Pugh, C. C. and Shub, M. 1977 Invariant Manifolds in "*Springer Lecture Notes in Mathematics*", No. 583, Springer-Verlag, New York.

Holmes, P., Marsden, J. and Scheurle, J. 1987 Exponentially Small Splitting of Separatrices, Preprint.

Irwin, M. C. 1980 *Smooth Dynamical Systems*, Academic Press, New York.

Kerr, R. M. 1985 Higher-Order Derivative Correlations and the Alignment of Small-Scale Structures in Isotropic Numerical Turbulence, *J. Fluid Mech.*, **153**, 31.

Kerstein, A. R. and Ashurst W. T. 1984 Lognormality of Gradients of Diffusive Scalars in Homogeneous, Two Dimensional Mixing Systems, *Phys. Fluids*, **27**, No. 12, 2819.

Khakhar, D. V., Chella, R., and Ottino, J. M. 1984 Stretching, Chaotic Motion and Elongated Droplets in Time Dependent Flows, *Advances in Rheology*, **2**, Fluids, 81-88, B. Mena, A. Garcia-Rejon and C. Kangel - Naifel editors.

Khakhar, D. V., Rising, H. III and Ottino, J. M. 1986 Analysis of Chaotic Mixing in Two Model Systems, *J. Fluid Mech.*, **172**, 419.

Marble, F. E. 1985 Growth of a Diffusion Flame in the Field of a Vortex, *Recent Advances in the Aerospace Sciences*, pp. 395, C. Casci editor, Plenum Publishing.

Mather, J. N. 1984 Non-Existence of Invariant Circles, *Ergod. Theory Dyn. Syst.*, **4**, 301.

Melnikov, V. K. 1963 On the Stability of the Center for Time Periodic Perturbations, *Trans. Moscow Math. Soc.*, **12**, 1.

Moffatt, H. K. and Proctor, M. R. E. 1985 Topological Constraints Associated with Fast Dynamo Action, *J. Fluid Mech.*, **154**, 493.

Moser, J. 1973 *Stable and Random Motions in Dynamical Systems*, Princeton University Press, Princeton.

Oseledec, V. I. 1968 A Multiplicative Ergodic Theorem. Lyapunov Characteristic Numbers for Dynamical Systems, *Trudy Moskov. Mat. OBSC, TOM 19. Trans. Moscow Math. Soc.*, **19**, 197.

Ottino, J. M. 1982 Description of Mixing with Diffusion and Reaction in Terms of the Concept of Material Surfaces, *J. Fluid Mech.*, **114**, 83.

Ottino, J. M. and Chella, R. 1983 Laminar Mixing of Polymeric Liquids; Brief Review and Recent Theoretical Developments, *Polymer Engng. Sci.*, **23**, 357.

Ottino, J. M., Leong, C. W., Rising, H. and Swanson, P. D. 1988 Morphological Structures Produced by Mixing in Chaotic Flows, to appear in *Nature.*

Percival, I. C. 1980 Variational Principles for Invariant Tori and Cantori. *Air Conference Proc., Nonlinear Dynamics and the Beam-Beam Interaction, Amer. Inst. Phys.*, **57**, New York. Mouth M. and Herrera J. C. editors.

Pope, S. B. 1987 Turbulent Premixed Flames, *Ann. Rev. Fluid Mech.*, **19**, 237.

Ralph, M. E. 1986 Oscillatory Flows in Wavy-Walled Tubes, *J. Fluid Mech.*, **168**, 515.

Rising, H., Leong, K. and Ottino, J. M. 1987 Morphological Structures Produced by Mixing in Chaotic Flows, to appear in *Nature.*

Shariff, K. 1987 Private Communication.

Shariff, K., Leonard, A., Zabusky, N. J., and Ferziger, J. H. 1987 Acoustics and Dynamics of Coaxial Interacting Fundamental Aspects of Vortex Motion, Tokyo, Japan.

Sobey, I. J. 1985 Dispersion Caused by Separation during Oscillatory Flow through a Furrowed Channel, *Chem. Eng. Sci.*, **40**, 2129.

Suresh, A. 1985 Point Vortex Interactions, Ph. D thesis, Princeton University.

Wiggins, S. 1987 Chaos in the Quasiperiodically Forced Duffing Oscillator, *Phy. Lett.*, **124A**, 138.

Wiggins, S. 1988 *Global Bifurcations and Chaos - Analytical Methods* to appear in "Springer Applied Mathematics Series".

Wolf, A., Swift, S. B., Swinney, H. L., and Vastano, J. A. 1985 Determining Lyapunov Exponents from a Time Series, *Physica*, **16D**, 285.

Yamada, H. and Matsui, T. 1978 in *An Album of Fluid Motion*, pp. 46, The Parabolic Press, M. Van Dyke editor.

PART II: TRANSPORT IN TWO DIMENSIONAL MAPS

1. Introduction

The study of transport phenomena is important in a variety of diverse fields. Webster's New International dictionary defines the word transport as follows:

> *To convey; esp., to carry or convey from one place or station to another, as by boat or rail; to transfer; as to* transport *goods or troops.*

Thus in any physical situation where transport is of importance there are three points which first need to be clarified. In the context of the above definition they are:

1. The *mechanisms* for conveyance or transference.
2. The *places or stations* to and from which things are transported.
3. The *quantity* that is being conveyed or transferred.

In this paper we study transport in the two dimensional phase space of C^r diffeomorphisms ($r \geq 1$) of two manifolds. The *places or stations* to and from which things are transported will consist of regions of the phase space bounded by pieces of the stable and unstable manifolds of hyperbolic fixed points, the *mechanism* for transport will be the dynamics of the diffeomorphism in the heteroclinic and/or homoclinic tangles, and the *quantity* that is being transported will be area elements of the phase space.

As examples of how this framework might arise in applications we offer the following two situations. First, consider the simple pendulum. It is well known that the phase space of this system possesses a pair of homoclinic orbits which separate the librational motion of the pendulum from the rotational motion. When the system is subjected to a periodic excitation the homoclinic orbits break up and thus a mechanism is created whereby orbits may start out librating and subsequently make a transition to rotational motion (or vice versa). Through a canonical procedure (see Guckenheimer and Holmes [1983] or Wiggins [1988]) the study of this system can be reduced to the study of an associated two dimensional Poincaré map (see section 6) and therefore our methods can be brought to bear on this problem. In

particular, our techniques allow us to compute the probability of the system going from libration to rotation or vice-versa based on the geometry of the homoclinic tangle. This allows us to give a statistical description of the dynamics in a region of phase space where the dynamics is chaotic.

Another example where our methods have potentially far reaching applications is in the field of fluid mechanics. Let $v(x,t)$, $x \in R^2$, be a solution of the two dimensional Navier-Stokes equations which is periodic in time. Then the ordinary differential equation describing the motion of fluid particles in the flow is given by

$$\dot{x} = v(x,t)$$

As in the above example, the temporal periodicity allows us to reduce the study of this system to the study of an associated two dimensional Poincaré map where in this example the "phase space" is actually the physical space. As a result our methods can be utilized to study questions of mixing and transport in fluid dynamics in situations where it is the convective nature of the flow (and not molecular diffusion) that is influencing these questions, see Rom-Kedar et al. [1988].

Transport phenomena in two dimensional area preserving maps have been studied extensively in the last few years. After it had been recognized that the motion in these systems can be both regular and chaotic, extensive numerical experiments were performed to investigate the influence of the chaotic regions on the transport rates (Chirikov [1979], Karney [1983]). The main theme in these works was to quantify the change in the transport rates as a result of the destruction of KAM tori and the appearance of cantori as the parameters vary.

Bensimon and Kadanoff [1984] and Mackay et al.[1984] made the first analytical attempts to quantify these transport rates. Bensimon and Kadanoff showed that the flux rates between different regions separated by the stable and unstable manifolds of periodic orbits are related to the generating function of the map evaluated along orbits homoclinic to these orbits and Mackay et al. showed that the flux rates between different regions separated by cantori are related to the generating function of the map evaluated along orbits homoclinic to the cantorus. Subsequently,

Mackay et al. applied these ideas to resonance bands [1987] and continuous time systems [1986]. However their methods did not consider the entire geometry of the homoclinic orbits and therefore they were not able to compute transport rates for more than a few iterations exactly. Our work shows that a consideration of the global geometry of the homoclinic orbits is essential. Incorporating their ideas into our framework (when the diffeomorphism is also area preserving and a twist map) seems promising and is discussed in section 6.

A statistical approach to transport phenomena in area preserving maps, presented in detail in Lichtenberg and Lieberman [1983], attempts to quantify the transport rates by modeling the transport mechanisms by statistical processes such as a Markov process. This results in a diffusion equation for the density distribution in phase space. Based on the mechanism described by Bensimon and Kadanoff [1984] and Mackay et al. [1984], Meiss and Ott [1986] developed an approximate statistical model for transport based on a Markov tree. Our method could be used along similar lines to improve this model.

In this paper we concentrate on investigating the transport as governed by intersections of stable and unstable manifolds of hyperbolic fixed points of maps. Being invariant curves, these manifolds supply natural boundaries for regions in phase space. These regions may be the resonance bands of an area preserving map, but may also represent any other region with boundaries consisting of stable and unstable manifolds. Note that the study presented here is based on the geometry of the manifolds only and does not require the system to be near integrable or area preserving.

The observation that boundaries consisting of segments of stable and unstable manifolds allow transport across them in a very specific manner, via exchange of "lobes", was found by various people, see Bensimon and Kadanoff [1984] or Mackay et al. [1984] for this account. The new observation presented in this paper is that following the evolution of these lobes, and using the invariance of the manifolds in the process, supplies a method for computing the exact transport rates between regions for all times, both in area preserving and non area preserving C^r diffeomor-

phisms ($r \geq 1$) of two manifolds. This work suggests that the appropriate statistical model should be developed for the dispersion of only a few "lobes" in phase space, since all the transport rates are completely determined by the transport rates of these lobes.

The paper is organized as follows: in section 2 we state the necessary definitions and the general principles that are discussed throughout the paper, in section 3 we demonstrate these principles and compute transport quantities for three examples, in section 4 we state the precise assumptions and theorems for the transport rates in area preserving maps, in section 5 we show how these concepts are generalized to non area preserving maps, in section 6 we discuss some aspects of the application of the proposed methods for computing the transport rates and in section 7 we demonstrate the method by performing a numerical investigation of the transport rates for the periodically forced undamped Duffing equation.

2. General Principles

Consider a two dimensional phase space, on which an area and orientation preserving diffeomorphism F is defined (e.g. F is a Poincaré map of a time dependent flow). Let $p_i, i = 1,..,N$, denote all the hyperbolic fixed points of F with their associated $2N$ branches of stable and $2N$ branches of unstable manifolds. We denote the stable manifold of the hyperbolic fixed point p_i by $W^s_{p_i}$ and its unstable manifold by $W^u_{p_i}$ (note that each manifold consist of two branches. When a differentiation between these branches is needed we will label each branch). The phase space can be divided into disjoint regions, using pieces of the stable and unstable manifolds of hyperbolic fixed points. We investigate the transport between such regions, where the precise manner in which these regions are defined is discussed later. The mechanisms for transport between the regions are associated with the intersections of the stable and unstable manifolds and the tangling of the manifolds resulting from these intersections. Poincaré [1899] was the first to recognize that an intersection of the stable and unstable manifolds leads to a very complicated geometrical structures, structures which Easton [1985] investigated and tried to classify, with success for a special class of maps. We use the properties of the tangling to investigate the transport, borrowing some ideas from Easton notation for the geometrical structures involved in the tangling of the manifolds.

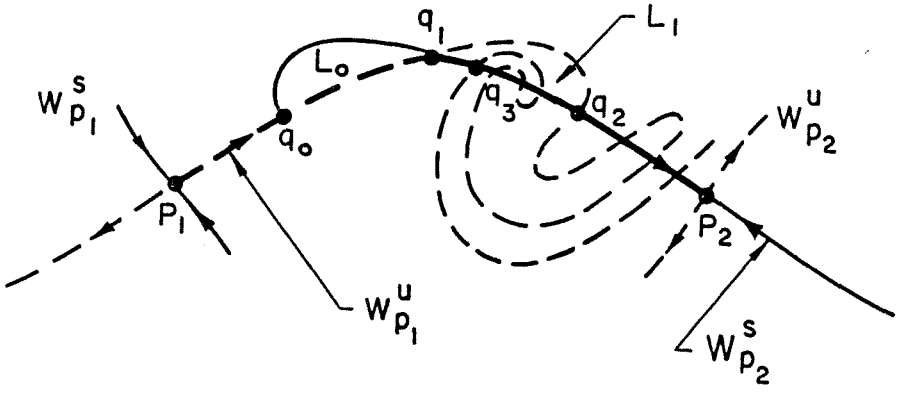

Figure 2.1 Definition of the Pip and the Lobe

q_0, q_1 and q_2 are pip's q_3 is not a pip. L_0 and L_1 are lobes.

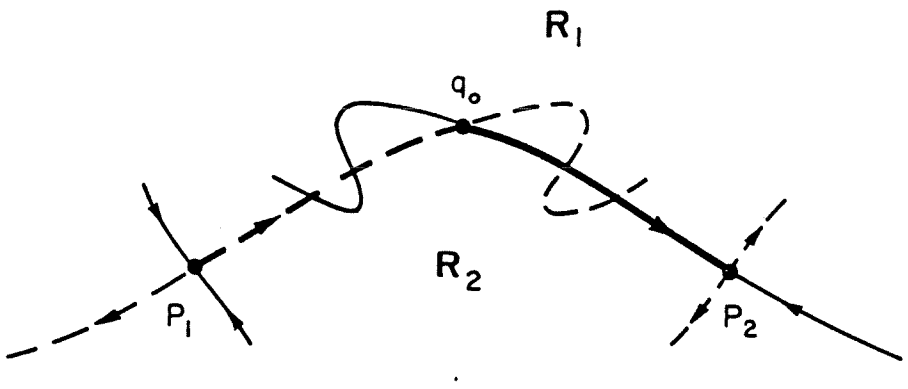

Figure 2.2 Transport across a Boundary

We start with a few definitions, then explain the mechanism for transport and the dynamics associated with the tangling, and then state a few properties of area and orientation preserving diffeomorphisms and their stable and unstable manifolds.

Definition 2.1 A point q_0 in phase space is called a **heteroclinic** point if it belongs to both a stable and an unstable manifold, namely $q_0 \in W^s_{p_i} \cap W^u_{p_j}$ for some p_i and p_j. The point q_0 is called **homoclinic** if $i = j$.

Definition 2.2 Consider a heteroclinic (or homoclinic) point $q_0 \in W^s_{p_i} \cap W^u_{p_j}$ and let $S[p_i, q_0]$ denote the segment of $W^s_{p_i}$ from p_i to q_0 and $U[p_j, q_0]$ denote the segment of $W^u_{p_j}$ from p_j to q_0. Then q_0 is called a **primary intersection point (pip)** if $S[p_i, q_0]$ and $U[p_j, q_0]$ intersect only in q_0 (and possibly at p_i if i = j). See Figure 2.1.

Definition 2.3 Let q_0 and q_1 be two adjacent pip's, i.e. there are no pip's on $U[q_0, q_1]$ and $S[q_0, q_1]$, the segments of $W^s_{p_i}$ and $W^u_{p_j}$ which connect q_0 and q_1. We refer to the region bounded by the segments $U[q_0, q_1]$ and $S[q_0, q_1]$ as a **lobe** . See Figure 2.1.

The Lobe Dynamics and the Transport Mechanism

The transport across a boundary which consists of a segment of a stable manifold and a segment of an unstable manifold, both segments starting at hyperbolic fixed points and ending at a common pip (see Figure 2.2), is governed by the motion of lobes, which in turn can be inferred by the motion of the pips defining them. We

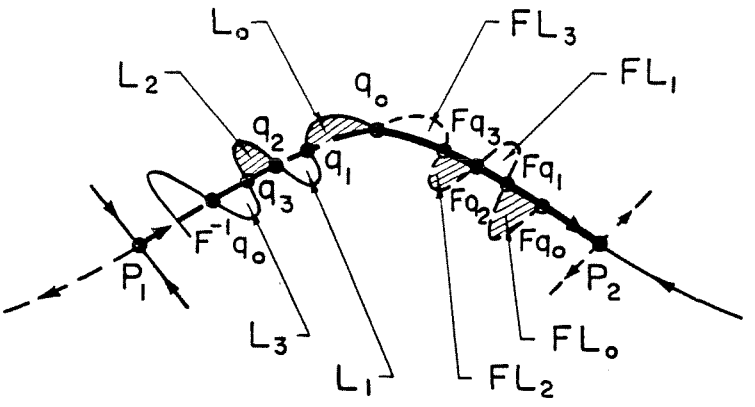

Figure 2.3 The Lobe Motion

therefore start with describing the dynamics associated with heteroclinic (homoclinic) points in general and pip's in particular and then show how this determines the lobe motion.

Note that the existence of a heteroclinic (homoclinic) point q_0 implies the existence of infinitely many heteroclinic (homoclinic) points; by the invariance of the manifolds all forward and backward iterations of q_0, $F^k q_0$, must stay on both the stable and the unstable manifolds, and therefore $F^k q_0$ are heteroclinic (homoclinic) points for all k. Moreover, by orientation preservation of F, if q_0 is a heteroclinic (homoclinic) point, the segments of the stable and unstable manifolds connecting q_0 and $F^{-1}q_0$ must intersect each other in an odd number of heteroclinic (homoclinic) points (see Abraham and Shaw [1982]). Now, let us consider the case were q_0 is a pip. It is easy to show that if q_0 is a pip so are $F^k q_0$ for all k (see Easton [1985]). By the previous statement, the segments of the manifolds connecting q_0 to $F^{-1}q_0$ intersect each other in an odd number of heteroclinic (homoclinic) points, of which $2m-1$ are pip's ($m \geq 1$). The $2m-1$ pip's, q_i, $i = 1,..2m-1$, together with q_0 and $F^{-1}q_0$ define $2m$ lobes, the motion of these allows transport across the boundary. Note that by orientation preservation of F, the interior of a closed curve is mapped to the interior of the curves image, and the ordering of the heteroclinic (homoclinic) points q_i along the curve is preserved; hence, the lobe L_i defined by the segments $S[q_i, q_{i+1}]$ and $U[q_i, q_{i+1}]$ (where $q_{2m} \equiv F^{-1}q_0$) is mapped to the lobe defined by $F(S[q_i, q_{i+1}])$ and $F(U[q_i, q_{i+1}])$, see Figure 2.3.

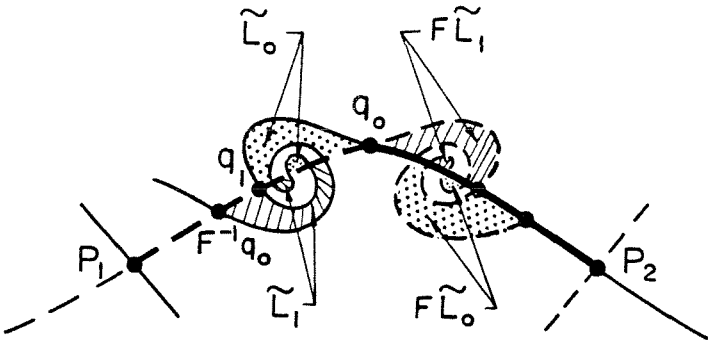

Figure 2.4 Redefinition of a Lobe

It is important to notice that a lobe is always mapped to a lobe, and that all the lobes and tangling associated with the pip q_0 are images or preimages of the L_i lobes, $i = 0, .., 2m-1$. In Figure 2.3 we draw a possible scenario in which $m = 2$ and there are only pip's on the segment connecting q_0 and Fq_0. Four lobes are created between q_0 and $F^{-1}q_0$ denoted by L_i, $i = 0, .., 3$. Under F, the L_0 and L_2 lobes are mapped from the region above the boundary $U[p_1, q_0] \cup S[p_2, q_0]$ to the region below it, while the L_1 and L_3 lobes are mapped from the lower region to the upper one. This is the mechanism for transport across the boundary! Note that the manifolds are stationary (they are invariant), hence on each iteration the same scenario occurs: L_0 and L_2 are mapped downward while L_1 and L_3 move upward. Therefore, the lobes which are mapped downward at iteration n are necessarily the $n-1$ preimages of L_0 and L_2.

Four remarks are now in order:

R1. With no loss of generality we can always assume that there is an exchange of exactly one lobe between neighboring regions (having a common boundary consisting of a segment of a stable and a segment of an unstable manifold starting at hyperbolic fixed points and ending at a common pip), since we can always define a generalized lobe which is the union of all the lobes moving from one region to the other under one iteration of the map.

R2. In practice the number of lobes crossing per iteration from one region to the other may be of interest. In previous work we have shown that when the splitting of the crossing of the manifolds is a result of a perturbation and Melnikov's technique

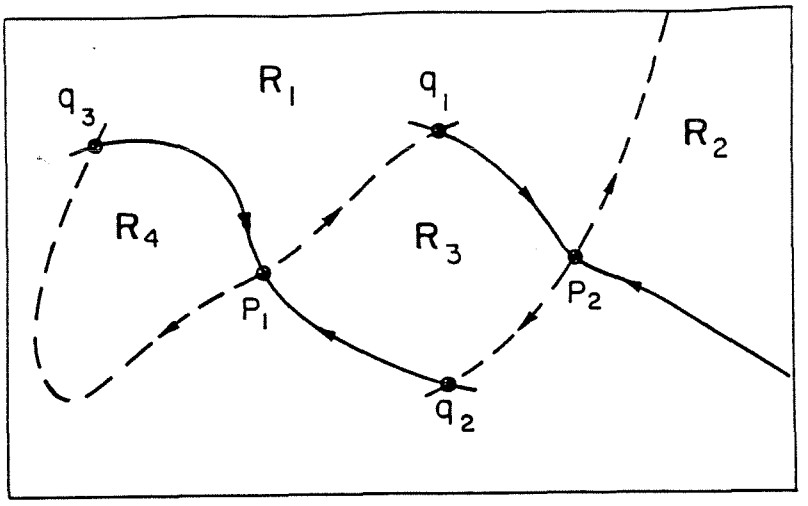

Figure 2.5 Phase Space division into Regions

can be employed, half the number of simple zeroes of the Melnikov function per period of the perturbation equals the number of lobes crossing from one side of the boundary to the other side each iteration (see Rom-Kedar et al. [1988]).

R3. With no loss of generality we can always assume that $U[q_0, F^{-1}q_0]$ and $S[q_0, F^{-1}q_0]$ intersect each other only in pip's, namely that the L_i lobes do not intersect each other. If they do, one can redefine the lobes to exclude the intersection portion, so that the new "lobes" do not intersect each other, see Figure 2.4. We will discuss this remark in more detail in the next section.

R4. Since F is an area preserving map, the intersections of the manifolds at the pip's are topologically transverse, i.e. if a tangency occurs at a pip it must be of an odd order, so that in practice it can be considered as a transverse intersection.

So far we described the motion of lobes near a pip. We now define the notion of regions, so that we can proceed in describing the transport between them as governed by the lobe motion.

Definition 2.4 A **region** is a simply connected domain of phase space with boundaries consisting of boundaries of the phase space and segments of stable and unstable manifolds starting at hyperbolic fixed points and ending at either pip's or at the boundary of the phase space (which can be infinity). See Figure 2.5.

Before embarking on the analysis of three examples for which we demonstrate

the use of the lobe motion for describing long time transport, we state a few key properties of the map F and the stable and unstable manifolds which one needs to bear in mind when dealing with the lobe dynamics:

1) A stable manifold cannot intersect itself or any other stable manifold, nor can an unstable manifold intersect an unstable manifold.
2) If a stable manifold intersects an unstable manifold at a heteroclinic (or homoclinic) point, then these manifolds intersect each other infinitely many times.
3) If q is a heteroclinic (or homoclinic) point, then the segments of the manifolds connecting q and Fq. intersect each other in an odd number of heteroclinic (homoclinic) points.
4) The interior of a closed curve is mapped to the interior of the curves image.

In the following section, we demonstrate for three simple configurations how the transport between regions is governed by the motion of lobes into and out of the regions. In these examples we illustrate the following basic rules:

1) The transport between the regions is determined by the initial distribution of the relevant lobes in the regions (the relevant lobes are the lobes which move from one region to the other under F).
2) The initial distribution of all the relevant lobes can be found by following the evolution of a few lobes which are images or preimages of all the relevant lobes.

3. Three Examples

Example 1:

Suppose that the map F, defined on R^2 has a hyperbolic fixed point p, and only one branch of the stable manifold, $W^s_{p,+}$, and one branch of the unstable manifold,$W^u_{p,+}$, are allowed to intersect with each other, see Figure 3.1.1. This phase space represents, for example, the Poincaré map of the motion of a particle in the presence of a nondegenerate cubic potential and a small forcing which is periodic in time.

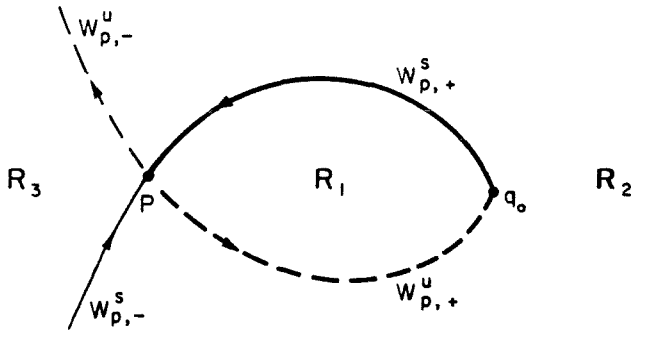

Figure 3.1.1 The Regions Geometry for Example 1

In this example, there are exactly three regions in the phase space which are separated by the stable and unstable manifolds of p. Since we assume that $W^u_{p,-}$ and $W^s_{p,-}$ do not contain any homoclinic points, region R_3, defined as the region bounded by $W^u_{p,-}$, $W^s_{p,-}$ and infinity, is separated from the rest of the phase space, and no transport can occur between R_3 and the other regions, see Figure 3.1.1. We will therefore be concerned with the transport between the two regions R_1 and R_2 which are defined as follows; let $q_0 \in W^s_{p,+} \cap W^u_{p,+}$ be a pip, denote the region bounded by the segments $S^+[p, q_0]$ and $U^+[p, q_0]$ by R_1 and the complement to R_1 and R_3 by R_2. The regions R_1 and R_2 can be defined in many different ways, depending on which pip, q_0, one chooses, however, the transport rates between R_1 and R_2 will not depend on this choice (this is not true when more regions are involved, since in general transport rates do depend on both initial distributions and definition of boundaries).

The question we wish to address is as follows:

If initially particles of species S_1 are uniformly distributed in region R_1 and particles of species S_2 are uniformly distributed in region R_2, what will be the distribution of S_1 and S_2 in regions R_1 and R_2 after n iterations of the map F?

Denote the amount of species S_i, $i = 1, 2$, which is contained in region R_j immediately after n iterations of the map by $\mathbf{T_{i,j}(n)}$.

The **flux** of species S_i through region R_j at iteration n is the change in the amount of species S_i in R_j namely $\mathbf{T_{i,j}(n) - T_{i,j}(n-1)}$. The flux is equal to the amount of species S_i entering region R_j at iteration n minus the amount of species S_i leaving R_j at iteration n.

Our goal is to determine $T_{i,j}(n)$, $i, j = 1, 2$ for all n. We assume that $T_{i,i}(0) = \mu(R_i)$, the area of region R_i while $T_{i,j}(0) = 0$ for $i \neq j$. Note that when $\mu(R_i)$ is infinite (e.g. for i=2,3) $T_{i,i}(n)$ is infinite too, though the flux is well defined and finite. In these cases we will refer to the flux instead of $T_{i,i}(n)$ and denote it by the same notation as in the finite area case namely $T_{i,i}(n) - T_{i,i}(n-1)$.

Note that area preservation implies relations between the $T_{i,j}(n)$, for example, conservation of S_i implies:

$$\sum_{j=1}^{2}(T_{i,j}(n) - T_{i,j}(n-1)) = 0. \quad i = 1, 2 \tag{3.1.1}$$

while area preservation of R_j implies:

$$\sum_{i=1}^{2}(T_{i,j}(n) - T_{i,j}(n-1)) = 0. \quad j = 1, 2 \tag{3.1.2}$$

(3.1.1) and (3.1.2) constitute three independent equations for the four unknowns $T_{i,j}(n) - T_{i,j}(n-1)$, hence solving for one of the $T_{i,j}(n)$'s provides the solution for all the other $T_{i,j}(n)$'s.

We now demonstrate that the amount of species S_i in the lobes (the lobe content) determines $T_{i,j}(n)$, then show how the content of the lobes is determined by the lobe intersections with each other, and finally show how the lobe dynamics

can be used to determine the initial intersections of the lobes. Ultimately this demonstrates that the structure of the lobes and their motion determines $T_{i,j}(n)$.

Consider Figure 3.1.2. In this figure we illustrate the motion of particles of species S_1 (black) and S_2 (white) under the map, where we assumed (see **R1**) that one lobe escapes and one lobe enters region R_1 at each iteration. Denote the lobe which leaves region R_1 and enters region R_2 immediately after n iterations by $L_{1,2}(n)$ and the one which leaves R_2 and enters R_1 after n iterations by $L_{2,1}(n)$. From the discussion in the previous section it follows that $L_{1,2}(n)$ is mapped to $L_{1,2}(1)$ after $n-1$ iterates, but at this point we ignore the dynamics and concentrate on the initial position of the lobes. The notation "$L_{1,2}(n)$" may seem a bit strange since $L_{1,2}(n)$ may not be entirely contained in R_1, however the important point is that after $n-1$ iterations, i.e. just before crossing the boundary of R_1, the lobe is entirely contained in R_1. We will discuss this point in more detail later on. Since the only mechanism to enter or leave region R_1 and R_2 is through these lobes, their content determines the flux of the various species through R_1 and R_2. In other words, denoting by $L^i_{k,l}(n)$ the part of lobe $L_{k,l}(n)$ containing particles of species S_i (so that $L_{k,l}(n) = L^1_{k,l}(n) \cup L^2_{k,l}(n)$), we have:

$$\begin{aligned} T_{i,j}(n) - T_{i,j}(n-1) &= \{\textit{flux of species } S_i \textit{ through region } R_j \textit{ at iteration } n\} \\ &= \{\textit{amount of } S_i \textit{ in the lobes entering region } R_j \textit{ at iteration } n\} \\ &\quad - \{\textit{amount of } S_i \textit{ in the lobes leaving region } R_j \textit{ at iteration } n\} \\ &= \mu(L^i_{k,j}(n)) - \mu(L^i_{j,k}(n)) \quad \text{for} \quad k \neq j. \end{aligned} \tag{3.1.3}$$

Let us describe in more detail the characteristic of the geometry of the manifolds as shown in Figure 3.1.2a. Note the following characteristics of the manifolds geometry in Figure 3.1.2a: $\mu(L^1_{2,1}(n)) = 0$ for all $n > 0$ (no black particles in these lobes), $\mu(L^1_{1,2}(1)) = \mu(L_{1,2}(1))$ (the whole lobe is black) but $\mu(L^1_{1,2}(2)) < \mu(L_{1,2}(2))$ (part of the lobe is white). (Note: the observation that $L_{1,2}(2)$ is the first lobe to have white particles is specific to the geometry described in Figure 3.1.2, where in general $L_{1,2}(k_f)$ can be the first lobe to have white particles, with any $k_f > 1$, and the same discussion presented for the case $k_f = 2$ applies. In particular, the formulas derived

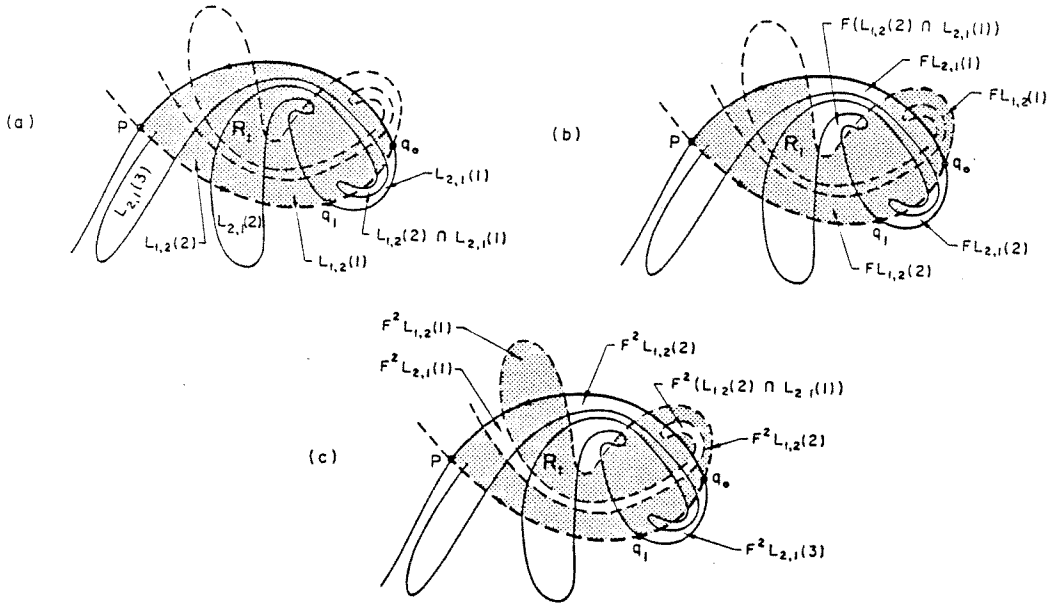

Figure 3.1.2 The species motion under the map

for this example are independent of k_f). As an example of a consequence of equation (3.1.3), substituting $i = j = 1$, for $n = 1, 2$, in this equation shows that the amount of black species in region R_1 decreases by the area of the lobe $L_{1,2}(1)$ after the first iteration and by $\mu(L^1_{1,2}(1))$ after the second one.

We now discuss how the content of the lobes depends on the lobe intersections associated with the chosen geometry. Since in this example all the $L_{2,1}(n)$ lobes are contained in region R_2 initially, namely they contain only white (S_2) particles: $L^1_{2,1}(n) = \emptyset$ and $L^2_{2,1}(n) = L_{2,1}(n)$ for all n, we have that:

$$\mu(L^1_{2,1}(n)) = 0 \quad \mu(L^2_{2,1}(n)) = \mu(L_{2,1}(n)) \tag{3.1.4}$$

Now we wish to describe $L^i_{1,2}(n), \quad i = 1, 2$ in terms of the lobe intersections. Consider Figure 3.1.2a. Note that $L_{1,2}(n)$ are contained mainly in R_1 for small n. The parts which are not contained in R_1 are contained in $L_{2,1}(k)$ for some $k < n$. For example, $L_{1,2}(1)$ is completely contained in R_1 and therefore contains only S_1 particles, while $L_{1,2}(2) \cap L_{2,1}(1)$ is a non-empty set and therefore $L_{1,2}(2)$ contains $\mu(L_{1,2}(2) \cap L_{2,1}(1))$ white (S_2) particles, namely

$$\mu(L^2_{1,2}(2)) = \mu(L_{1,2}(2) \cap L_{2,1}(1))$$

$$\mu(L^1_{1,2}(2)) = \mu(L_{1,2}(2)) - \mu(L^2_{1,2}(2))$$

Or in general:

$$\begin{aligned} L^2_{1,2}(n) &= \bigcup_{k=1}^{n-1} (L_{1,2}(n) \cap L_{2,1}(k)) \\ L^1_{1,2}(n) &= L_{1,2}(n) - L^2_{1,2}(n) \end{aligned} \tag{3.1.5}$$

In obtaining formula (3.1.5) we use the following properties:

a) Particles belonging to $L^2_{1,2}(n)$ must be in R_2 initially and must enter R_1 before iteration n, hence they are contained in a lobe which leaves region R_2 and enters region R_1 before iteration n, namely in an $L_{2,1}(k)$ lobe with $k < n$.

b) $L^2_{1,2}(n) \subset L_{1,2}(n)$

c) All the $L_{2,1}(k)$ lobes are completely contained in R_2, hence we are guaranteed that the right hand side of the first equation in (3.1.5) contains only particles of species S_2.

The observation that there is a correspondence between lobe intersections and lobe content, as manifested in equation (3.1.5) for this example, is one of the back bones of this work. We prove in the next section that a similar formula holds in the general case.

Using equations (3.1.3), (3.1.4) and (3.1.5) we can now write $T_{1,2}(n)$ in terms of the area of the intersections of the lobes $L_{1,2}(n)$ and $L_{2,1}(k)$ for $k < n$:

$$\begin{aligned} T_{1,2}(n) - T_{1,2}(n-1) &= \mu(L^1_{1,2}(n)) - \mu(L^1_{2,1}(n)) = \\ &= \mu(L_{1,2}(n)) - \mu(\bigcup_{k=1}^{n-1} (L_{1,2}(n) \cap L_{2,1}(k))). \end{aligned} \tag{3.1.6}$$

Now we use the dynamics of the lobes to demonstrate that the measures of all these intersections can be obtained by, for example, the measure of the intersection between the lobe $L_{1,2}(1)$ and the $n-1$ forward iterations of $L_{2,1}(1)$. The rules which enable us to achieve this result are as follows:

A1. By definition after $k-1$ iterations of the map the lobe $L_{2,1}(k)$ is mapped to lobe $L_{2,1}(1)$, similarly after $k-1$ iterations, lobe $L_{1,2}(k)$ is mapped to $L_{1,2}(1)$.

A2. By area preservation, for any set A in phase space, $\mu(A) = \mu(F^k(A))$ for all k.

A3. The $L_{2,1}(k)$ lobes are disjoint, namely $L_{2,1}(k) \cap L_{2,1}(l) = \emptyset$ for $k \neq l$.

Using the first two rules, we obtain the following result:

$$\mu(L_{1,2}(n)\cap L_{2,1}(k)) = \mu(F^{-n+1}L_{1,2}(1)\cap F^{-k+1}L_{2,1}(1)) = \mu(L_{1,2}(1)\cap F^{n-k}L_{2,1}(1)) \tag{3.1.7}$$

Therefore, using (3.1.5) and (3.1.7) we find:

$$\begin{aligned}\mu(L^2_{1,2}(n)) &= \mu(\bigcup_{k=1}^{n-1}(L_{1,2}(n)\cap L_{2,1}(k)) = \sum_{k=1}^{n-1}\mu(L_{1,2}(1)\cap F^{n-k}L_{2,1}(1)) \\ &= \sum_{l=1}^{n-1}\mu(L_{1,2}(1)\cap F^{l}L_{2,1}(1)) \\ \mu(L^1_{1,2}(n)) &= \mu(L_{1,2}(n)) - \mu(L^2_{1,2}(n)) = \mu(L_{1,2}(1)) - \mu(L^2_{1,2}(n))\end{aligned} \tag{3.1.8}$$

Where we used the third rule to obtain that the area of the union of the lobe intersections is equal to the sum of their areas. Substituting (3.1.8) in (3.1.6) and using $\mu(L_{2,1}(n)) = \mu(L_{2,1}(1))$ we find:

$$T_{1,2}(n) - T_{1,2}(n-1) = \mu(L_{1,2}(1)) - \sum_{l=1}^{n-1}\mu(L_{1,2}(1)\cap F^{l}L_{2,1}(1))$$

Hence,

$$\begin{aligned}T_{1,2}(n) &= T_{1,2}(0) + \sum_{k=1}^{n}\Big[\mu(L_{1,2}(1)) - \sum_{l=1}^{k-1}\mu(L_{1,2}(1)\cap F^{l}L_{2,1}(1))\Big] \\ &= n\mu(L_{1,2}(1)) - \sum_{l=1}^{n-1}(n-l)\mu(L_{1,2}(1)\cap F^{l}L_{2,1}(1)).\end{aligned}$$

And using (3.1.1) and (3.1.2) we find that all the other $T_{i,j}(n)$ can be obtain from the above quantity since:

$$\begin{aligned}T_{1,2}(n) - T_{1,2}(n-1) &= -[T_{1,1}(n) - T_{1,1}(n-1)] = \\ &-[T_{2,2}(n) - T_{2,2}(n-1)] = T_{2,1}(n) - T_{2,1}(n-1).\end{aligned}$$

Hence, the only quantities one needs to compute in order to find $T_{i,j}(k)$ for $k \leq n$ are :

1) $\mu(L_{1,2}(1))$

2) $\mu(L_{1,2}(1)\cap F^{l}L_{2,1}(1))$ for $l = 1,..,n-1$

To summarize example 1, we distinguish between properties special to this case ,which make it the "simplest" interesting problem, and properties which hold generally.

The following properties are special to example 1:

a) The $L_{2,1}(k)$ lobes are all contained in R_2, which also implies that once an $L_{1,2}(k)$ lobe leaves region R_1 it cannot enter it again.

b) The $L_{1,2}(k)$ lobes cannot intersect each other nor can the $L_{2,1}(k)$ lobes intersect each other.

c) The area of the intersections of all the lobes can be obtained from the area of intersections of the forward iterations of only one lobe with another lobe.

P1-P5 are of a general nature:

P1. With no loss of generality, one can always assume that only one lobe is exchanged between neighboring regions.

P2. The quantities $T_{i,j}(n)$ are determined by the lobe content.

P3. The lobe content is determined by the lobe intersections.

P4. The lobe dynamics gives a tool to compute the lobe intersections.

P5. Area conservation gives global results about the relations between the total transport rates between the different regions.

Remark We discuss here in some more detail remark **R3**. In this example, as well as in all the others, we assume that $L_{2,1}(1) \cap L_{1,2}(1) = \emptyset$ (and hence $L_{2,1}(n) \cap L_{1,2}(n) = \emptyset$ for all n). However, in practice the situation may be different, for example we expect that if the forcing of the particle in the cubic potential has large amplitude and slow time dependence this intersection will not be empty. If $L_{2,1}(1) \cap L_{1,2}(1) \neq \emptyset$, then by the definition of the lobes this intersection stays in the same region under an iteration of the map, see Figure 3.1.3. This is an inconvenience, since it does not fit into our description of the flux mechanism where particles in $L_{1,2}(1)$ leave region R_1 while particles in $L_{2,1}(1)$ enter it. We therefore redefine the lobes so that to exclude the intersection region, and using the redefined lobes we proceed with the same formulas, see Figure 3.1.3. So, we continue to assume that $L_{2,1}(1) \cap L_{1,2}(1) = \emptyset$, being aware of the need to redefine the lobes

in case the usual lobe definition does not satisfy this condition. An alternative (and more complicated) approach would be to modify the formulas to include this possibility.

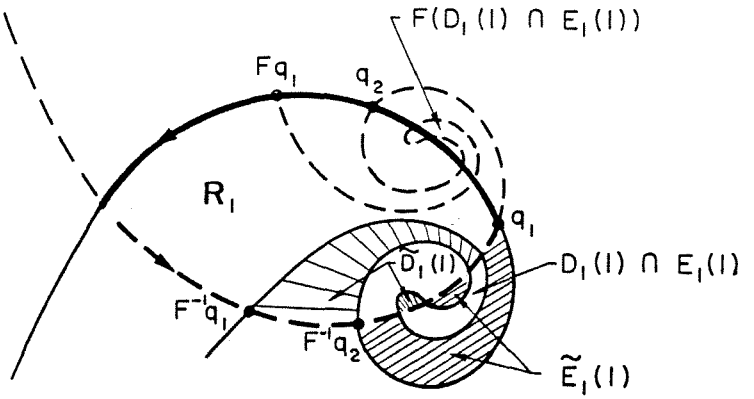

Figure 3.1.3 Redefining a Lobe

The redefined lobes: $\tilde{E}_1(1) = E_1(1) - E_1(1) \cap D_1(1)$, $\tilde{D}_1(1) = D_1(1) - D_1(1) \cap E_1(1)$.

Example 2:

Suppose that the map F, defined on R^2 has one hyperbolic fixed point p, and both branches of the stable and unstable manifolds are allowed to intersect with each other, see Figure 3.2.1. This phase space represents, for example, the Poincaré map of the Duffing equation with no damping and with negative linear stiffness term which models the motion of a magneto elastic beam (see Guckenheimer and Holmes [1983] for physical motivation and references). The motion near the right elliptical fixed point, in R_1, corresponds to the beam vibrations with the tip pointing to the right magnet, while motion near the left elliptical point corresponds to the tip pointing to the left.

In this example, there are again three regions in the phase space, but this time all the regions participate in the transport game. The regions are defined as follows (see Figure 3.2.1): let $q_1^+ \in W^s_{p,+} \cap W^u_{p,+}$ be a pip, and denote the region bounded by the segments $S^+[p, q_1^+]$ and $U^+[p, q_1^+]$ by R_1, similarly, let $q_1^- \in W^s_{p,-} \cap W^u_{p,-}$ be a pip, and denote the region bounded by the segments $S^-[p, q_1^-]$ and $U^-[p, q_1^-]$ by R_2. Let R_3 be the complement of R_1 and R_2.

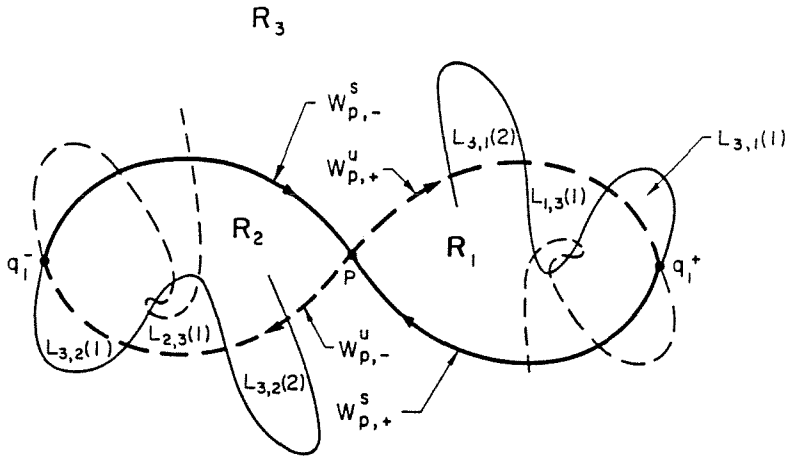

Figure 3.2.1 The regions Geometry for example 2

As in the previous example, we wish to address the following question:

If initially particles of species S_i are uniformly distributed in region R_i, for $i = 1, 2, 3$, what will be the distribution of S_i in region R_j for $i, j = 1, 2, 3$ after n iterations of the map F?

We again denote the amount of species S_i, $i = 1, 2, 3$, which is contained in region R_j just after n iterations of the map by $T_{i,j}(n)$, and our goal is to determine $T_{i,j}(n)$, $i, j = 1, 2, 3$, for all n.

As an example of the use of these quantities, $T_{1,2}(n)/\mu(R_1)$, is the fraction of particles which start in R_1 and end up in R_2 after n iterations of the map, hence is equal to the probability that a magneto elastic beam initially pointing to the right magnet will point to the left magnet after n periods of the forcing.

First let us describe some consequences of the conservation of $\mu(R_j)$ and S_i (i.e. **P5**). Analytically, this is expressed by the following equations:

$$\begin{aligned} &\sum_{j=1}^{3}(T_{i,j}(n) - T_{i,j}(n-1)) = 0 \quad i = 1, 2, 3 \\ &\sum_{i=1}^{3}(T_{i,j}(n) - T_{i,j}(n-1)) = 0 \quad j = 1, 2, 3. \end{aligned} \tag{3.2.1}$$

constituting five independent equations for the nine unknowns $T_{i,j}(n) - T_{i,j}(n-1)$.

If the map F has a symmetry under a 180° rotation about the hyperbolic fixed point p, so that regions R_1 and R_2 are actually identical, then the following three

relations between the $T_{i,j}(n)$'s hold:

$$\begin{aligned} T_{1,2}(n) &= T_{2,1}(n) \\ T_{1,3}(n) &= T_{2,3}(n) \\ T_{3,1}(n) &= T_{3,2}(n) \end{aligned} \tag{3.2.2}$$

and these relations together with (3.2.1) constitute eight equations for the nine unknowns, hence finding one $T_{i,j}(n)$ is sufficient for obtaining a complete solution for all the transport rates $T_{i,j}(n)$'s.

We now follow the same steps as in the previous example in order to obtain an expression for $T_{i,j}(n)$ in terms of the area of lobe intersections. Using **P1** and **R3** we can assume that the flux mechanism between the regions is as described in Figure 3.2.1, namely that one lobe, $L_{3,j}(n)$, enters and one lobe, $L_{j,3}(n)$, leaves region R_j, $j = 1, 2$, on iteration n. As before, we can write easily how the $T_{i,j}(n)$'s depend on the content of the lobes:

$$T_{i,j}(n) - T_{i,j}(n-1) = \sum_{k=1}^{3} \{\mu(L^i_{k,j}(n)) - \mu(L^i_{j,k}(n))\} \tag{3.2.3}$$

where the superscript i for the lobes denotes the part of the lobe which contains particles of species S_i, and $L_{1,2}(n) = L_{2,1}(n) = L_{i,i}(n) = \emptyset$ for $i = 1, 2, 3$. Equation (3.2.3) is the manifestation of **P2** for this example. To proceed, we want to represent the portion of a lobe containing a given species as an intersection of lobes. This is the manifestation of **P3** discussed earlier. Example 2 is more complicated than example 1 at this stage, since lobes which leave one region can reenter the same region at a later time and lobes from the same "family" may intersect each other, namely $L_{j,k}(n) \cap L_{j,k}(m)$ is not necessarily empty. Before we write down the rules which connect the lobe content to their intersections, let us describe the geometry of some of the lobe intersections as illustrated in Figure 3.2.2. Consider the $L_{3,1}(n)$ lobes in Figure 3.2.2, and say we are interested in finding the portion of these lobes which are filled with particles of species S_2, namely $L^2_{3,1}(n)$. For $n = 1, 2, 3$, the lobes $L_{3,1}(n)$ are completely contained in region R_3 and therefore $\mu(L^2_{3,1}(n)) = 0$ for $n = 1, 2, 3$ (note: for illustrating the methods we need to take a specific configuration

of the lobe intersections, but the general formulas are independent of this choice. For example we could have the first k lobes completely contained in R_3 where k is any number greater than 1). However, $L_{3,1}(4)$ has a portion which is contained in R_2, and hence contains particles of species S_2. Now this portion is also contained in lobe $L_{2,3}(1)$, a lobe which leaves R_2 after one iteration. Geometrically, since $W^s_{p,+}$ cannot intersect $W^s_{p,-}$, the only route for the $L_{3,1}(n)$ lobes to invade region R_2 is through the $L_{2,3}(k)$ lobes, where $k < n$. An analytical justification for this statement is that since $n-1$ iterations of F map $L_{3,1}(n)$ to $L_{3,1}(1)$, which is completely contained in R_3, any portion of $L_{3,1}(n)$ which is contained in R_2 must leave R_2 before the $n-1$ iteration, and therefore must be contained in a $L_{2,3}(k)$ lobe with $k \leq n-1$. So $L^2_{3,1}(n)$ is contained in the union of the lobes which leave R_2 before iteration n:

$$L^2_{3,1}(n) \subset \left[L_{3,1}(n) \cap \bigcup_{k=1}^{n-1} L_{2,3}(k)\right] \tag{3.2.4}$$

The same argument applies to all the lobes, namely:

Any part of the lobe $L_{j,k}(n)$ which is contained in a region R_i, $i \neq j$ must be contained in a lobe which leaves region R_i before iteration n.

Now we want to change the "$\subset$" sign in (3.2.4) to an equality. For lobe $L_{3,1}(4)$ we can do this, since $L_{3,1}(4) \cap L_{2,3}(1)$ is completely contained in R_2. However, looking at Figure 3.2.2 it is not hard to imagine that for large n and k, $L_{3,1}(n) \cap L_{2,3}(k)$ may have portions which are not contained in R_2 (for example, $L_{3,1}(5) \cap L_{2,3}(2)$ in the figure) and therefore, to obtain an "=" sign in (3.2.4) we need to replace $L_{2,3}(k)$ by $L^2_{2,3}(k)$, the portion of $L_{2,3}(k)$ which is contained in R_2:

$$L^2_{3,1}(n) = \left[L_{3,1}(n) \cap \bigcup_{k=1}^{n-1} L^2_{2,3}(k)\right] \tag{3.2.5}$$

In other words we need to subtract the portions of the lobe intersections which are not contained in R_2.

However, (3.2.5) is still not good enough since we want to express $L^2_{3,1}(n)$ in terms of lobe intersections so that we can use the lobe dynamics, as in the first

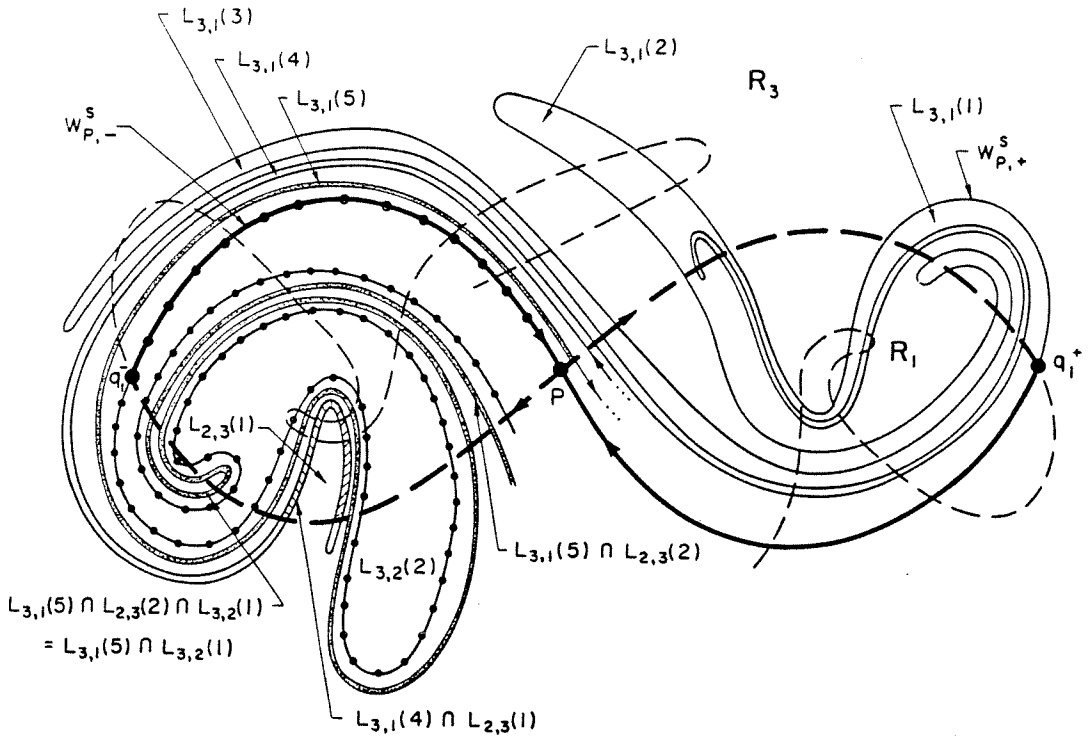

Figure 3.2.2 The Lobe Intersections

example, for obtaining simplified expressions for the transport rates. Using the same argument which led to (3.2.4), we find that any portion of $L^2_{3,1}(n)$ which is contained in a $L_{2,3}(k)$ lobe but is not contained in R_2 must also belong to the portion of a $L_{3,2}(m)$ lobe which is not contained in R_2, where $m < k < n$, i.e.:

$$L^2_{3,1}(n) = \bigcup_{k=1}^{n-1} \left(L_{3,1}(n) \cap L_{2,3}(k)\right) - \bigcup_{k=1}^{n-1} \bigcup_{\substack{i=1 \\ i \neq 2}}^{3} \bigcup_{m=1}^{k-1} \left(L_{3,1}(n) \cap L_{2,3}(k) \cap L^i_{3,2}(m)\right) \quad (3.2.6)$$

Consider for example figure 3.2.2; the portion of $L_{3,1}(5) \cap L_{2,3}(2)$ which is not contained in R_2 is contained in $L_{3,2}(1)$, so that

$$L^2_{3,1}(5) = L_{3,1}(5) \cap L_{2,3}(1) \bigcup L_{3,1}(5) \cap L_{2,3}(2) - L_{3,1}(5) \cap L_{2,3}(2) \cap L_{3,2}(1).$$

Moreover, note that the only route for $L_{3,1}(5)$ to intersect $L_{3,2}(1)$ is through an $L_{2,3}(m)$ lobe where $1 < m < 5$. Specifically, in this example, we have:

$$L_{3,1}(5) \cap L_{2,3}(2) \cap L_{3,2}(1) = L_{3,1}(5) \cap L_{3,2}(1).$$

Or in general, the only route for the $L_{3,1}(n)$ lobe to intersect with the $L_{3,2}(m)$ lobes is through the $L_{2,3}(k)$ lobes and therefore we can always replace the triple intersection by the intersection of two lobes:

$$\bigcup_{k=1}^{n-1}\bigcup_{\substack{i=1\\ i\neq 2}}^{3}\bigcup_{m=1}^{k-1} L_{3,1}(n)\cap L_{2,3}(k)\cap L^i_{3,2}(m) = \bigcup_{\substack{i=1\\ i\neq 2}}^{3}\bigcup_{m=1}^{n-1} L_{3,1}(n)\cap L^i_{3,2}(m) \qquad (3.2.7)$$

Therefore, using (3.2.6) and (3.2.7) we obtain:

$$\mu(L^2_{3,1}(n)) = \mu\left(\bigcup_{k=1}^{n-1}\left(L_{3,1}(n)\cap L_{2,3}(k)\right)\right) - \mu\left(\bigcup_{m=1}^{n-1}\bigcup_{\substack{i=1\\ i\neq 2}}^{3}\left(L_{3,1}(n)\cap L^i_{3,2}(m)\right)\right). \qquad (3.2.8)$$

Now, for small n, we expect that $L^2_{3,2}(m) = \emptyset$ for $m < n$, hence

$$\bigcup_{\substack{i=1\\ i\neq 2}}^{3} L^i_{3,2}(m) = L_{3,2}(m).$$

Moreover, for such a small n the sets under the union sign in (3.2.8) are disjoint, in which case (3.2.8) becomes:

$$\mu(L^2_{3,1}) = \sum_{k=1}^{n-1}\mu(L_{3,1}(n)\cap L_{2,3}(k)) - \sum_{m=1}^{n-1}\mu(L_{3,1}(n)\cap L_{3,2}(m)) \qquad (3.2.9)$$

The somewhat surprising result is that (3.2.9) is valid for all n, even when $L^2_{3,2}(m) \neq \emptyset$ and the sets under the union in (3.2.8) are not disjoint. Losely speaking, the interchange of the union and area sign which leads to (3.2.9) exactly compensates for disregarding the superscript i in that equation. Disregarding the superscript corresponds to the subtraction of the parts of $L_{3,1}(n)$ which originated in R_2 and belonged to at least two sets of lobe intersections: $L_{3,1}(n) \cap L_{2,3}(k)$ and $L_{3,1}(n) \cap L_{3,2}(m)$ for some $m < k < n$. However, the portion of $L_{3,2}(m)$ which belongs to R_2 must also belong to a lobe which leaves R_2 before the m^{th} iterate, i.e. to a $L_{2,3}(l)$ lobe with $l < m$, which shows that the area of this portion is added twice through the first sum in (3.2.9) and subtracted once through the second sum. We show in the general proof that in fact this portion must belong to $t+1$ $L_{2,3}(k)$ lobes and to t

$L_{3,2}(m)$ lobes, where $t \geq 1$, hence the effect of interchanging the union and area sign and ignoring the content of the $L_{3,2}(m)$ lobes give exactly the right counting. Note that the above scenario occurs for n large enough so that the lobes $L_{2,3}(k)$ are no longer disjoint, namely an $L_{2,3}(k)$ $(k < n)$ lobe is so stretched that it gets out of region R_2 through an $L_{3,2}(m)$ lobe, encircles region R_1 and comes back to R_2 from the outer side to intersect an $L_{2,3}(l)$ lobe with $l < k$ (it is much too complicated to draw $L_{2,3}(k)$ in this case. We suggest that the reader stare at Figure 3.2.2 and imagine the route $L_{2,3}(k)$ goes through).

The general formulation gives us formulas like (3.2.9) for all the families of lobes $L_{k,j}(n)$ and all the species S_i:

$$\mu(L^i_{k,j}(n)) = \sum_{s=1}^{3}\sum_{m=1}^{n} \mu(L_{k,j}(n) \cap L_{i,s}(m)) - \sum_{s=1}^{3}\sum_{m=1}^{n-1} \mu(L_{k,j}(n) \cap L_{s,i}(m)) \quad (3.2.10)$$

where the first sum on m is from 1 to n so that (3.2.10) applies also to the case $k = i$, in which $L_{i,j}(n)$ itself is contained mainly in R_i, and therefore has to be added in through the first sum.

This demonstrates **P3** for this example. We next simplify (3.2.10) by using the lobe dynamics. This illustrates **P4** discussed earlier. The rules for the lobe dynamics, which are equivalent to A1 and A2 of the first example, are given by:

B1. By definition the lobe $L_{k,j}(n)$ is mapped to lobe $L_{k,j}(1)$ after $n-1$ iterations, or in general $F^l L_{k,j}(n)$ is mapped to $L_{k,j}(n-l)$ for $n > l$.

B2. For any set A in phase space $\mu(F^k(A)) = \mu(A)$ for all k.

Using these two rules we can play with formula (3.2.9) to obtain:

$$\begin{aligned}
\mu(L^2_{3,1}) &= \sum_{k=1}^{n} \mu(F^{-n+1}L_{3,1}(1) \cap F^{-k+1}L_{2,3}(1)) - \\
&\qquad \sum_{m=1}^{n-1} \mu(F^{-n+1}L_{3,1}(1) \cap F^{-m+1}L_{3,2}(1)) \\
&= \sum_{k=1}^{n} \mu(L_{3,1}(1) \cap F^{n-k}L_{2,3}(1)) - \sum_{m=1}^{n-1} \mu(L_{3,1}(1) \cap F^{n-m}L_{3,2}(1)) \\
&= \sum_{k=1}^{n} \mu(F^{k-n}L_{3,1}(1) \cap L_{2,3}(1)) - \sum_{m=1}^{n-1} \mu(F^{m-n}L_{3,1}(1) \cap L_{3,2}(1))
\end{aligned} \quad (3.2.11)$$

Which shows that we need to find the $n-1$ forward iterations of $L_{2,3}(1)$ and $L_{3,2}(1)$ or the $n-1$ backward iterations of $L_{3,1}(1)$ to determine $L^2_{3,1}(k)$ for $k = 1, .., n$. Similarly, using (3.2.10), B1 and B2 we can write:

$$\begin{aligned}\mu(L^2_{1,3}) &= \sum_{m=1}^{n} \mu(L_{1,3}(n) \cap L_{2,3}(m)) - \sum_{m=1}^{n-1} \mu(L_{1,3}(n) \cap L_{3,2}(m)) \\ &= \sum_{m=1}^{n} \mu(L_{1,3}(1) \cap F^{n-m} L_{2,3}(1)) - \sum_{m=1}^{n-1} \mu(L_{1,3}(1) \cap F^{n-m} L_{3,2}(1))\end{aligned} \tag{3.2.12}$$

And therefore, using (3.2.3) for $i = 2,\ j = 1$, we can compute $T_{2,1}(n)$, the amount of species S_2 in region R_1 after n iterations of the map, by computing the $n-1$ forward iterations of $L_{2,3}(1)$ and $L_{3,2}(1)$:

$$\begin{aligned}T_{2,1}(n) =& T_{2,1}(0) + \sum_{l=1}^{n} [\mu(L^2_{3,1}(l)) - \mu(L^2_{1,3}(l))] \\ =& 0 + \sum_{l=1}^{n} \Big\{ \sum_{m=0}^{l-1} \mu(L_{3,1}(1) \cap F^m(L_{2,3}(1)) - \sum_{m=1}^{l-1} \mu(L_{3,1}(1) \cap F^m(L_{3,2}(1)) - \\ & \sum_{m=0}^{l-1} \mu(L_{1,3}(1) \cap F^m(L_{2,3}(1)) + \sum_{m=1}^{l-1} \mu(L_{1,3}(1) \cap F^m(L_{3,2}(1)) \Big\} \\ =& \sum_{m=1}^{n-1} (n-m) \Big\{ \mu(L_{3,1}(1) \cap F^m(L_{2,3}(1)) - \mu(L_{3,1}(1) \cap F^m(L_{3,2}(1)) - \\ & \mu(L_{1,3}(1) \cap F^m(L_{2,3}(1)) + \mu(L_{1,3}(1) \cap F^m(L_{3,2}(1)) \Big\}\end{aligned} \tag{3.2.13}$$

We could write the corresponding expressions for all the $T_{i,j}(n)$'s in a similar fashion, or compute three more $T_{i,j}(n)$'s and use the conservation of $\mu(R_j)$ and S_i, namely equations (3.2.1), to find all the $T_{i,j}(n)$'s.

If the map F has a symmetry under a 180° we can use (3.2.1) and (3.2.2) which constitute eight equations for the nine unknowns together with (3.2.9) to obtain a complete solution for all the transport rates $T_{i,j}(n)$'s from the intersections of the $n-1$ forward iterations of $L_{2,3}(1)$ and $L_{3,2}(1)$ with $L_{1,3}(1)$ and $L_{3,1}(1)$.

Example 3:

Suppose that the map F, defined on the cylinder, denoted by $T \times (a, b)$ where T is the circle, has a hyperbolic fixed point p and both branches of the stable and

unstable manifolds are allowed to intersect with each other, as in Figure 3.3.1a. The interval (a,b) can be finite or infinite, and the boundaries a,b may depend on the T co-ordinate, x. It is easier to visualize the phase space embedded in $R \times (a,b)$, so that instead of viewing x on a circle we consider $x \in R$ and lift F to its universal cover and view it as a map from $R \times (a,b)$ into $R \times (a,b)$ where it is periodic in the x variable, see Figure 3.3.1b. This phase portrait appears in many applications. For example, the 1/1 resonance band of a two dimensional area preserving diffeomorphism, the Poincaré map of a pendulum with time periodic forcing and the Poincaré map, in the physical space, of a Kelvin-Stuart Cat's Eye flow with time and space periodic perturbations. The way one chooses the boundary does not affect the formulation (the KAM tori and the phase space boundaries are two natural candidates for the boundaries in many applications).

For $x \in [0, 2\pi)$ there are three regions in phase space and all of them participate in the transport, where the same picture repeats itself in all the strips $x \in [2n\pi, 2(n+1)\pi)$ for all n. The regions are defined as follows (see Figure 3.3.1b): let $q_1^+ \in W^s_{p,+} \cap W^u_{p,+}$ be a pip, and denote by R_1 the region which is bounded from below by the segments $S^+[p,q_1^+]$ and $U^+[p,q_1^+]$ and from above by the curve y=b, similarly, let $q_1^- \in W^s_{p,-} \cap W^u_{p,-}$ be a pip, and denote the region bounded by the segments $S^+[p,q_1^+]$, $U^+[p,q_1^+]$, $S^-[p,q_1^-]$ and $U^-[p,q_1^-]$ by R_2, and finally, denote the complement of R_1 and R_2 by R_3. Assuming that initially particles of species S_i are uniformly distributed in region R_i, $i = 1,2,3$, we want to determine $T_{i,j}(n)$, the amount of species S_i, $i = 1,2,3$, which are contained in region R_j just after n iterations of the map.

As an example of the use of the transport quantities, $T_{2,1}(n)/\mu(R_2)$ is the fraction of particles which start in R_2 and end up in R_1 after n iterations of the map. Or, more physically, it is the probability that a pendulum initially oscillating will begin rotating with positive velocity after n periods of the forcing, or the probability that fluid starting inside the Cat's Eyes will be transported to the upper half plane after n periods of the perturbation.

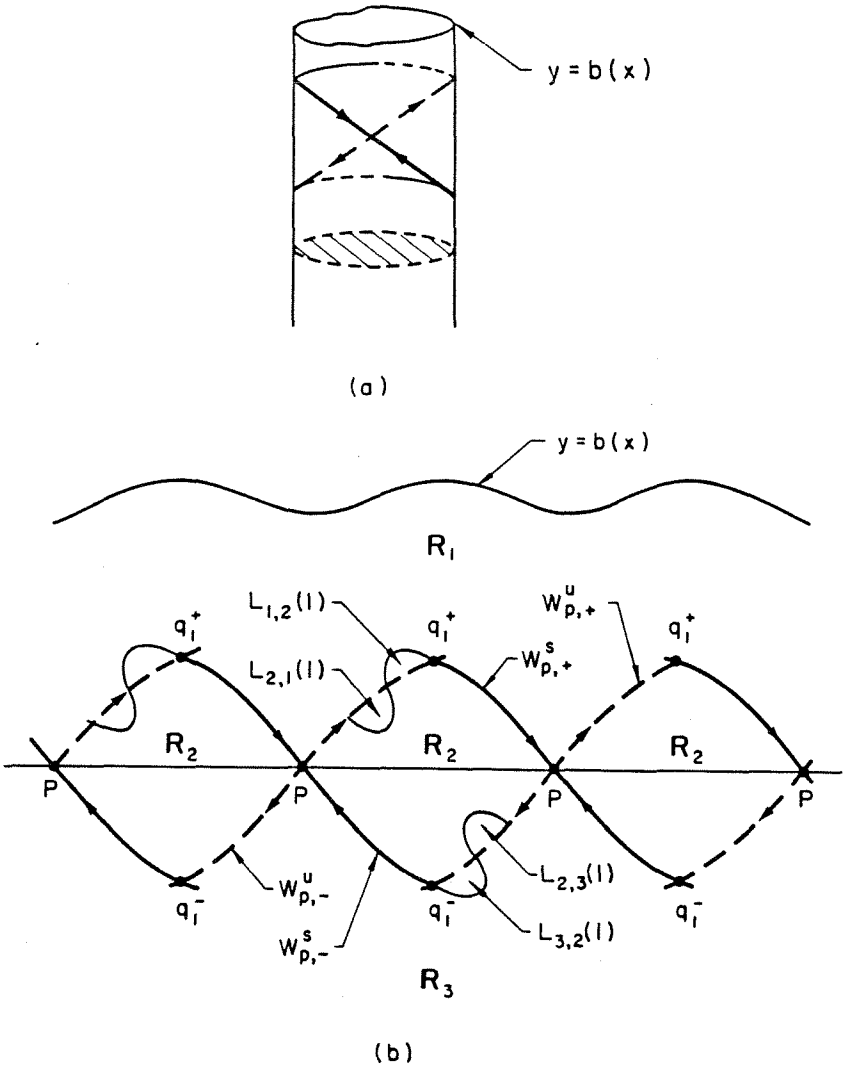

Figure 3.3.1 The Regions Geometry For Example 3.

As before, conservation of $\mu(R_j)$ and S_i (i.e. **P5**) implies:

$$\begin{aligned} \sum_{j=1}^{3}(T_{i,j}(n) - T_{i,j}(n-1)) = 0 \quad i = 1,2,3 \\ \sum_{i=1}^{3}(T_{i,j}(n) - T_{i,j}(n-1)) = 0 \quad j = 1,2,3. \end{aligned} \tag{3.3.1}$$

constituting five independent equations for the nine unknowns $T_{i,j}(n) - T_{i,j}(n-1)$.

If the map F has a symmetry under a 180° rotation about the origin, so that regions R_1 and R_3 are actually identical, then the following three relations between

the $T_{i,j}(n)$'s hold:

$$\begin{aligned} T_{1,3}(n) &= T_{3,1}(n) \\ T_{2,1}(n) &= T_{2,3}(n) \\ T_{1,2}(n) &= T_{3,2}(n) \end{aligned} \tag{3.3.2}$$

and these relations together with (3.3.1) constitute eight equations for the nine unknowns, hence finding one $T_{i,j}(n)$ is sufficient for obtaining a complete solution for all the transport rates $T_{i,j}(n)$'s.

We now follow the same steps as in the previous example in order to obtain an expression for $T_{i,j}(n)$ in terms of the area of lobe intersections. Using **P1** and **R3** we can assume that the flux mechanism between the regions is as described in Figure 3.3.1b, namely that one lobe, $L_{2,j}(n)$, enters and one lobe, $L_{j,2}(n)$, leaves region R_j, $j = 1, 3$, immediately after iteration n. As before we can write easily how the $T_{i,j}(n)$'s depend on the content of the lobes:

$$T_{i,j}(n) - T_{i,j}(n-1) = \sum_{k=1}^{3} \{\mu(L^i_{k,j}(n)) - \mu(L^i_{j,k}(n))\} \tag{3.3.3}$$

where the superscript i for the lobes denotes the part of the lobe which contains particles of species S_i, and

$$L_{1,3}(n) = L_{3,1}(n) = L_{i,i}(n) = \emptyset \quad \text{for } i = 1, 2, 3 \tag{3.3.4}$$

Equation (3.3.3) is the manifestation of **P2** for this example. To proceed, we want to show how **P3** is applied here. The reader has probably noticed by now that this example is very similar to example 2, and actually the same formulas and remarks apply. We illustrate this by reproducing (3.2.10) below (and using (3.3.4) in the process) for $k = 1$, $j = 2$ and $i = 2, 3$.

$$\begin{aligned} \mu(L^2_{1,2}(n)) = &\sum_{m=1}^{n} \left[\mu(L_{1,2}(n) \cap L_{2,1}(m)) + \mu(L_{1,2}(n) \cap L_{2,3}(m))\right] \\ &- \sum_{m=1}^{n-1} \left[\mu(L_{1,2}(n) \cap L_{1,2}(m)) + \mu(L_{1,2}(n) \cap L_{3,2}(m))\right] \end{aligned} \tag{3.3.5}$$

$$\mu(L^3_{1,2}(n)) = \sum_{m=1}^{n} \mu(L_{1,2}(n) \cap L_{3,2}(m)) - \sum_{m=1}^{n-1} \mu(L_{1,2}(n) \cap L_{2,3}(m)) \tag{3.3.6}$$

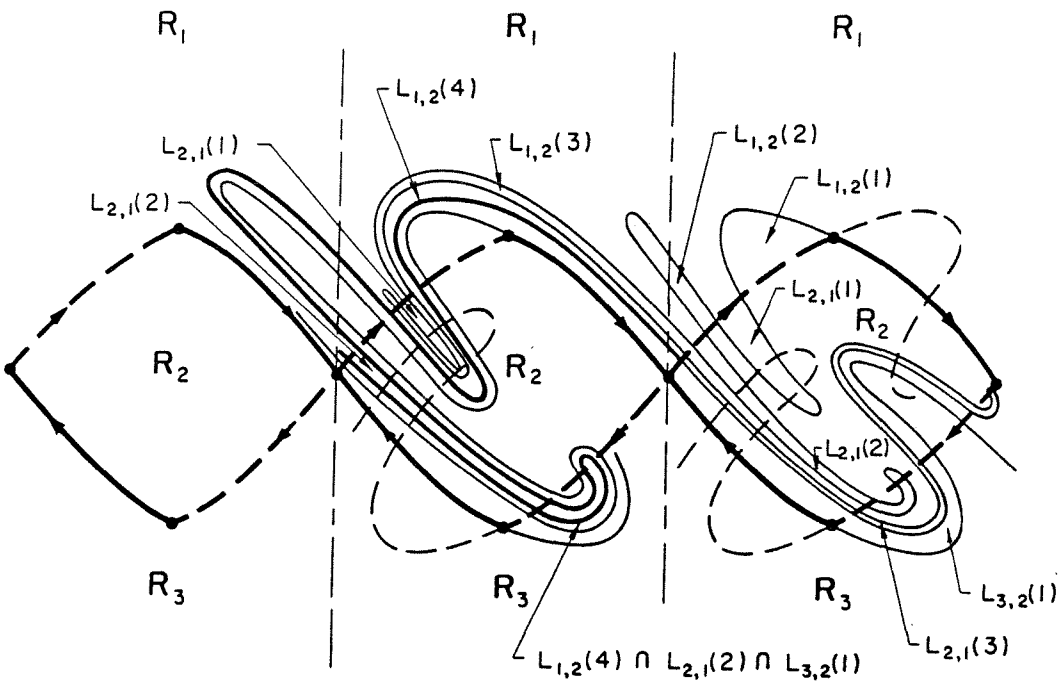

Figure 3.3.2 The Lobe intersections

We now argue that (3.3.5) and (3.3.6) hold for this example based on the geometry of the lobes in Figure 3.3.2. And indeed, consider the $L_{1,2}(n)$ lobes in Figure 3.3.2; for $n = 1, 2$ these lobes are completely contained in R_1 and therefore do not contain any S_2 or S_3 species. For $n = 1$ this is the case by definition. For $n = 2$, we learn from (3.3.5) that intersections of $L_{1,2}(2)$ with either $L_{2,1}(1)$ or $L_{2,3}(1)$ could contribute species S_2 to $L_{1,2}(2)$, but in this example these intersections are empty. Therefor, by (3.3.5), $\mu(L^2_{1,2}(2) = 0$ which is confirmed by looking at the figure. For $n = 3$ we observe that $L_{1,2}(3)$ contains particles of species S_2, and these are all contained in the set $L_{1,2}(3) \cap L_{2,1}(1)$, the only non empty set counted in (3.3.5) for $n = 3$. Finally $L_{1,2}(4)$ intersects the lobes $L_{2,1}(1)$, $L_{2,1}(2)$ and $L_{3,2}(1)$, and equation (3.3.5) tells us that $L^2_{1,2}(4)$ is given by the area of the intersection of $L_{1,2}(4)$ with the first two lobes minus the area of the intersection with the third lobe. Looking at Figure (3.3.2) we see that indeed the last intersection is exactly the portion of $L_{1,2}(4) \cap L_{2,1}(2)$ which does not belong to R_2 and had to be subtracted. Moreover, this is exactly the portion of $L_{1,2}(4)$ which contains particles of species S_3, and this is manifested by equation (3.3.6) for n=4.

Note that $\mu(L^1_{1,2}(n))$ can be obtained either from (3.2.10) or from:

$$\mu(L_{1,2}(n)) = \sum_{s=1}^{3} \mu(L^i_{1,2}(n))$$

resulting in exactly the same expression.

We can now simplify (3.3.5) and (3.3.6) by using the lobe dynamics as stated previously by **P4**, expressing the lobe content in terms of intersections of forward iterations of two lobes with two other lobes. For example, to obtain $L^3_{1,2}(n)$ we need to find the $n-1$ forward iterations of $L_{2,3}(1)$ and $L_{3,2}(1)$ since (3.3.6) implies:

$$\mu(L^3_{1,2}(n)) = \sum_{m=0}^{n-1} \mu(L_{1,2}(1) \cap F^m L_{3,2}(1)) - \sum_{m=1}^{n-1} \mu(L_{1,2}(1) \cap F^m L_{2,3}(1)) \quad (3.3.7)$$

Or in general, (3.2.10) implies:

$$\mu(L^i_{k,j}(n)) = \sum_{s=1}^{3} \sum_{l=0}^{n-1} \mu(L_{k,j}(1) \cap F^l L_{i,s}(1)) - \sum_{s=1}^{3} \sum_{l=1}^{n-1} \mu(L_{k,j}(1) \cap F^l L_{s,i}(1)) \quad (3.3.8)$$

which shows that we can immediately write:

$$\mu(L^3_{2,1}(n)) = \sum_{m=0}^{n-1} \mu(L_{2,1}(1) \cap F^m L_{3,2}(1)) - \sum_{m=1}^{n-1} \mu(L_{2,1}(1) \cap F^m L_{2,3}(1)) \quad (3.3.9)$$

hence we can find $T_{3,1}(n)$, the portion of particles transported from the lower half plane to the upper half plane, in terms of the $n-1$ forward intersections of the lobes $L_{2,3}(1)$ and $L_{3,2}(1)$ with the lobes $L_{1,2}(1)$ and $L_{2,1}(1)$ (for more details see equation (3.2.13)):

$$\begin{aligned} T_{3,1}(n) =& T_{3,1}(0) + \sum_{l=1}^{n} [\mu(L^3_{2,1}(l)) - \mu(L^3_{1,2}(l))] \\ =& \sum_{m=1}^{n-1} (n-m) \Big\{ \mu(L_{2,1}(1) \cap F^m(L_{3,2}(1)) - \mu(L_{2,1}(1) \cap F^m(L_{2,3}(1)) - \\ & \mu(L_{1,2}(1) \cap F^m(L_{3,2}(1)) + \mu(L_{1,2}(1) \cap F^m(L_{2,3}(1)) \Big\} \end{aligned} \quad (3.3.10)$$

and as before, we can compute the other $T_{i,j}(n)$'s using either (3.3.3) and (3.3.8) or the conservation laws and the symmetries (equation (3.3.1) and (3.3.2)).

To conclude, we demonstrated that equation (3.2.10) governs the transport in this geometry as well, which saved us the need to go through the same steps as in example 2 in order to find how to express the content of the lobes in terms of the lobe intersections, namely we made a major shortcut in showing that step **P3** holds in this example. This is essentially the roll of the general formulation and its proof, to guarantee that in any given geometry in which transport is governed by the motion of lobes, one can find out from the lobe definitions (e.g. (3.3.4) in this example) and from the general formulas which lobes and which intersections are needed for finding the transport rates.

Note that this example has the same geometry as a typical 1/1 resonance band. One of the questions addressed in the study of transport in area preserving maps is the influence of the resonance bands, called also the island chains, on the transport. The main reason for these studies is the observation that statistical approaches for predicting the transport rates are quite successful in the absence of islands but fail when they are present, see Lieberman and Lichtenberg [1983]. Karney [1983] addressed the question of the "stickiness" of an island chain by numerically iterating a map which models the behavior near a resonance. He started the iteration with an initial condition outside the island and computed the trapping statistics f_t of the orbit, defined to be proportional to the number of orbit segments which have a length t, the idea being that if a trajectory is trapped in a p/q resonance band it will circle the origin p times in q iterations and therefore the segment of length $t = p/q$ will appear frequently. The transport rates supply an alternative way to define the stickiness of an island chain; define the interior of the islands to be region R_2, and the bounded regions above and below the chain which are tested for the "stickiness" to be R_1 and R_3 respectively, then:

$$stickiness = \frac{T_{1,2}(n) + T_{3,2}(n)}{\mu(R_1) + \mu(R_3)}.$$

The average of the above quantity over n should be equal to the average of the trapping statistics over the regions R_1 and R_3. This suggests that an alternative way to examine the island chain stickiness is by computing $T_{1,2}(n)$ and $T_{3,2}(n)$,

where the trapping statistics may be used to approximate the lobe intersections by choosing initial conditions in the lobes $L_{2,3}(1)$ and $L_{3,2}(1)$.

4. General Formulation

In this section we present the definition of the general problem addressed in this paper, and state the main theorems which are the mathematical formulation of **P2, P3, P4** and **P5** for a general configuration.

Assumptions and Notation

Consider a two dimensional phase space, on which an area and orientation preserving diffeomorphism F is defined. Let p_i, $i = 1, .., N$, denote the hyperbolic fixed points of the map with their associated $2N$ branches of stable and $2N$ branches of unstable manifolds. Let R_j, $j = 1, .., N_R$ denote the **regions** (see definition 2.4) in phase space, and we assume that the regions are well defined so that they are distinct and their union covers all phase space. This assumption implies that when transport is permitted between neighboring regions, R_k and R_j, the boundary between them consists of a segment of a stable and a segment of an unstable manifold, and that the only mechanism for transport is the motion of lobes, as described previously for the three examples. With no loss of generality (see **R1**), we assume that across the boundaries which allow transport, only one lobe is exchanged every iteration.

Denote the lobe which leaves region R_k and enters region R_j after n iterations by $\mathbf{L_{k,j}(n)}$.

$L_{k,j}(n) = \emptyset$ when transport is not permitted, namely when R_k and R_j do not have a common boundary which consists of both stable and unstable segments which intersect each other topologically transversely, or when $k = j$. With no loss of generality (see **R3** and section 3), we assume that the lobe $L_{k,j}(n)$ is well defined in the sense that after $n - 1$ iterations, just before the crossing of the boundary between regions R_k and R_j, the lobe is completely contained in region R_k and after iteration n, just after the crossing, it is completely contained in region R_j (this condition is trivially satisfied when the lobe is the empty set), which is equivalent to requiring that:

$$L_{k,j}(n) \cap L_{l,m}(n) = \emptyset \quad \text{whenever } k \neq l \text{ or } j \neq m \tag{4.1}$$

We assume that initially particles of species S_i are uniformly distributed in region R_i, and we are interested in the redistribution of the species throughout the different regions by the map F

Denote by $\mathbf{T_{i,j}(n)}$ the amount of species S_i in region R_j just after n iterations of F.

Denote by $\mathbf{L^i_{k,j}(n)}$ the portion of lobe $L_{k,j}(n)$ which is occupied with species S_i.

Denote by $\mu(\mathbf{A})$ the area of a set A in phase space.

Theorems

By definition, $T_{i,j}(n)$ is equal to the area of the portion of R_j occupied by the species S_i immediately after the n^{th} iterate of F. The following theorem connects this area to the amount of species S_i in the lobes and is the quantitative manifestation of property **P2**.

Theorem 4.1 Given the above assumptions, the following relation between the transport rate $T_{i,j}(n)$ and the lobe content $L^i_{k,l}(n)$ holds:

$$T_{i,j}(n) - T_{i,j}(n-1) = \sum_{k=1}^{N_R} [\mu(L^i_{k,j}(n)) - \mu(L^i_{j,k}(n))] \tag{4.2}$$

proof: By the definitions of the lobes and $T_{i,j}(n)$,

$$T_{i,j}(n) - T_{i,j}(n-1) = \mu(\bigcup_{k=1}^{N_R} F^n L^i_{k,j}(n)) - \mu(\bigcup_{k=1}^{N_R} F^n L^i_{j,k}(n))$$

Since F is an area preserving map this implies:

$$T_{i,j}(n) - T_{i,j}(n-1) = \mu(\bigcup_{k=1}^{N_R} L^i_{k,j}(n)) - \mu(\bigcup_{k=1}^{N_R} L^i_{j,k}(n)) \tag{4.3}$$

By definition $L^i_{k,j}(n) \subset L_{k,j}(n)$, and by assumption (4.1) holds, hence the union in (4.3) is of disjoint sets and therefore the area of the union equals the sum of the areas, resulting in equation (4.2).

□.

The second theorem is the quantitative manifestation of **P3** and, as shown in the examples, involves more delicate questions regarding the right counting of

areas, which is not a trivial task when the sets involved intersect each other many times. Theorem 4.2 saves us the unpleasant mind boggling task of understanding the geometry and the correct counting for each individual configuration as done in the examples. Since the proof for this theorem is lengthy and its details are not enlightening, we present here only the outline, and leave the details for the appendix.

Theorem 4.2 Given the above assumptions, the following relation between the lobe content $L^i_{k,j}(n)$ and the lobe intersections holds:

$$\mu(L^i_{k,j}(n)) = \sum_{s=1}^{N_R} \sum_{m=1}^{n} \mu(L_{k,j}(n) \cap L_{i,s}(m)) - \sum_{s=1}^{N_R} \sum_{m=1}^{n-1} \mu(L_{k,j}(n) \cap L_{s,i}(m)) \quad (4.4)$$

outline of the proof: As demonstrated in the examples, for small n or for "simple" geometries equation (4.4) is obtained by interchanging union and area signs of disjoint sets, while for the more complicated geometries the sets are not disjoint and one has to prove that interchanging the signs leaves the counting right. We break down the proof of Theorem 4.2 into two cases as described below. Even though case 1 is contained in case 2, we discuss it separately since we feel that it gives more insight into the issues that are involved.

We start by proving that the the following relation holds:

$$L^i_{k,j}(n) = \bigcup_{s=1}^{N_R} \bigcup_{m=1}^{n} [L_{k,j}(n) \cap L^i_{i,s}(m)] \quad (4.5)$$

Then we distinguish between the simple (**case 1**) and the more complicated (**case 2**) cases:

case 1: $L^i_{s,i}(m) = \emptyset$ for $m = 1,..,n$ and $s = 1,...,N_R$.

case 2: $L^i_{s,i}(m) \neq \emptyset$ for some m,s, $1 \leq m \leq n$ and $1 \leq s \leq N_R$.

outline of the proof for case 1: The proof of case 1 consists of showing the following six steps:

A1. Regarding i as fixed and m and s as variable, the sets $L^i_{i,s}(m)$ are disjoint.

B1. The set $L^i_{i,s}(m)$ is given by:

$$L^i_{i,s}(m) = L_{i,s}(m) - \bigcup_{r=1}^{N_R} \bigcup_{l=1}^{m-1} [L_{i,s}(m) \cap L_{r,i}(l)] \quad (4.6)$$

C1. Regarding i as fixed and l and r as variable, the lobes $L_{r,i}(l)$ are disjoint.

D1. Regarding i, r and l as fixed and m and s as variable, the sets $L_{i,s}(m) \cap L_{r,i}(l)$ are disjoint.

E1. The following identity holds:

$$L_{k,j}(n) \cap L_{r,i}(l) \cap \{\bigcup_{s=1}^{N_R} \bigcup_{m=l+1}^{n} L_{i,s}(m)\} = L_{k,j}(n) \cap L_{r,i}(l) \qquad (4.7)$$

F1. Substitute equations (4.6) and (4.7) into equation (4.5), reindex and use A1 C1 and D1 to interchange the union and the area signs in the new equation gives (4.4).

outline of the proof for case 2:

In this case we show, using elementary set theory, that equation (4.4) gives the right counting, namely, if a "small" set A (note: "small" will be explained in detail in the appendix) is contained in $L^i_{k,j}(n)$ then $\mu(A)$ is added N_A times through the first sum in equation (4.4) and subtracted $N_A - 1$ times through the second sum, so that $\mu(A)$ is counted exactly once. Similarly, if A is not contained in $L^i_{k,j}(n)$ its area is added and subtracted M_A times through the first and second sum (respectively) to yield zero contribution to the right hand side of (4.4). The number of times $\mu(A)$ is counted depends on the number of lobes containing A and is essentially equal to the number of times A enters and leaves region R_i until iteration n.

Theorem 4.2 supplies us with the relation between the lobe content and the lobe intersections. We now want to employ the relation between the lobe intersections and the lobe dynamics, to transform equation (4.4) to a more useful form (i.e. express **P4** for the general case). As seen in the examples this step is trivial, all we need to use is the lobe dynamics rule, namely that $L_{i,j}(n)$ is mapped under l iterations to $L_{i,j}(n-l)$, and the invariance of the area under iterations of F to obtain:

Corollary 4.3: The following relations between the lobe content and the lobe intersections hold:

$$\mu(L^i_{k,j}(n)) = \sum_{s=1}^{N_R} \sum_{l=0}^{n-1} \mu(L_{k,j}(1) \cap F^l L_{i,s}(1)) - \sum_{s=1}^{N_R} \sum_{l=1}^{n-1} \mu(L_{k,j}(1) \cap F^l L_{s,i}(1)) \quad (4.9a)$$

$$\mu(L^i_{k,j}(n)) = \sum_{s=1}^{N_R}\sum_{l=0}^{n-1}\mu(F^{-l}L_{k,j}(1)\cap L_{i,s}(1)) - \sum_{s=1}^{N_R}\sum_{l=1}^{n-1}\mu(F^{-l}L_{k,j}(1)\cap L_{s,i}(1)) \tag{4.9b}$$

The last theorem deals with the conservation laws and is the basis of **P5**.

Theorem 4.4: The following $2N_R$ conservation laws hold:

$$\sum_{i=1}^{N_R}(T_{i,j}(n) - T_{i,j}(n-1)) = 0 \quad j = 1,...,N_R. \tag{4.10a}$$

$$\sum_{j=1}^{N_R}(T_{i,j}(n) - T_{i,j}(n-1)) = 0 \quad i = 1,...,N_R \tag{4.10b}$$

and (4.10) constitute $2N_R - 1$ independent equations for the $(N_R)^2$ unknowns $T_{i,j}(n) - T_{i,j}(n-1)$.

Proof: The first equation states that the total flux of all species through region R_j must be zero, since $\mu(R_j)$ is conserved. The second equation states that the total flux of species S_i through all the regions is zero, since the amount of S_i in phase space is conserved.

It is easy to see that at least one equation of the $2N_R$ equations in (4.10) is dependent of the others since the sum of the first N_R equations minus the sum of the last N_R equations is identically zero. To show that any $2N_R - 1$ equations from (4.10) are independent, note that the first N_R equations are clearly independent and so are the last N_R equations. Excluding one of the equations of the first set, we find that every equation in the second set includes terms which are not contained in any of the other $2N_R - 2$ equations, and hence the $2N_R - 1$ equations are independent.

□.

Other quantities which may be of interest are the portion of orbits which do not leave region R_i until iteration n, called $P_i(n)$, and the portion of retrapped orbits for each region, namely $T_{i,i}(n) - P_i(n)$. $P_2(n)/\mu(R_2)$ in example 3, for example, is the probability that the pendulum will oscillate for at least n periods of the forcing, while $[T_{2,2}(n) - P_2(n)]/T_{2,2}(n)$ is the probability that a pendulum, going through an oscillatory motion before the first and after the $n-1^{th}$ periods of the forcing

are completed, has gone through other forms of motion in between the first and the n^{th} iterations.

We express the $P_i(n)$'s in terms of lobe intersections as follows:

$$\begin{aligned} P_i(n) - P_i(n-1) &= -\sum_{j=1}^{N_R} \{\textit{portion of } L_{i,j}(n) \textit{ which belongs to } R_i \\ &\qquad \textit{and leaves it for the first time at iteration } n\} \\ &= -\sum_{j=1}^{N_R} \{\mu(L_{i,j}(n)) - \textit{portion of } L_{i,j}(n) \textit{ which} \\ &\qquad \textit{belongs to lobes which enter } R_i \textit{ before iteration } n\} \\ &= -\sum_{j=1}^{N_R} \{\mu(L_{i,j}(n)) - \mu(\bigcup_{m=1}^{n-1} \bigcup_{k=1}^{N_R} (L_{i,j}(n) \cap L_{k,i}(m)))\} \\ &= -\sum_{j=1}^{N_R} \{\mu(L_{i,j}(1)) - \mu(\bigcup_{m=1}^{n-1} \bigcup_{k=1}^{N_R} (L_{i,j}(1) \cap F^m L_{k,i}(1)))\} \end{aligned} \tag{4.11}$$

In this case we cannot interchange the union and the area signs since for large n the lobe intersections are not disjoint and as opposed to (4.4) we do not have a second sum to balance this effect. However, in practice, finding the area of the union is even easier than finding the sum of the areas of the lobe intersections; we showed that any set which is contained in two different lobes which enter region R_i must be also contained in a lobe which leaves that region in between the two entries. Hence, if one tests for intersections of $F^m L_{k,i}(1)$ with $L_{i,j}(1)$ and disregards all portions of $F^m L_{k,j}(1)$ which have left region R_i between iteration 1 and n one gets exactly the area of the union, in other words once a portion of the lobe leaves region R_i one need not keep track of its evolution.

5. Dissipative Systems

In many applications the map F is not area preserving (NAP), for example when the continuous time dynamical system has dissipation the resulting Poincaré map is not an area preserving map. Hence a natural generalization of the previous analysis is to NAP maps. It turns out that with some modifications most of the analysis holds.

Note that intersection of the manifolds in the NAP case has the same consequences regarding the tangling of the manifolds and the flux mechanism. The major difference is that the lobe area is not conserved under the evolution of the map, hence one needs to be more careful when referring to the dynamics of the lobes. Another difference, which is relevant to the assumptions on the regions geometry and not to the analysis, is that in NAP systems the presence of manifold intersections is less common than in conservative systems. In many cases the appearance of manifold intersections depends on the ratio between the amplitude of the forcing and the dissipation rate, where for sufficiently large dissipation there are no intersections of the manifolds, see Guckenheimer and Holmes [1983]. In this section we modify the formulation given in section 4 for NAP maps, where we point out how the formulation applies in this case and supply the modifications when necessary.

Assumptions and Notation

With the exception of F being a NAP map, so that $\mu(FA) \neq \mu(A)$ where A is a set in phase space, all the assumptions and notations are the same as in section 4.

Theorems

Following the same lines as in the previous section, we start with stating the relation between the transport rates and the lobe content. Note that in this case we need to specify at which iteration those quantities are related since the area occupied by the species varies under the evolution of the map. The expression for the flux across the boundary is very similar to the one obtained for the area preserving maps but the formula for the transport rates $T_{i,j}(n)$ is very different,

the reason being that in the NAP case the area occupied by species S_i in region R_j changes under the action of the map due to two effects:

1. Flux of species S_i across the boundary of R_j at iteration n, denoted by $a_{i,j}(n)$.
2. Change of the area occupied by species S_i within the region R_j.

Where in the area preserving case only the first effect played a roll, which made the relation between the transport rates $T_{i,j}(n)$ and the flux trivial.

We start with stating the result for the flux $a_{i,j}(n)$.

Theorem 5.1 Given the above assumptions, the following relation between the flux $a_{i,j}(n)$ and the lobe content $L^i_{k,l}(n)$ holds:

$$a_{i,j}(n) = \sum_{k=1}^{N_R} [\mu(F^n L^i_{k,j}(n)) - \mu(F^n L^i_{j,k}(n))] \tag{5.1}$$

Proof: By the definitions of the lobes and $T_{i,j}(n)$,

$$a_{i,j}(n) = \mu(\bigcup_{k=1}^{N_R} F^n L^i_{k,j}(n)) - \mu(\bigcup_{k=1}^{N_R} F^n L^i_{j,k}(n)) \tag{5.2}$$

By definition $L^i_{k,j}(n) \subset L_{k,j}(n)$, and by assumption (4.1) holds, hence

$$F^n L^i_{k,j}(n) \cap F^n L^i_{r,j}(n) = \emptyset \quad \text{for all } r \neq k$$

and similarly the $F^n L^i_{j,k}$ lobes are disjoint, hence the union in (5.2) is of disjoint sets and the area of the union equals the sum of the areas, resulting in equation (5.1).

□.

Theorem 5.2 Given the above assumptions, the following relation between the transport rate $T_{i,j}(n)$ and the lobe content $L^i_{k,j}(l)$ holds:

$$T_{i,j}(n) = \delta_{i,j}\mu(F^n R_j) + \sum_{k=1}^{N_R}\sum_{l=1}^{n} [\mu(F^n L^i_{k,j}(l)) - \mu(F^n L^i_{j,k}(l))] \tag{5.3}$$

where $\delta_{i,j}$ is the Kronecker delta.

Proof: To express the change in $T_{i,j}(n)$ we use recursively the effects of the flux and the change in area within R_j on the set $A_{i,j}(n)$, defined as the set of particles of species S_i which are in region R_j immediately after iteration n, so that by definition

$$T_{i,j}(n) = \mu(A_{i,j}(n)). \tag{5.4}$$

The recursion relation between the sets $A_{i,j}(n)$ is obtained directly from their definition and the definition of the lobes:

$$A_{i,j}(n) = \{ \textit{ image of the portion of } A_{i,j}(n-1) \textit{ which stays in } R_j \} \cup \{ \textit{ flux of species } S_i \textit{ into } R_j \textit{ on the } n^{th} \textit{ iterate } \}$$
$$= F\big(A_{i,j}(n-1) - \bigcup_{k=1}^{N_R} F^{n-1} L^i_{j,k}(n)\big) \cup \bigcup_{k=1}^{N_R} F^n L^i_{k,j}(n) \tag{5.5}$$

using (5.5) and the same reasoning as in the proof of Theorem 5.1 to argue that the sets under the union sign are disjoint we obtain:

$$\mu(A_{i,j}(n)) = \mu(F\ A_{i,j}(n-1)) - \sum_{k=1}^{N_R} \mu(F^n L^i_{j,k}(n)) + \sum_{k=1}^{N_R} \mu(F^n L^i_{k,j}(n)) \tag{5.6}$$

Using (5.6) recursively n times together with (5.4) we obtain:

$$T_{i,j}(n) = \mu(F^n A_{i,j}(0)) - \sum_{k=1}^{N_R} \sum_{l=1}^{n} \mu(F^n L^i_{j,k}(l)) + \sum_{k=1}^{N_R} \sum_{l=1}^{n} \mu(F^n L^i_{k,j}(l)) \tag{5.7}$$

now, by the definition of $A_{i,j}(n)$, $A_{j,j}(0) = R_j$ and $A_{i,j}(0) = \emptyset$ for $i \neq j$, hence (5.3) is a direct result of (5.7).

□.

For $i \neq j$ (5.3) supplies an expression for the transport rates $T_{i,j}(n)$ in terms of the lobe content. As in the area preserving case we can express the lobe content in terms of lobe intersections, leading to a computable expression for the $T_{i,j}(n)$'s. When $i = j$ we need to find $\mu(F^n(R_j))$. Luckily, we can express this quantity in terms of the other $T_{i,j}(n)$'s.

Lemma 5.3

$$\mu(F^n R_j) = \mu(R_j) - \sum_{\substack{i=1 \\ i \neq j}}^{N_R} T_{i,j}(n) + \sum_{\substack{i=1 \\ i \neq j}}^{N_R} T_{j,i}(n) \tag{5.8}$$

Proof: By the definition of the sets $A_{i,j}(n)$ the following relations hold:

$$F^n R_j = \bigcup_{i=1}^{N_R} A_{j,i}(n)$$
$$R_j = \bigcup_{i=1}^{N_R} A_{i,j}(n) \tag{5.9}$$

and since by definition the sets $A_{i,j}(n)$ are disjoint (5.9) implies:

$$\begin{aligned}\mu(A_{j,j}(n)) &= \mu(F^n R_j) - \sum_{\substack{i=1\\ i\neq j}}^{N_R} \mu(A_{j,i}(n)) \\ &= \mu(R_j) - \sum_{\substack{i=1\\ i\neq j}}^{N_R} \mu(A_{i,j}(n))\end{aligned} \tag{5.10}$$

Rearranging equation (5.10) and using (5.4) results in (5.8).

□.

We now show how to relate expressions like $\mu(F^n L^i_{j,k}(l))$ appearing in (5.1) and (5.3) to the lobe intersections. Note that in the proof of theorem 4.2 we used only the lobe and the region definitions, hence the theorem applies also for NAP maps, namely the initial lobe content is given in terms of lobe intersections by:

$$\mu(L^i_{k,j}(l)) = \sum_{s=1}^{N_R}\sum_{m=1}^{l} \mu(L_{k,j}(l) \cap L_{i,s}(m)) - \sum_{s=1}^{N_R}\sum_{m=1}^{l-1} \mu(L_{k,j}(l) \cap L_{s,i}(m)) \tag{5.11}$$

Using the lobe dynamics we can write:

$$\begin{aligned}\mu(L^i_{k,j}(l)) = &\sum_{s=1}^{N_R}\sum_{m=1}^{l} \mu(F^{-l+1} L_{k,j}(1) \cap F^{-m+1} L_{i,s}(1)) \\ &- \sum_{s=1}^{N_R}\sum_{m=1}^{l-1} \mu(F^{-l+1} L_{k,j}(1) \cap F^{-m+1} L_{s,i}(1))\end{aligned} \tag{5.12}$$

The right hand side of (5.12) is not a convenient expression to work with since the n backward iterations of all the lobes appearing in the equation are needed. Furthermore, we cannot alter it by shifting in F, as we did in the area preserving case to obtain (4.9), since F is not area preserving. Note that the flux and the transport rates are given in terms of the area of forward iterations of $L^i_{k,j}(l)$. It turns out that since F is a diffeomorphism we can just "operate" with F^n on equation (5.12), resulting in an expression similar to (4.9a) for $\mu(F^n L^i_{k,j}(l))$.

Theorem 5.4 Given the above assumptions, the following relation between the

area of $F^n L^i_{k,j}(l)$ and the lobe intersections holds:

$$\begin{aligned}\mu(F^n L^i_{k,j}(l)) = &\sum_{s=1}^{N_R}\sum_{m=0}^{l-1}\mu(F^{n-l+1}(L_{k,j}(1)\cap F^m L_{i,s}(1))) \\ &-\sum_{s=1}^{N_R}\sum_{m=1}^{l-1}\mu(F^{n-l+1}(L_{k,j}(1)\cap F^m L_{s,i}(1)))\end{aligned} \tag{5.13}$$

Proof: Since F is a diffeomorphism, for all sets A, B in phase space we have:

$$\begin{aligned} A\subset B &\Leftrightarrow F^nA\subset F^nB \qquad \text{for all } n \\ A\cap B=\emptyset &\Leftrightarrow F^nA\cap F^nB=\emptyset \quad \text{for all } n\end{aligned} \tag{5.14}$$

In addition, we showed in the proof of theorem 4.2 that for a "small enough" set A:

1. If $A\subset L^i_{k,j}(l)$ then

$$\begin{aligned}&\{A\subset L_{k,j}(l)\cap L_{i,s_t}(m_t),\ t=1,\ldots,N_A \text{ where } N_A\le l\}\Leftrightarrow \\ &\quad\{A\subset L_{k,j}(l)\cap L_{s'_t,i}(m'_t),\ t=1,\ldots,N_A-1 \text{ where } N_A\le l\}\end{aligned} \tag{5.15a}$$

2. If $A\cap L^i_{k,j}(l)=\emptyset$ then

$$\begin{aligned}&\{A\subset L_{k,j}(l)\cap L_{i,s_t}(m_t),\ t=1,\ldots,M_A \text{ where } M_A\le l\}\Leftrightarrow \\ &\quad\{A\subset L_{k,j}(l)\cap L_{s'_t,i}(m'_t),\ t=1,\ldots,M_A \text{ where } M_A\le l\}\end{aligned} \tag{5.15b}$$

Therefore, using (5.14) and (5.15) for a set $D=F^nA$ we obtain:

1. If $D\subset F^n(L^i_{k,j}(l))$ then

$$\begin{aligned}&\{D\subset F^n(L_{k,j}(l)\cap L_{i,s_t}(m_t)),\ t=1,\ldots,N_A \text{ where } N_A\le l\}\Leftrightarrow \\ &\quad\{D\subset F^n(L_{k,j}(l)\cap L_{s'_t,i}(m'_t)),\ t=1,\ldots,N_A-1 \text{ where } N_A\le l\}\end{aligned}$$

2. If $D\cap F^nL^i_{k,j}(l)=\emptyset$ then

$$\begin{aligned}&\{D\subset F^n(L_{k,j}(l)\cap L_{i,s_t}(m_t)),\ t=1,\ldots,M_A \text{ where } M_A\le l\}\Leftrightarrow \\ &\quad\{D\subset F^n(L_{k,j}(l)\cap L_{s'_t,i}(m'_t)),\ t=1,\ldots,M_A \text{ where } M_A\le l\}\end{aligned}$$

which shows that the following relation holds:

$$\mu(F^nL^i_{k,j}(l))=\sum_{s=1}^{N_R}\sum_{m=1}^{l}\mu[F^n(L_{k,j}(l)\cap L_{i,s}(m))]-\sum_{s=1}^{N_R}\sum_{m=1}^{l-1}\mu[F^n(L_{k,j}(l)\cap L_{s,i}(m))]$$

Using $F^n(A \cap B) = F^nA \cap F^nB$ together with the lobe dynamics in the above expression results in (5.13).

□.

Note that in the area preserving case we have the freedom to "operate" with F^k with different k's for different sets in an equation, leading to expressions like (4.9b), while for the NAP case the same k must be used for the whole equation.

(5.1) together with (5.13) supply a convenient expression for the flux in terms of intersections of forward iterations of $L_{i,s}(1)$ and $L_{s,i}(1)$ with $FL_{k,j}(1)$, while (5.3) together with (5.13) supply the expression for the transport rates $T_{i,j}(n)$ in terms of forward iterations of these intersections.

To obtain the equivalent equations for the conservation laws (4.10) we deduce first the following equations from (5.4) and (5.9):

$$\sum_{i=1}^{N_R} T_{i,j}(n) = \sum_{i=1}^{N_R} T_{i,j}(n-1) = \mu(R_j) \quad j = 1, \ldots, N_R \qquad (5.16a)$$

$$\sum_{j=1}^{N_R} T_{i,j}(n) = \mu(F^n R_i) \qquad i = 1, \ldots, N_R \qquad (5.16b)$$

(4.10a) and (5.16a) are identical and are actually a direct result from the definition of the $T_{i,j}(n)$'s. In general, the N_R conservation laws of (4.10b) do not have equivalent equations in the NAP case since there is no obvious relation between $\mu(F^nR_i)$ and $\mu(F^{n-1}R_i)$. However, if the map F contracts (or expands) areas at a uniform rate δ, so that $\mu(FA) = \delta\mu(A)$ for any set A, then using (5.16b) one can write the following analog for the second N_R conservation laws:

$$\sum_{j=1}^{N_R} T_{i,j}(n) = \delta \sum_{j=1}^{N_R} T_{i,j}(n-1) \quad j = 1, ..., N_R \qquad (5.17)$$

and the relation between (5.12) and (5.13) becomes trivial.

We find the equivalent quantities for the $P_i(n)$'s in the same fashion we found the transport rates for the NAP case. Define the set $B_i(n)$ to be the set of particles of species S_i which have not left R_i until iteration n, so that

$$P_i(n) = \mu(B_i(n)). \qquad (5.18)$$

Then the following recursion relation between the $B_i(n)$'s holds:

$$\begin{aligned} B_i(n) &= \{\textit{image of } B_i(n-1) \textit{ which is contained in } R_i \ \} \\ &= F(B_i(n-1) - F^{n-1}\{ \textit{ portion of } L_{i,k}(n) \textit{ lobes which have not left } R_i\}) \\ &= F(B_i(n-1)) - \bigcup_{k=1}^{N_R} \Big[F^n L_{i,k}(n) - \bigcup_{s=1}^{N_R}\bigcup_{m=1}^{n-1} F^n(L_{i,k}(n) \cap L_{s,i}(m))\Big] \end{aligned} \tag{5.19}$$

therefore,

$$\mu(B_i(n)) = \mu(F\ B_i(n-1)) - \sum_{k=1}^{N_R}\Big[\mu(F^n L_{i,k}(n)) - \mu\Big(\bigcup_{s=1}^{N_R}\bigcup_{m=1}^{n-1} F^n(L_{i,k}(n)\cap L_{s,i}(m))\Big)\Big] \tag{5.20}$$

where the first union sign can be interchanged with the area sign by the same argument as in the proof of theorem 5.1, and the second union sign cannot be interchanged since the sets under it are not disjoint. Using (5.20) recursively n times, together with (5.18) we find:

$$P_i(n) = \mu(F^n\ B_i(0)) - \sum_{k=1}^{N_R}\sum_{l=1}^{n}\Big[\mu(F^n L_{i,k}(l)) - \mu\Big(\bigcup_{s=1}^{N_R}\bigcup_{m=1}^{l-1} F^n(L_{i,k}(l)\cap L_{s,i}(m))\Big)\Big] \tag{5.21}$$

where by definition $B_i(0) = R_i$ hence the first term in (5.21) can be obtained using (5.8). Using the lobe dynamics we can simplify (5.21) farther to obtain:

$$\begin{aligned} P_i(n) = \mu(F^n R_i) - \sum_{k=1}^{N_R}\sum_{l=1}^{n}\Big[&\mu(F^{n-l+1} L_{i,k}(1)) - \\ &-\mu\Big(\bigcup_{s=1}^{N_R}\bigcup_{m=1}^{l-1} F^{n-l+1}(L_{i,k}(1)\cap F^m L_{s,i}(1))\Big)\Big] \end{aligned} \tag{5.21}$$

and the method to evaluate this quantity is similar to the one in the area preserving case with the additional complexity of having to iterate the lobe intersections.

Finally, we remark that these results may provide tools for understanding the structure of strange attracting sets of two dimensional diffeomorphisms. Recall (see Guckenheimer and Holmes [1983]) that a strange attracting set is an attracting set which contains a transverse homoclinic orbit. The transverse homoclinic orbit gives rise to a lobe structure exactly as described in this paper (see Abraham and Shaw

[1982]) and is the chaotic heart of the strange attracting set. Our results imply that the only way an orbit may asymptotically approach the strange attracting set is through the lobes. Therefore a detailed investigation of the lobe motion should reveal the structure of the strange attracting set.

6. The Application

In this section we explain how to apply the presented formulation to a given two dimensional diffeomorphism. After discussing the application of the formulation for maps, we conclude with a few notes about the construction of the Poincaré map, the tool which enables us to reduce the study of a two dimensional time periodic ordinary differential equation to a two dimensional map.

We now describe the steps one has to go through when applying the proposed method for computing the transport rates for a diffeomorphism F. With the exception of the last step, all the steps are fairly easy to perform when one has some idea about the global behavior of the map (e.g. when the map is composed of a perturbation of an integrable system or after an extensive numerical investigation of the global structure of the map has been performed) and the techniques involved can be found in several papers, for example in Ling[1986], or Mackay et al. [1987]. Therefore the main emphasis is on the last step which involves the computation of the intersections of the relevant lobes. The steps are as follows:

1: Find hyperbolic fixed points of the map.

2: Find the segments of the stable and unstable manifolds of the hyperbolic fixed points up to the pip's q_i which determine the regions appropriately (the regions should be defined according to definition 2.4 and the requirement that the regions are distinct and their union covers the phase space).

3: Find the segments $S[q_i, Fq_i]$, and define the lobes according to definition 2.3 and remarks **R1** and **R3**.

4: After labeling the regions determine which of the regions do not have a common boundary allowing transport. This will show for which r, s the $L_{r,s}(n)$ lobes are defined to be the empty sets for all n.

5: Write the conservation laws (equation (4.10)) and the symmetry laws to find which of the $T_{i,j}(n)$ are needed in order to find all the interesting transport rates for the specific map.

6: Write the relevant $T_{i,j}(n)$'s in terms of the lobe intersections and find which lobes need to be iterated (equations (4.2) and (4.9)). At this stage it is some-

times beneficial to use conservation laws and symmetries in terms of the lobes themselves:

$$\begin{aligned} \sum_{j=1}^{N_R} \mu(L_{k,j}(n)) &= \sum_{j=1}^{N_R} \mu(L_{j,k}(n)) \qquad k = 1, ..., N_R \\ \sum_{i=1}^{N_R} \mu(L^i_{k,j}(n)) &= \mu(L_{k,j}) \qquad\qquad j, k = 1, ..., N_R. \end{aligned} \tag{6.1}$$

7: Find the intersections of the lobes which appear in the formulas for the relevant transport rates derived in step 6. This step is much easier said then done. Note that after using the lobe dynamics the transport rates are expressed in terms of intersections of forward iterations of a few lobes, called the *relevant lobes*, with other $L_{r,s}(1)$ lobes (for example, in example 2 equation (3.2.13) shows that $T_{2,1}(n)$ can be found in terms of the intersection of the forward iterations of the two *relevant lobes* $L_{2,3}(1)$, $L_{3,2}(1)$ and the other lobes, $L_{r,s}(1)$, $r, s = 1, 3$). We present three approaches for computing the intersections of the *relevant lobes*:

   a. The brute force method - construct an array of grid points in the *relevant lobes* and obtain the area of their intersections with the other lobes by iterating the grid points and checking for their invasion of the other $L_{r,s}(1)$ lobes.

   b. The boundary method - follow the boundary of the *relevant lobes* and check for the intersection of the *relevant lobe* boundaries with the $L_{r,s}(1)$ lobes.

   c. The generating function method - when F is an area preserving and a twist map and is periodic in one co-ordinate (in some co-ordinate system), use the generating function of the map F for computing the area of the intersections.

We now discuss in some more detail the advantages and disadvantages of the three approaches and, in particular, provide some more detail regarding the third one.

The brute force method:

The advantages of the brute force method are simplicity and robustness with

respect to numerical round-off errors. Given the $L_{r,s}(1)$ lobe boundaries which were found in step 3, the algorithm for deciding whether a grid point is contained in such a lobe after iteration m is rather simple and the area of the intersection of the m^{th} iteration of a relevant lobe with an $L_{r,s}(1)$ lobe is approximated by the number of grid points found in an $L_{r,s}(1)$ lobe after iteration m times the area element associated with the grid points. Using a sufficiently refined grid provides an accurate measurement of the area of the lobe intersections since the numerical round-off errors can be thought of as a distortion of the grid which, on the average, should not affect the results (this was confirmed numerically for a geometry similar to the one of example 1 in Rom-Kedar et al. [1988]). The third advantage of this method is that one has an a-priori estimate of the amount of computations involved which depends linearly on the number of grid points.

The deficiency of this method is that it requires a vast amount of computations. Although it supplies a major reduction in computation when compared with a "grand scale brute force" calculation of the transport rates, i.e. the construction of an array of grid points covering the whole region of interest, it uses the same philosophy.

The boundary method:

The second method involves the computation of the evolution of the lobe boundaries; namely, the computation of larger and larger segments of the manifolds. It is a much more elegant approach then the previous one and in addition it supplies the manifold length; namely, the length of the interface between the different species which is of interest in many applications. However, there are several severe problems with this method; first, the manifolds stretch exponentially fast in time which makes them impossible to follow with reasonable accuracy after rather short times (see Franjione and Ottino [1987]). Secondly, even if the manifolds could be followed it would be a non-trivial task to distinguish between the interior and exterior of the lobe (a resolution of this problem can be found by an argument similar to the one presented for the next method), and finally this method would be very sensitive to numerical round-off errors.

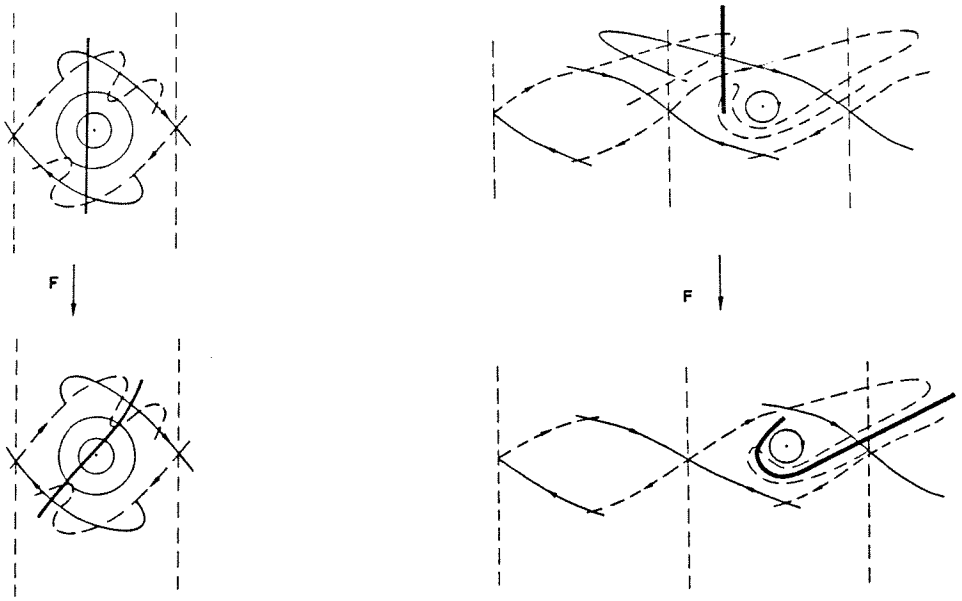

Figure 6.1 The Action of "Fast" and "Slow" Chaos on a Vertical Line.

The generating function method

The third approach appears to be the most elegant and promising one, but its implementation raises serious technical difficulties. This approach is based on the work of Mackay Meiss and Percival [1984] and the work of Bensimon and Kadanoff [1984] in which they show that for *area preserving twist maps* the *algebraic area* enclosed by the segments $S[r_0, r_1]$ and $U[r_0, r_1]$ is given by sums of the *generating function* of the map, Φ, evaluated along the orbits of r_0 and r_1. We will very briefly describe their results and concentrate on pointing out its relation to our work.

Note that this method would apply only if the map F is a twist map in a co-ordinate system for which F is periodic in the first co-ordinate:

$$F : (x, y) \mapsto (x', y') \qquad x \in T, \quad y \in R \text{ or } T$$
$$\frac{\partial x'}{\partial y} \neq 0 \quad \text{for all } x, y$$

where (x, y) may represent a new co-ordinate system in which the twist condition is satisfied. The assumption that F is periodic in x is necessary for using the results regarding the relations between the generating function and areas but it seems as if

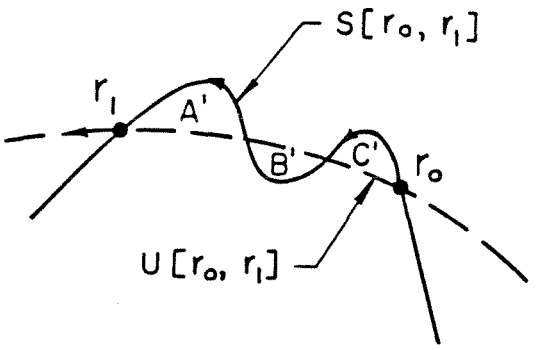

Figure 6.2 The Geometric and Algebraic Areas
The algebraic area $= \mu(A') + \mu(C') - \mu(B')$.

one could generalize the results to the non-periodic case. From the three examples that were presented in section 3, the only candidate for which this method can be applied is the third example, in which F is periodic in x. In this example, thought of as the Poincaré map of a pendulum, the twist condition is satisfied only in the "fast chaos" case in which vertical lines are not convoluted too badly after one iteration of the map, see Figure 6.1 for an illustration of the different action of the slow and fast chaos systems on a vertical segment in this geometry (the terms "slow" and "fast" refer to the frequency of the forcing in the continuous time system for which example 3 represents the Poincaré map, see Escande [1987]).

The *generating function* of an area preserving twist map F satisfies:

$$y = -\frac{\partial \Phi(x,x')}{\partial x} \qquad y' = \frac{\partial \Phi(x,x')}{\partial x'}.$$

The *algebraic area* enclosed by $S[r_0, r_1]$ and $U[r_0, r_1]$ (so that r_0, r_1 are heteroclinic, or homoclinic, points which asymptote in forward and backward times to the same fixed points) is the area enclosed underneath $S[q_0, q_1]$ (and above some reference line) minus the area enclosed underneath $U[q_0, q_1]$, see Figure 6.2, and is given by:

$$\Delta(r_0, r_1) = \sum_{t=-\infty}^{\infty} \left(\Phi(F^t r_1, F^{t+1} r_1) - \Phi(F^t r_0, F^{t+1} r_0)\right) \tag{6.2}$$

for a detailed explanation of this result and the roll of generating functions see Bensimon and Kadanoff [1984] or Mackay et al. [1984].

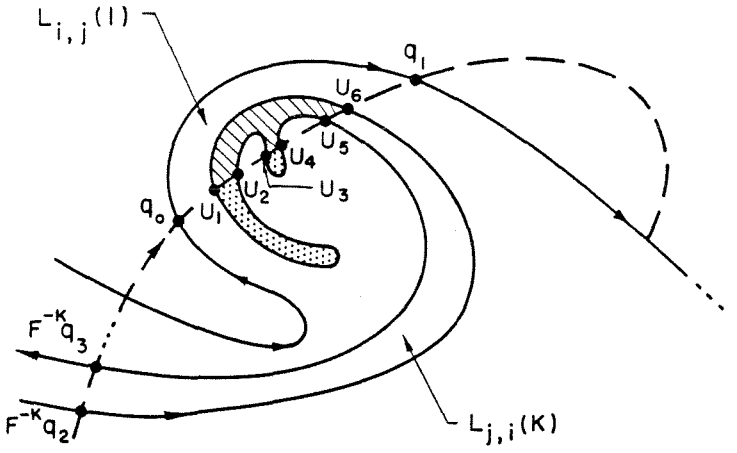

Figure 6.3 The Ordering of the Heteroclinic Points.

Back to the transport rates, note that all the lobe intersections in (4.9) are sets which are bounded by segments of stable and unstable manifolds. Hence, if F can be written as a twist map in some co-ordinate system and the heteroclinic (or homoclinic) points which determine the lobe intersections are known, one can use the above formulation for determining the area of the lobes intersections.

The relation between the algebraic and geometric areas does not pose a major difficulty; consider Figure 6.3. Let u_t, $t = 1, \ldots, 2n$ denote all the heteroclinic (or homoclinic) points which are contained in both $U[q_0, q_1]$ and $F^{-k}S[q_2, q_3]$, i.e. these are all the points which belong to the boundary of the two lobes $L_{i,j}(1)$ and $L_{l,m}(k)$, ordered according to there position along the unstable manifold so that u_1 is the closest to q_0 and u_{2n} is the closest to q_1 along the unstable manifold (note that in the figure $q_2 = q_1$, $q_3 = Fq_0$ and $l = j$, $m = i$). Since by the definition of the u_t's the segments $U[u_t, u_{t+1}]$, $S[u_t, u_{t+1}]$ do not intersect each other (excluding the end points), the algebraic and geometric areas enclosed by these segments are the same up to a minus sign. In fact, we can write:

$$\mu\big(L_{i,j}(1) \cap L_{l,m}(k)\big) = \Big| \sum_{t=1}^{n} \Delta(u_{2t-1}, u_{2t}) \Big| \tag{6.3}$$

since opposite signs of $\Delta(u_t, u_{t+1})$ indicates areas which have opposite manifolds orientation, the areas which have opposite sign to the sign of the sum in (6.3) are not contained in $L_{i,j}(1)$. The assumption that *all* the heteroclinic points contained

in both $U[q_0, q_1]$ and $F^{-k}S[q_1, q_2]$ are labeled, implies that such areas (dotted in the figure) are added and subtracted the same amount of times, hence their area does not contribute to the right hand side of (6.3).

The major difficulty with this method is the computation of the heteroclinic (or homoclinic) points, a computation which must be done sufficiently accurately to determine the area of the lobe intersections correctly. Mackay et al. [1987] addressed this problem and suggested two methods; the first is essentially equivalent to the boundary method, since one needs to compute the manifolds and use a bisection method to find the heteroclinic points. The second method involves the use of periodic orbits to limit on the heteroclinic (or homoclinic) orbits, where the periodic orbits themselves are found via minimization of sums of the generating function (called action). In particular the second method is beneficial when the action is known explicitly and this is not the case when dealing with continuous time systems. The minimization of the action in the continuous time systems corresponds to the minimization of the integral of the lagrangian among heteroclinic (or homoclinic) orbits, see Mackay and Meiss [1986].

Constructing the Poincaré map

Before we discuss some aspects of the computation of the transport rates for ordinary differential equation using the Poincaré map, we set the notation for describing it. We assume familiarity with the concept of the Poincaré map which is discussed in detail in Guckenheimer and Holmes [1983] or Wiggins [1988]. When the dynamical system is given by a conservative two dimensional system of ordinary differential equations with time periodic vector field with period Θ:

$$\begin{aligned} \dot{x} &= \frac{\partial H(x,y,t)}{\partial y} \\ \dot{y} &= -\frac{\partial H(x,y,t)}{\partial x} \end{aligned} \qquad H(x,y,t+\Theta) = H(x,y,t) \tag{6.4}$$

one can embed the system in a three dimensional space so that it has the form of a time independent three dimensional vector field by introducing the phase of the vector field as a new dependent variable:

$$\theta(t) = 2\pi t/\Theta \mod 2\pi$$

in which case (6.4) can be written as:

$$\begin{aligned} \dot{x} &= \frac{\partial H(x,y,\theta)}{\partial y} \\ \dot{y} &= -\frac{\partial H(x,y,\theta)}{\partial x} \\ \dot{\theta} &= 2\pi/\Theta. \end{aligned} \tag{6.5}$$

A two dimensional *cross-section* of the three dimensional phase space of (6.5) is given by:

$$\Sigma^{\overline{\theta}} = \{(x,y,\theta)|\theta = \overline{\theta} \in (0,2\pi]\}$$

and the Poincaré map of $\Sigma^{\overline{\theta}}$ into $\Sigma^{\overline{\theta}}$ is defined as:

$$\begin{aligned} F_{\overline{\theta}} &: \Sigma^{\overline{\theta}} \to \Sigma^{\overline{\theta}} \\ (x(\overline{\theta}), y(\overline{\theta})) &\mapsto (x(\overline{\theta}+2\pi), y(\overline{\theta}+2\pi)). \end{aligned} \tag{6.6}$$

So studying the flow via the Poincaré map is equivalent to sampling particle trajectories at time intervals equal to the period of the vector field.

Now we can apply the formulation described in the previous section to the Poincaré map $F_{\overline{\theta}}$ defined on the cross section $\Sigma^{\overline{\theta}}$. The transport rates found for $F_{\overline{\theta}}$ are the physical transport rates between the regions, sampled at intervals of the vector field period.

Four notes regarding the relations between the Poincaré map and (6.4) are now in order:

1. In most cases we do not expect to find the Poincaré map explicitly. Two alternative approaches for computing the orbit of an initial condition under $F_{\overline{\theta}}$ are:
   a. Integrate the system (6.5) for the initial condition and, starting at an initial phase $\overline{\theta}$, sample the trajectory every period Θ.
   b. Construct a numerical version of the Poincaré map by integrating (6.5) for one period (starting at the phase $\overline{\theta}$) for an array of grid points in $\Sigma^{\overline{\theta}}$, creating a table of the grid points and their images under one iteration of the map. Then, given an initial condition find its map via an appropriate extrapolation between the images of the closest grid points.

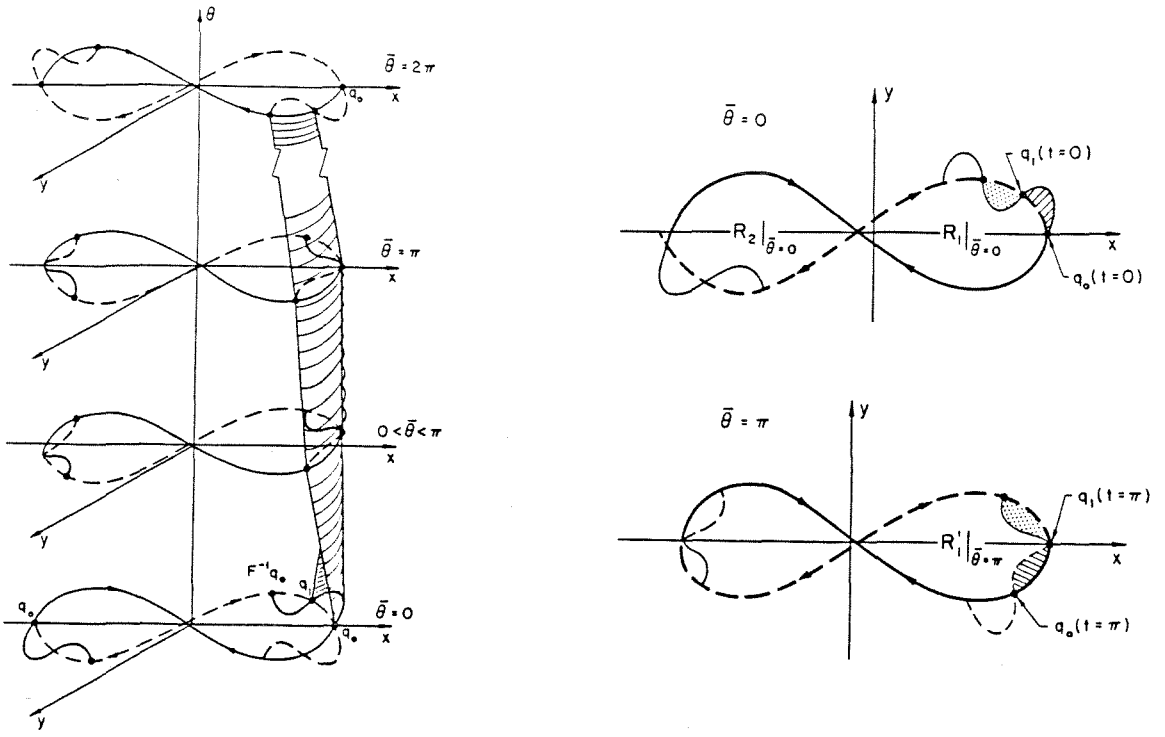

Figure 6.4 Lobe Motion in Different Poincaré Maps.

a) View of the lobe motion in the continuous time system

b) Two Poincaré sections of Figure 6.4a.

2. In many cases one can choose the phase $\overline{\theta}$ in such a way that the Poincaré map $F_{\overline{\theta}}$ has additional symmetries (see for example Rom-Kedar et al.[1988]). Such a choice of $\overline{\theta}$ reduces the amount of computations required for determining the manifolds and the transport rates. We demonstrate these reductions in the next section where we calculate the transport rates for the undamped Duffing equation.

3. It is sometimes helpful to visualize how the motion of the lobes is manifested in terms of the continuous time system (6.5). In Figure 6.4a we plot the manifolds of the undamped Duffing equation (example 2) embedded in the three dimensional space (x, y, θ), and in Figure 6.4b we plot the intersection of the manifolds with the the two Poincaré sections $\Sigma^{\overline{\theta}}$, $\overline{\theta} = 0, \pi$ (these sections have the additional symmetry of reflection about the x-axis combined with time re-

versal). One conclusion from this plot is that the difference in area between the regions $R_1|_{\overline{\theta}=0}$ and $R_1'|_{\overline{\theta}=\pi}$ (see Figure 6.4b) is exactly the area of one lobe. This observation is particularly useful for obtaining an approximation for the lobe area when one has an approximation for the area of the R_1's with an error term which is much smaller then the area of the lobe. An example for such a case is the forced pendulum where the forcing is of large amplitude and of a small frequency ε (Kaper [1988], Escande [1987]). In this case, the R_1's boundaries are ε-close to the boundaries of the equivalent regions of the unforced pendulums (the "frozen separatrices" in Escande terminology), while the lobe area is of order one. The above observation was in fact inspired by numerical evidence, found by T. Kaper, that the lobe area asymptotes to half the difference between the areas enclosed by the "frozen separatrices", corresponding to the the phases 0 and π/ε, as $\varepsilon \to 0$ (the half is needed since in this geometry two identical lobes enter region R_1 after π/ε, one from the upper and one from the lower half plane).

4. The generating function approach for the Poincaré map is equivalent to the lagrangian formulation for the continuous time system. In particular, the flux in the continuous time system is related to the integral of the lagrangian evaluated along a heteroclinic (or homoclinic) orbits, see Mackay and Meiss [1986].

7. An Example - The Undamped Duffing Equation

The Duffing equation serves as a classical example for the complicated dynamics associated with nonlinear oscillators exhibiting phenomena like chaos and strange attractors. For parameter values for which the equation is near integrable, analytical methods such as averaging and Melnikov techniques have been used to understand the structure of this equation (see Guckenheimer and Holmes [1983] and references therein). In this section, we do not attempt to investigate the rich behavior associated with the Duffing equation but merely use it as an example for demonstrating our method. Hence we pick specific parameter values which supply us with a nice geometry, and in particular, we choose the non-dissipative case in which additional symmetries are present. An interesting question, which is beyond the scope of this paper, is the relation between the lobe dynamics and the strange attractor in the dissipative case.

The Duffing equation with a negative linear stiffness term is given by:

$$\ddot{x} + \delta\dot{x} - x - x^3 = \gamma\cos(\omega t) \qquad x \in R \tag{7.1a}$$

the parameters values which we use are:

$$\delta = 0.0 \qquad \gamma = 0.5 \qquad \omega = 3.0 \tag{7.1b}$$

and from now on we will omit the dissipation term $\delta\dot{x}$ from the equations.

Equation (7.1), a second order time dependent differential equation, can be written in the form of a three dimensional time independent system as follows:

$$\begin{aligned} \dot{x} &= y \\ \dot{y} &= x - x^3 + \gamma\cos(\theta) \qquad\qquad q = (x, y, \theta) \in R \times R \times T \\ \dot{\theta} &= \omega \end{aligned} \tag{7.2}$$

where T is a circle of length 2π and the analysis is done in Poincaré sections of (7.2). Note that (7.2) can be written as a Hamiltonian system (this is not true when $\delta \neq 0$), hence its Poincaré maps, defined as in (6.6), are area preserving maps.

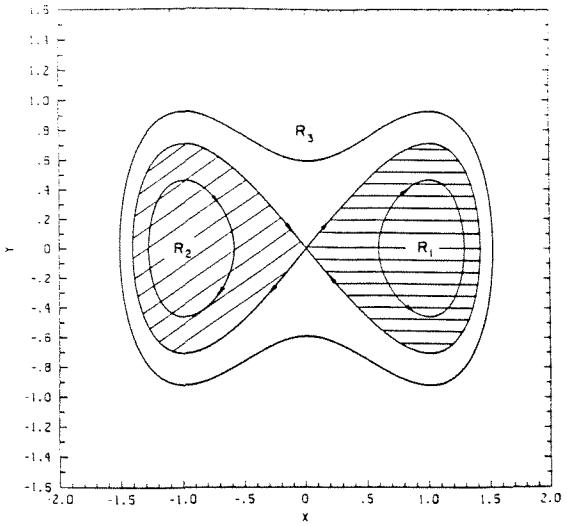

Figure 7.1 Phase Space of the Unperturbed Duffing Equation.

The global structure of (7.2) can be inferred from the analysis of the integrable system one obtains when setting $\gamma = 0$ in (7.2). The Poincaré map of the integrable system is shown in Figure 7.1. Note that in the integrable case the origin is a hyperbolic fixed point, connected to itself by two homoclinic loops. These loops divide phase space into three separate regions, shown in Figure 7.1. For small γ one can calculate the Melnikov function and prove that the stable and unstable manifolds of the perturbed fixed point intersect each other transversely, hence for $\gamma \neq 0$ (with $\delta = 0$) (7.2) is non-integrable and we expect to see geometrical structure similar to the one discussed in example 2 of section 3.

To begin our analysis we need to find the position of the perturbed fixed point and its stable and unstable manifolds. It turns out that even in this early stage the use of symmetry in the Poincaré sections can reduce our calculations significantly, hence we begin with describing the Poincaré maps symmetries.

Poincaré Map Symmetries

There are two types of symmetries of the Poincaré maps $F_{\overline{\theta}}$ which are of interest:

1. Symmetries which relate orbits of different Poincaré maps:
   given that $\{(x_n, y_n)\}_{n=-\infty}^{\infty}$ is an orbit of $F_{\overline{\theta}}$ (i.e. there exists a solution q(t) of (7.2) such that $q(\overline{\theta} + 2\pi n/\omega) = (x_n, y_n, \overline{\theta})$) the symmetry action supplies an

orbit $\{(\tilde{x}_m, \tilde{y}_m)\}_{m=-\infty}^{\infty}$ of the Poincaré map $F_{\tilde{\theta}}$.

2. Symmetries which relate orbits of a Poincaré map to orbits of the same map; given that $\{(x_n, y_n)\}_{n=-\infty}^{\infty}$ is an orbit of $F_{\overline{\theta}}$ the symmetry action supplies an orbit $\{(\tilde{x}_m, \tilde{y}_m)\}_{m=-\infty}^{\infty}$ of the same Poincaré map $F_{\overline{\theta}}$.

The symmetries may depend on the phase $\overline{\theta}$, and different maps may have different numbers of symmetries.

For the undamped Duffing equation we find that there exists one symmetry of the first kind, relating orbits of every Poincaré map $F_{\overline{\theta}}$ to orbits of the Poincaré map $F_{\overline{\theta}+\pi}$, and there are two symmetries of the second kind, one symmetry for the Poincaré maps F_0 and F_π and the other for the maps $F_{\frac{\pi}{2}}$ and $F_{\frac{3\pi}{2}}$.

Finding the Poincaré Map Symmetries

To obtain the image of an initial condition (x_0, y_0) under the map $F_{\overline{\theta}}$ one has to integrate (7.2) for one period $2\pi/\omega$ starting with the initial conditions $(x, y, \theta) = (x_0, y_0, \overline{\theta})$, which is equivalent to solving the system

$$\begin{aligned} \dot{x} &= y \\ \dot{y} &= x - x^3 + \gamma \cos(\theta + \overline{\theta}) \\ \dot{\theta} &= \omega \end{aligned} \tag{7.3}$$

with the initial condition $(x, y, \theta) = (x_0, y_0, 0)$ for one period.

Hence, finding symmetries of the Poincaré maps corresponds to finding symmetries of (7.3), where for symmetries of the first kind $\overline{\theta}$ is variable and for the symmetries of the second kind it is fixed.

It is easy to check that (7.3) has the following symmetries:

1. Symmetry of the first kind:

$$x \mapsto -x, \quad y \mapsto -y, \quad \overline{\theta} \mapsto \overline{\theta} + \pi \qquad \text{for all } \overline{\theta}.$$

This symmetry relates Poincaré maps which are 180° apart in $\overline{\theta}$ by a 180° rotation about the origin.

2. Symmetry of the second kind:

$$x \mapsto -x, \quad t \mapsto -t \qquad \text{for } \overline{\theta} = \frac{\pi}{2} \text{ or } \overline{\theta} = \frac{3\pi}{2}.$$

This symmetry implies that the Poincaré maps $F_{\frac{\pi}{2}}$ and $F_{\frac{3\pi}{2}}$ are symmetric with respect to reflection about the y-axis with a time reversal. Note that the notion of symmetry with time reversal is very useful since it relates stable and unstable manifolds!

3. Symmetry of the second kind:

$$y \mapsto -y, \quad t \mapsto -t \qquad \text{for } \overline{\theta} = 0 \text{ or } \overline{\theta} = \pi.$$

This symmetry implies that the Poincaré maps F_0 and F_π are symmetric with respect to reflection about the x-axis with time reversal.

We begin the analysis of equation (7.2) according to the plan proposed in section 6. In general it is sufficient to investigate the dynamics of one Poincaré map since all the Poincaré maps are differentiably equivalent and in particular the transport rates are identical in all of them. We choose a map which has as many symmetries as possible, so that for the undamped Duffing equation the maps $F_0, F_\pi, F_{\frac{\pi}{2}}$ and $F_{\frac{3\pi}{2}}$ are good candidates. We choose to work with F_0.

Finding the Fixed Point of F_0

Since F_0 is symmetric with respect to reflection about the x-axis with time reversal, the fixed point must lie on the x-axis. Hence, after obtaining an analytical first approximation to the fixed point location, we numerically bracket it on the x-axis (in the Poincaré section $\overline{\theta} = 0$) to get higher order corrections for its location.

To get a first approximation for the fixed point location we construct an expansion in γ about the origin:

$$p(t) = (x(t), y(t), \theta(t)) = \gamma p_1(t) + \gamma^2 p_2(t) + \dots$$

plug it in (7.3) and impose periodicity to obtain:

$$\begin{aligned} x(t) &= -\frac{\gamma}{1+\omega^2}\cos(\omega t) + O(\gamma^3) \\ y(t) &= \frac{\gamma\omega}{1+\omega^2}\sin(\omega t) + O(\gamma^3) \\ \theta(t) &= \omega t \end{aligned}$$

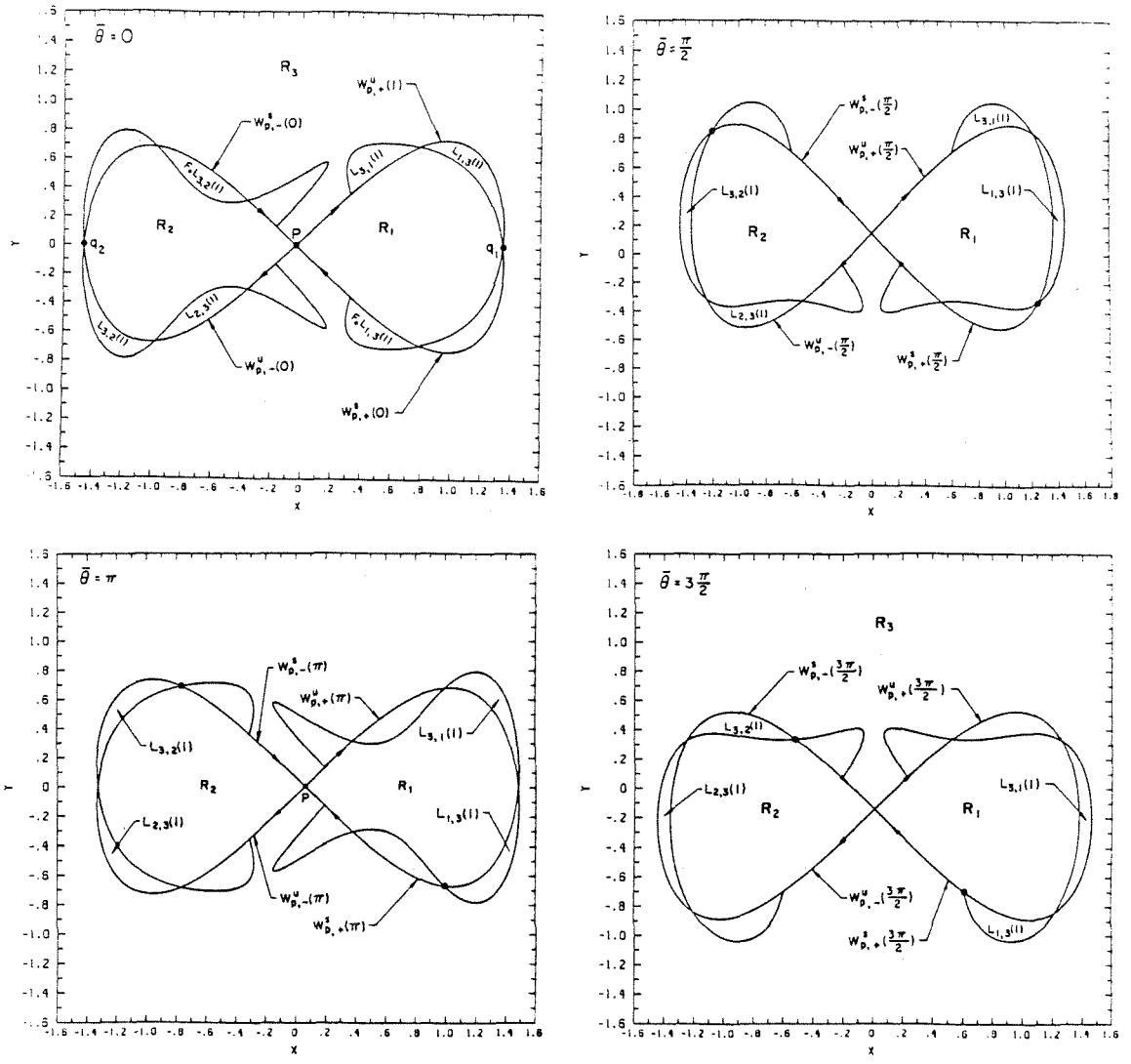

Figure 7.2 Lobe Motion in Different Poincaré Maps

and in particular, we obtain that the fixed point of F_0 is located at:

$$p(0) = (x(0), y(0), 0) = (-\frac{\gamma}{1+\omega^2}, 0, 0) + O(\gamma^3).$$

For the parameter values $\gamma = 0.5, \omega = 3.0$ we find that the error term is much smaller than γ^3, and we obtain numerically that $p(0) = (-0.0500097 + O(10^{-8}), 0, 0)$.

Finding the Stable and Unstable Manifolds of p under F_0 At this step the use of the symmetries reduces the calculations by a factor of four. Since we expect the homoclinic connections to break up, four branches of the fixed point p need to be computed. Denote the four branches of p at the Poincaré section $\Sigma^{\bar{\theta}}$ by $W^u_{p,+}(\bar{\theta}), W^u_{p,-}(\bar{\theta}), W^s_{p,+}(\bar{\theta})$ and $W^s_{p,-}(\bar{\theta})$, see Figure 7.2a.

Note that the symmetries of the Poincaré maps relate the different branches of the manifolds :

1. The first symmetry shows that the "+" branches of the stable and unstable manifolds of the Poincaré map $F_{\overline{\theta}}$ are mapped under rotation of 180° to the "-" branches of the stable and unstable manifolds (respectively) of $F_{\overline{\theta}+\pi}$, compare for example Figures 7.2a and 7.2c.
2. The second symmetry shows that for $\overline{\theta} = \pi/2,\ 3\pi/2$, the "+" branches of the stable and unstable manifolds are mapped under reflection about the y-axis to the "-" branches of the unstable and stable manifolds (respectively), see Figure 7.2b or 7.2d.
3. The third symmetry shows that for $\overline{\theta} = 0,\ \pi$, the "+" and "-" branches of the stable manifold are mapped under reflection about the x-axis to the "+" and "-" branches (respectively) of the unstable manifold, see Figure 7.2a or 7.2c.

Combining these three observations, we can create Figure 7.2 by computing only one branch of the manifolds, say $W^u_{p,-}(\overline{\theta})$ for $\overline{\theta} = 0,\ \pi/2,\ \pi,\ 3\pi/2$, which means in practice that we compute only one branch of the unstable manifold, and sample the trajectories four times per period instead of only one time (as one does when computing the manifolds usually).

Figure 7.2a for example is obtained as follows: a reflection of $W^u_{p,-}(0)$ about the x-axis gives $W^s_{p,-}(0)$, a rotation by 180° of $W^u_{p,-}(\pi)$ about the origin gives $W^u_{p,+}(0)$, and a reflection of $W^u_{p,+}(0)$ about the x-axis gives $W^s_{p,+}(0)$.

Defining the Regions and Finding the Relevant Lobes The symmetries are useful in defining the regions and lobes, where the point of the first intersection of a branch with the axis of symmetry is the natural choice for the q_i's. We therefore define R_1 to be the region bounded by the segments of $W^u_{p,+}(0)$ and $W^s_{p,+}(0)$ starting at p and ending at the first intersection of these branches with the x-axis, denoted by q_1. We define R_2 similarly, and define R_3 to be the compliment of R_1 and R_2, see Figure 7.3. Note that if one prefers to define the regions using different pips, it is an easy task to find the relation between the transport rates found for the differently defined regions.

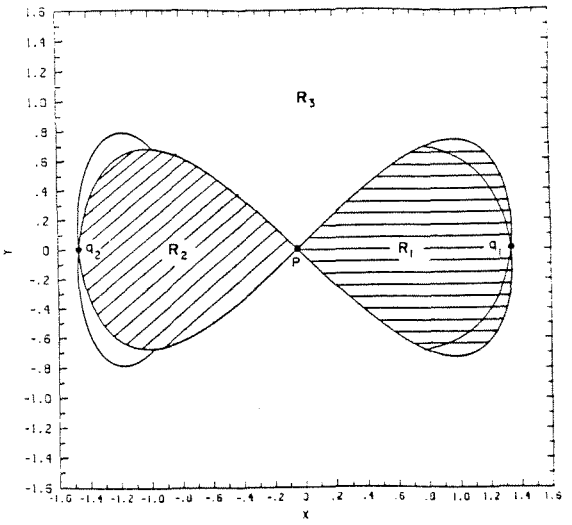

Figure 7.3 Definition of the Regions

As in example 2 of section 3, we note that the geometry of the regions implies that the lobes $L_{1,2}(n)$ and $L_{2,1}(n)$ are the empty set for all n.

To demonstrate the transport rate calculation, we will compute $T_{1,2}(n)$ and $T_{2,1}(n)$ which are given in terms of lobe intersections by (see (3.2.13) and the general formulation):

$$\begin{aligned} T_{2,1}(n) = \sum_{m=1}^{n-1}(n-m)\Big\{&\mu(L_{3,1}(1)\cap F_0^m(L_{2,3}(1)) - \mu(L_{3,1}(1)\cap F_0^m(L_{3,2}(1)) \\ &- \mu(L_{1,3}(1)\cap F_0^m(L_{2,3}(1)) + \mu(L_{1,3}(1)\cap F_0^m(L_{3,2}(1))\Big\} \\ T_{1,2}(n) = \sum_{m=1}^{n-1}(n-m)\Big\{&\mu(L_{3,2}(1)\cap F_0^m(L_{1,3}(1)) - \mu(L_{3,2}(1)\cap F_0^m(L_{3,1}(1)) \\ &- \mu(L_{2,3}(1)\cap F_0^m(L_{1,3}(1)) + \mu(L_{2,3}(1)\cap F_0^m(L_{3,1}(1))\Big\} \end{aligned} \tag{7.4}$$

(7.4) shows that to compute $T_{2,1}(n)$ we need to compute the areas of the four lobe intersections:

$$L_{3,1}(1)\cap F_0^m(L_{2,3}(1)),\ \ L_{3,1}(1)\cap F_0^m(L_{3,2}(1)),$$

$$L_{1,3}(1)\cap F_0^m(L_{2,3}(1)),\ \ L_{1,3}(1)\cap F_0^m(L_{3,2}(1))$$

for $m = 1, \ldots, n-1$ and similarly, to compute $T_{1,2}(n)$ we need to compute the areas of the four lobe intersections:

$$L_{3,2}(1)\cap F_0^m(L_{1,3}(1)),\ \ L_{3,2}(1)\cap F_0^m(L_{3,1}(1)),$$

$$L_{2,3}(1)\cap F_0^m(L_{1,3}(1)),\ \ L_{2,3}(1)\cap F_0^m(L_{3,1}(1))$$

for $m = 1, \ldots, n-1$ and therefore, the relevant lobes which we need to integrate are $L_{2,3}(1)$, $L_{3,2}(1)$ $L_{1,3}(1)$ and $L_{3,1}(1)$.

Computing the lobe Intersections

Note that the symmetries supply relations between the different lobe intersections, for example:

1. By the symmetry with respect to reflection about the y-axis with time reversal of the Poincaré map $F_{\frac{\pi}{2}}$, see Figure 7.2b, we obtain that

$$\mu(F_{\frac{\pi}{2}}^m L_{3,2}(1) \cap L_{3,1}(1)) = \mu(F_{\frac{\pi}{2}}^{-m} L_{1,3}(1) \cap F_{\frac{\pi}{2}} L_{2,3}(1))$$

   and since area is preserved, this implies that

$$\begin{aligned}\mu(F_0^m L_{3,2}(1) \cap L_{3,1}(1)) &= \mu(F_0^{-m} L_{1,3}(1) \cap F_0 L_{2,3}(1)) \\ &= \mu(L_{1,3}(1) \cap F_0^{m+1} L_{2,3}(1))\end{aligned}$$

   hence two of the first four intersections that we need to find are related.

2. By the symmetry with respect to reflection about the x-axis and with time reversal of the Poincaré map F_0, see Figure 7.2a, we obtain that

$$\begin{aligned}\mu(F_0^m L_{2,3}(1) \cap L_{3,1}(1)) &= \mu(F_0^{-m} F_0 L_{3,2}(1) \cap F_0 L_{1,3}(1)) \\ &= \mu(F_0^m L_{1,3}(1) \cap L_{3,2}(1))\end{aligned}$$

   supplying a relation between two other intersections.

3. By the symmetry with respect to 180° rotation between the Poincaré maps F_0 and F_π, see Figure 7.2a and 7.2c, we obtain that

$$\begin{aligned}\mu(F_0^m F_0 L_{2,3}(1) \cap L_{1,3}(1)) &= \mu(F_\pi^m L_{1,3}(1) \cap L_{2,3}(1)) \\ &= \mu(F_0^m L_{1,3}(1) \cap L_{2,3}(1)).\end{aligned}$$

Using the same arguments for the different maps and symmetries, we obtain the following relations:

$$\begin{aligned}\mu(L_{3,2}(1) \cap F_0^m L_{1,3}(1)) &= \mu(L_{3,1}(1) \cap F_0^m L_{2,3}(1)) \quad = e_1(m) \\ \mu(L_{3,2}(1) \cap F_0^m L_{3,1}(1)) &= \mu(L_{2,3}(1) \cap F_0^{m-1} L_{1,3}(1)) \\ &= \mu(L_{1,3}(1) \cap F_0^m L_{2,3}(1)) \\ &= \mu(L_{3,1}(1) \cap F_0^{m-1} L_{3,2}(1)) = e_2(m-1) \\ \mu(L_{2,3}(1) \cap F_0^m L_{3,1}(1)) &= \mu(L_{1,3}(1) \cap F_0^m L_{3,2}(1)) = e_3(m)\end{aligned}$$

Therefore it is sufficient to integrate two lobes, say $L_{2,3}(1)$ and $L_{3,2}(1)$, and the transport rates $T_{1,2}(n)$ and $T_{2,1}(n)$ are given in terms of the e_i's by:

$$\begin{aligned} T_{2,1}(n) &= \sum_{m=1}^{n-1}(n-m)[e_1(m) - e_2(m) - e_2(m-1) + e_3(m)] \\ T_{1,2}(n) &= \sum_{m=1}^{n-1}(n-m)[e_1(m) - e_2(m-1) - e_2(m) + e_3(m)] \end{aligned} \tag{7.5}$$

so actually $T_{2,1}(n) = T_{1,2}(n)$.

We use the "brute force" method for computing the lobe intersections. The symmetry is utilized in the code; first we initialize the lobes $L_{3,2}(1)$ and $F_0L_{2,3}(1)$ using the same grid construction reflected about the x-axis, then we perform the test for the trapping of the grid points in the lobes $L_{3,1}$ and $L_{1,3}$ in the Poincaré section $\overline{\theta} = \pi$, where these lobes are the exact reflection of $L_{3,2}(1)$ and $F_0L_{2,3}(1)$ about the y-axis. So that we use only one calculation of a lobe boundary for initializing the grid points and performing the tests.

In Figure 7.4 we show the evolution of the lobe $L_{2,3}(1)$ under the map F_0 for 8 iterations where as explained above we start with distributing grid points in $F_0L_{2,3}(1)$ to save the computation of another lobe boundary. We use a mesh size of 0.005, resulting in 3169 grid points in the lobe. We use a fourth order Runge-Kutta scheme for the integration. The results of the computation of the areas of the lobe intersections, normalized by the lobe area, are given in table 7.1, and the transport rates, normalized by the total flux through the regions untill iteration n, i.e. $n\mu(L_{1,3}(1)$, is given in table 7.2. The mesh size we use is crude, and as seen in Figure 7.4 the rapid stretching separates the grid points to the extend that the lobe does not appear to be connected after 6 iterates of the map. Decreasing the grid mesh size to 0.004 or decreasing the integration step size by a factor of 2 shows that one gets an error at the most significant digit after 7 iterations of the map. This result shows that if one uses enough grid points and enough accuracy in the integration scheme, the results will converge to the transport rates. It also demonstrates that "enough" can be rather large. A significant improvement in the accuracy of the computation can be achieved by using schemes which preserve areas

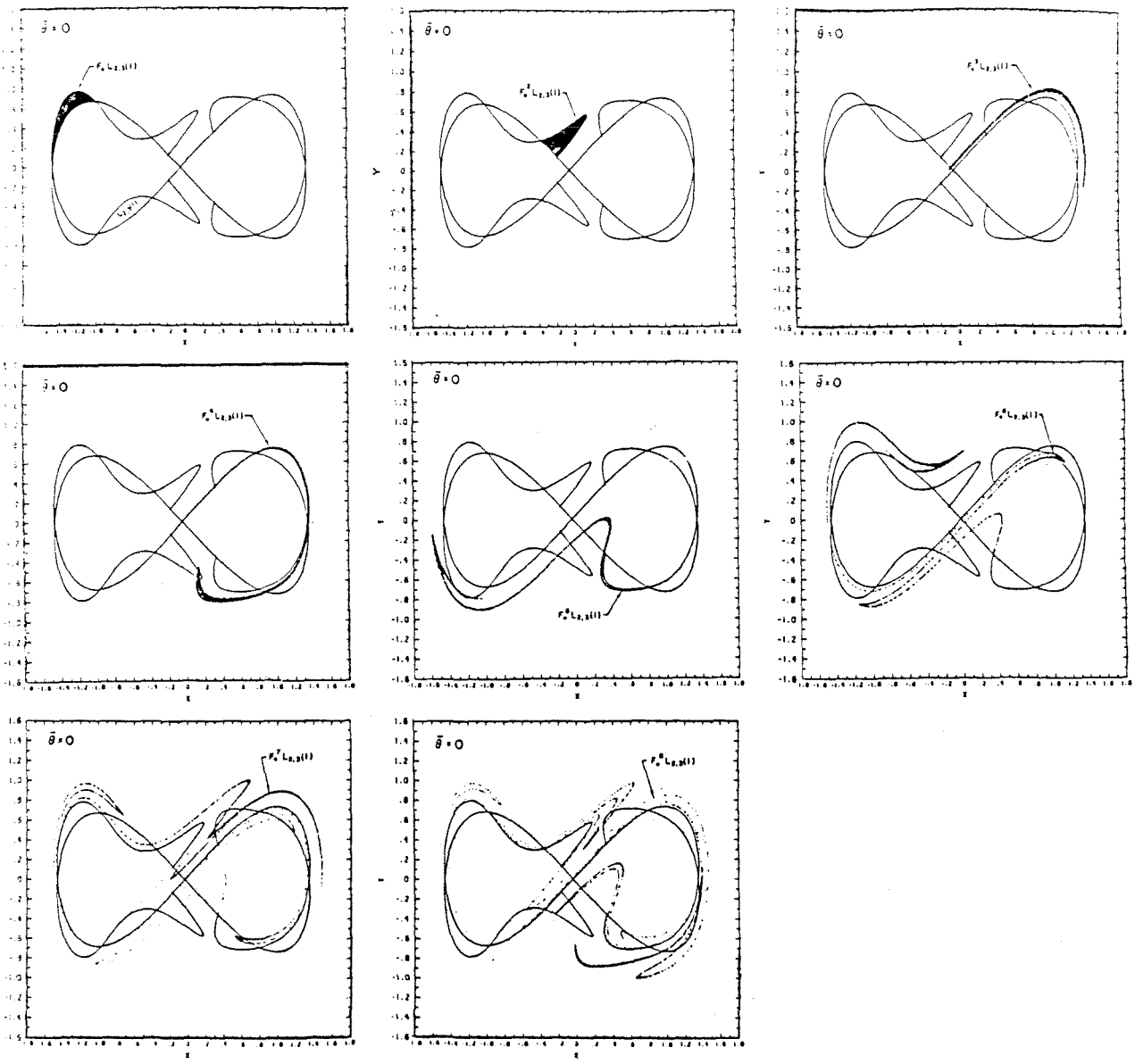

Figure 7.4 Numerical Iterates of the Lobe $L_{2,3}(1)$

in the Poincaré map such as symplectic integration algorithms, see Channell and Scovel [1988].

n	e_1	e_2	e_3
1	0.0000	0.0000	0.0000
2	0.0000	0.0000	0.0000
3	0.1918	0.0000	0.0000
4	0.0362	0.0000	0.0000
5	0.0047	0.0732	0.0000
6	0.0006	0.0369	0.0000
7	0.0902	0.0072	0.0000
8	0.0268	0.0249	0.0274
9	0.0059	0.0113	0.0236
10	0.0022	0.0426	0.0072

Table 7.1 The Area of the Lobe Intersections.

n	$T_{1,2}(n)$	$T_{1,2}(n) - T_{1,2}(n-1)$
1	0.0000	0.0000
2	0.0000	0.0000
3	0.0000	0.0000
4	0.0479	0.0479
5	0.0840	0.0456
6	0.0966	0.0266
7	0.0899	0.0071
8	0.0907	0.0120
9	0.0938	0.0131
10	0.0956	0.0111

Table 7.2 The Transport Rates and the Flux.

Appendix 1: Proof of Theorem 4.2

Before embarking on the proof as outlined in section 4, we prove the following four lemmas which are used in both the proof of case 1 and case 2:

Lemma A1.1 : If a point p is contained in two different lobes which leave region R_i at iteration n_1 and n_2 respectively, where $n_1 < n_2 - 1$, i.e. for some s_1 and s_2 $p \in L_{i,s_1}(n_1) \cap L_{i,s_2}(n_2)$, then p is also contained in a lobe which enters R_i at iteration m, where $n_1 < m < n_2$, i.e. there exists an s_3 such that $p \in L_{s_3,i}(m)$.

Lemma A1.2 : If a point p is contained in two different lobes which enter region R_i at iteration n_1 and n_2 respectively, where $n_1 < n_2 - 1$, i.e. for some s_1 and s_2 $p \in L_{s_1,i}(n_1) \cap L_{s_2,i}(n_2)$, then p is also contained in a lobe which leaves R_i at iteration m, where $n_1 < m < n_2$, i.e. there exists an s_3 such that $p \in L_{i,s_3}(m)$.

Lemma A1.3 : If the intersection of two different lobes which enter region R_i at iteration n_1 and n_2 respectively, where $n_1 < n_2 - 1$, is non empty, i.e. for some s_1 and s_2 $L_{s_1,i}(n_1) \cap L_{s_2,i}(n_2) \neq \emptyset$, then there exists a lobe which enters region R_i at iteration $n_2 - n_1$ and contains species S_i. Specifically, it will follow that $L^i_{s_2,i}(n_2 - n_1) \neq \emptyset$.

Lemma A1.4 : The following relation holds for all $k, j, r, i \in \{1, \ldots, N_R\}$ and $1 \leq l < n$:

$$L_{k,j}(n) \cap L_{r,i}(l) \subset \bigcup_{s=1}^{N_R} \bigcup_{m=l+1}^{n} L_{i,s}(m). \qquad (A1.1)$$

Lemma A1.5: If $p \in L^i_{k,j}(l)$ then there exist r', l', such that $p \in L_{i,r'}(l')$ and $l' < l$.

Proof of Lemma A1.1 :

$$\left.\begin{array}{l} p \in L_{i,s_1}(n_1) \Rightarrow F^{n_1}p \quad \notin R_i \\ p \in L_{i,s_2}(n_2) \Rightarrow F^{n_2-1}p \in R_i \end{array}\right\} \Rightarrow F^{n_1}p \in L_{s_3,i}(n') \quad \text{where} \quad 1 \leq n' \leq (n_2 - n_1 - 1)$$

$$\Rightarrow p \in F^{-n_1} L_{s_3,i}(n') = L_{s_3,i}(m) \quad \text{where} \quad m = n' + n_1, \quad \text{hence} \quad n_1 < m < n_2. \quad \square$$

Proof of Lemma A1.2 :

$$\left.\begin{array}{l} p \in L_{s_1,i}(n_1) \Rightarrow F^{n_1}p \quad \in R_i \\ p \in L_{s_2,i}(n_2) \Rightarrow F^{n_2-1}p \notin R_i \end{array}\right\} \Rightarrow F^{n_1}p \in L_{i,s_3}(n') \quad \text{where} \quad 1 \leq n' \leq (n_2 - n_1 - 1)$$

$\Rightarrow p \in F^{-n_1} L_{i,s_3}(n') = L_{i,s_3}(m)$ where $m = n' + n_1$, hence $n_1 < m < n_2$. □.

Proof of Lemma A1.3 :

$$\left.\begin{array}{l} p \in L_{s_1,i}(n_1) \Rightarrow F^{n_1} p \in R_i \\ p \in L_{s_2,i}(n_2) \Rightarrow F^{n_1} p \in L_{s_2,i}(n_2 - n_1) \end{array}\right\} \Rightarrow F^{n_1} p \in L^i_{s_2,i}(n_2 - n_1)$$

$\Rightarrow L^i_{s_2,i}(n_2 - n_1) \neq \emptyset$. □.

Proof of Lemma A1.4 : If $L_{k,j}(n) \cap L_{r,i}(l) = \emptyset$ then the relation (A1.1) is trivially satisfied. Let us assume that $L_{k,j}(n) \cap L_{r,i}(l) \neq \emptyset$ and that (A1.1) is not satisfied, namely there exists a p such that:

$$p \in L_{k,j}(n) \cap L_{r,i}(l) \qquad (A1.2)$$

but

$$p \notin \bigcup_{s=1}^{N_R} \bigcup_{m=l+1}^{n} L_{i,s}(m). \qquad (A1.3)$$

From (A1.2) we obtain:

$$a) \quad F^n p \in R_j, \qquad b) \quad F^{n-1} p \notin R_j \qquad c) \quad F^l p \in R_i \qquad (A1.4)$$

Since (A1.3) shows that p cannot leave region R_i after iteration l, and $A1.4c$ shows that $F^l p$ is indeed in R_i we obtain

$$F^{l'} p \in R_i \qquad \text{for } l' = l, \ldots, n. \qquad (A1.5)$$

Now, if $i \neq j$, $A1.4a$ and $A1.5$ contradict each other, and if $i = j$ $A1.4b$ and $A1.5$ contradict each other, hence either $L_{k,j}(n) \cap L_{r,i}(l) = \emptyset$ or

$$p \in \bigcup_{s=1}^{N_R} \bigcup_{m=l+1}^{n} L_{i,s}(m).$$

□.

Proof of lemma A1.5: $p \in L^i_{k,j}(l)$ implies that $p \in R_i$ and that $F^m p \notin R_i$, where $m = l$ if $i = j$ and $m = l - 1$ if $i \neq j$, which shows that p is contained in a lobe which leaves R_i until iteration m, namely in a $L_{i,r'}(l')$ lobe with $l' \leq l$.

□.

We now start with the proof of Theorem 4.2 as outlined in section 4.

We begin with the proof of equation (4.5):

$$L^i_{k,j}(n) = \bigcup_{s=1}^{N_R} \bigcup_{m=1}^{n} [L_{k,j}(n) \cap L^i_{i,s}(m)] \tag{4.5}$$

We prove first that the left hand side (lhs) of equation (4.5) is contained in the right hand side (rhs) of this equation:

Let a point in phase space p, be contained in the lhs of (4.5), $p \in L^i_{k,j}(n)$. Then, by lemma A1.5 there exist an s and an m such that $m \leq n$ and $p \in L_{i,s}(m)$. Therefore, using $p \in R_i$ and $p \in L_{k,j}(n)$ we obtain that there exist m and s such that $p \in L_{k,j}(n) \cap L^i_{i,s}(m)$ with $m \leq n$, hence that the lhs is contained in the rhs.

We complete the proof by showing that the rhs is contained in the lhs:

Proving that the rhs is contained in the lhs of (4.5) is trivial: if a point p is contained in the union of the sets then there exists an m and an s such that

$$p \in L_{k,j}(n) \cap L^i_{i,s}(m)$$

hence p belongs to the portion of the lobe $L_{i,s}(m)$ which is contained in R_i, and in particular $p \in R_i$. But by (A1.4) $p \in L_{k,j}(n)$ and therefore by definition $p \in L^i_{k,j}(n)$ which shows that the rhs is contained in the lhs of equation (4.5).

□.

Proof of Case 1: Recall that in case 1, by assumption:

$$L^i_{s,i}(m) = \emptyset \quad \text{for all } m,\ s \text{ such that } \ 1 \leq m \leq n, \ \ 1 \leq s \leq N_R. \tag{A1.6}$$

We prove that equation (4.4) is correct for this case by proving statements A1-E1, and then performing step F1.

A1. Regarding i as fixed and m and s as variable, the sets $L^i_{i,s}(m)$ are disjoint.

Proof of A1: We need to show that for $(s_1, m_1) \neq (s_2, m_2)$ the set $A = L^i_{i,s_1}(m_1) \cap L^i_{i,s_2}(m_2)$ is the empty set for all s_1, s_2, m_1, m_2 such that $1 \leq s_1, s_2 \leq N_R$ and

$1 \leq m_1, m_2 \leq n$, and let us assume that $m_1 \leq m_2$. We assume that $A \neq \emptyset$ and show that this assumption leads to a contradiction of either the lobe definition (i.e. the assumption that a lobe $L_{k,j}(l)$ is defined so that it is completely contained in R_k after iteration $l-1$ an completely contained in R_j after iteration l cf. **R3**) or (A1.6).

If $A \neq \emptyset$ then there exists a point p such that $p \in A$.

$$p \in A \Rightarrow \{p \in R_i \text{ and } p \in L_{i,s_1}(m_1) \cap L_{i,s_2}(m_2)\}$$

a) If $m_1 = m_2$ then, unless $s_1 = s_2$, $p \in L_{i,s_1}(m_1) \cap L_{i,s_2}(m_2)$ contradicts the assumption on the well definedness of the lobes, namely equation (4.1).

b) if $m_1 = m_2 - 1$ then $p \in L_{i,s_1}(m_1) \cap L_{i,s_2}(m_2)$ implies that p leaves region R_i in two consecutive iterations, which contradicts the lobe definition.

c) if $m_1 < m_2 - 1$ then by lemma A1.1 $p \in L_{i,s_1}(m_1) \cap L_{i,s_2}(m_2)$ implies that there exist m and s such that $p \in L_{s,i}(m)$ and $m_1 < m < m_2$. But $p \in A$ also implies that $p \in R_i$, hence $p \in L^i_{s,i}(m)$ for some $1 < m < n-1$ and $1 \leq s \leq N_R$ which contradicts the assumption of case 1, namely equation (A1.6).

B1. The set $L^i_{i,s}(m)$ is given by:

$$L^i_{i,s}(m) = L_{i,s}(m) - \bigcup_{r=1}^{N_R} \bigcup_{l=1}^{m-1} [L_{i,s}(m) \cap L_{r,i}(l)] \tag{4.6}$$

Proof of B1: We prove first that the lhs of (4.6) is contained the rhs:

$p \in L^i_{i,s}(m) \Rightarrow \{p \in R_i \text{ and } p \in L_{i,s}(m)\}$. However, by equation (A1.6), $p \in R_i$ implies that $p \notin L_{r,i}(l)$ for all $1 \leq r \leq N_R$ and $1 \leq l \leq m$, and using $p \in L_{i,s}(m)$ we obtain that $p \in L_{i,s}(m) - \bigcup_{r=1}^{N_R} \bigcup_{l=1}^{m-1} [L_{i,s}(m) \cap L_{r,i}(l)]$.

We complete the proof by showing that the rhs is contained in the lhs.

$$p \in L_{i,s}(m) - \bigcup_{r=1}^{N_R} \bigcup_{l=1}^{m-1} [L_{i,s}(m) \cap L_{r,i}(l)] \Rightarrow$$

$$\{p \in L_{i,s}(m) \text{ and } p \notin L_{r,i}(l) \text{ for all } 1 \leq l \leq m-1, \quad 1 \leq r \leq N_R$$

We show that the above statement implies that $p \in R_i$ and since p is also contained in $L_{i,s}(m)$ this shows that the rhs is contained in the lhs. Since

$p \notin L_{r,i}(l)$ for all $1 \leq l \leq m-1$ and all r, p does not enter R_i before iteration m, hence if p is not initially in R_i, $F^{m-1}p \notin R_i$. However, by the lobe definition $F^{m-1}L_{i,s}(m) \subset R_i$, hence, if $p \notin R_i$ then $p \notin L_{i,s}(m)$, which contradicts the assumption that p is contained in the rhs of (4.6).

C1. Regarding i as fixed and l and r as variable, the lobes $L_{r,i}(l)$ are disjoint.

Proof of C1: We need to show that for $(s_1, m_1) \neq (s_2, m_2)$ the set $A = L_{s_1,i}(m_1) \cap L_{s_2,i}(m_2)$ is the empty set for all s_1, s_2, m_1, m_2 such that $1 \leq s_1, s_2 \leq N_R$ and $1 \leq m_1, m_2 \leq n$, and let us assume that $m_1 \leq m_2$. We assume that $A \neq \emptyset$ and show that this assumption leads to a contradiction of either the definition of the lobes or (A1.6). If $A \neq \emptyset$ then there exists a point $p \in L_{s_1,i}(m_1) \cap L_{s_2,i}(m_2)$.

a) If $m_1 = m_2$ then, unless $s_1 = s_2$, $p \in L_{s_1,i}(m_1) \cap L_{s_2,i}(m_2)$ contradicts the assumption on the well definedness of the lobes, namely equation (4.1).

b) if $m_1 = m_2 - 1$ then $p \in L_{s_1,i}(m_1) \cap L_{s_2,i}(m_2)$ implies that p enters region R_i in two consecutive iterations, which contradicts the lobe definition.

c) if $m_1 < m_2 - 1$ then by lemma A1.3 $L^i_{s_2,i}(m_2 - m_1) \neq \emptyset$ which contradicts the assumption of case 1, namely equation (A1.6).

D1. Regarding i, r and l as fixed and m and s as variable, the sets $L_{i,s}(m) \cap L_{r,i}(l)$ are disjoint for all $m > l$.

Proof of D1: Assume the sets are not disjoint, namely there exists a p such that $p \in L_{i,s_1}(m_1) \cap L_{i,s_2}(m_2) \cap L_{r,i}(l)$ and $l < m_1 < m_2 - 1$ (as before the cases $m_1 = m_2$ or $m_1 = m_2 - 1$ are ruled out by the definition of the lobes). Therefore, by lemma A1.1 $p \in L_{s_3,i}(m_3)$ where $m_1 < m_3 < m_2$ and specifically $m_3 > l$. Therefore, if D1 is false then p belongs to two different lobes which enter region R_i, contradicting C1.

E1. The following identity holds:

$$L_{k,j}(n) \cap L_{r,i}(l) \cap \{\bigcup_{s=1}^{N_R} \bigcup_{m=l+1}^{n} L_{i,s}(m)\} = L_{k,j}(n) \cap L_{r,i}(l) \tag{4.7}$$

Proof of E1: This is a direct consequence of lemma A1.4.

F1. We now substitute equations (4.6) and (4.7) into equation (4.5), reindex and use A1, C1 and D1 to interchange the union and the area signs in the new equation which results in (4.4).

"Operating" with the area symbol on equation (4.5) and using A1 to interchange union and area symbols we obtain:

$$\mu(L^i_{k,j}(n)) = \sum_{s=1}^{N_R}\sum_{m=1}^{n}\mu(L_{k,j}(n)\cap L^i_{i,s}(m))$$

Substituting equation (4.6) into the above expression gives:

$$\begin{aligned}\mu(L^i_{k,j}(n)) &= \sum_{s=1}^{N_R}\sum_{m=1}^{n}\mu\left(L_{k,j}(n)\cap\left\{L_{i,s}(m)-\bigcup_{r=1}^{N_R}\bigcup_{l=1}^{m-1}[L_{i,s}(m)\cap L_{r,i}(l)]\right\}\right)\\ &= \sum_{s=1}^{N_R}\sum_{m=1}^{n}\mu(L_{k,j}(n)\cap L_{i,s}(m))-\\ &\quad\sum_{s=1}^{N_R}\sum_{m=1}^{n}\mu\left(L_{k,j}(n)\cap\bigcup_{r=1}^{N_R}\bigcup_{l=1}^{m-1}[L_{i,s}(m)\cap L_{r,i}(l)]\right)\end{aligned}$$

Therefore, using C1 and D1 and reindexing leads to:

$$\begin{aligned}\mu(L^i_{k,j}(n)) &= \sum_{s=1}^{N_R}\sum_{m=1}^{n}\mu(L_{k,j}(n)\cap L_{i,s}(m))-\\ &\quad\mu\left(\bigcup_{s=1}^{N_R}\bigcup_{m=1}^{n}\left[L_{k,j}(n)\cap\bigcup_{r=1}^{N_R}\bigcup_{l=1}^{m-1}[L_{i,s}(m)\cap L_{r,i}(l)]\right]\right)\\ &= \sum_{s=1}^{N_R}\sum_{m=1}^{n}\mu(L_{k,j}(n)\cap L_{i,s}(m))-\\ &\quad\mu\left(\bigcup_{r=1}^{N_R}\bigcup_{l=1}^{n-1}\left[L_{k,j}(n)\cap L_{r,i}(l)\cap\bigcup_{s=1}^{N_R}\bigcup_{m=l+1}^{n}L_{i,s}(m)\right]\right)\end{aligned}$$

and using equation (4.7) we obtain:

$$\mu(L^i_{k,j}(n)) = \sum_{s=1}^{N_R}\sum_{m=1}^{n}\mu(L_{k,j}(n)\cap L_{i,s}(m)) - \mu\left(\bigcup_{s=1}^{N_R}\bigcup_{l=1}^{n-1}[L_{k,j}(n)\cap L_{r,i}(l)]\right)$$

And therefore, using C1 once more we obtain equation (4.4):

$$\mu(L^i_{k,j}(n)) = \sum_{s=1}^{N_R}\sum_{m=1}^{n}\mu(L_{k,j}(n)\cap L_{i,s}(m)) - \sum_{s=1}^{N_R}\sum_{l=1}^{n-1}\mu(L_{k,j}(n)\cap L_{r,i}(l))$$

□.

Proof of Case 2: We show first that if $A \subset L^i_{k,j}(n)$ then $\mu(A)$ is added N_A times through the first sum in equation (4.4) and subtracted $N_A - 1$ times through the second sum, then we show that if $A \not\subset L^i_{k,j}(n)$ $\mu(A)$ is added and subtracted M_A times through the first and second sums respectively. We assume that A is small enough so that all the members of A are contained in the same lobes $L_{r,s,}(m)$ where $m \leq n$ which implies that writing $A \not\subset B$, where B is an intersection set of such lobes, is equivalent to writing $A \cap B = \emptyset$. This assumption implies that we assume that after each iteration A is completely contained in one region, at least up to iteration n.

We start with a proposition which contain all the necessary ingredients for this part of the proof.

Proposition A1.6:

Let $p \in L^i_{k,j}(n)$,

a) If $p \notin L_{k,j}(n) \cap L^i_{r,i}(l)$ for all $1 \leq r \leq N_R$ and all $1 \leq l \leq n$ then there exists a unique r' and a unique l' such that $p \in L_{i,r'}(l')$.

b) If $p \in L_{k,j}(n) \cap L^i_{r,i}(l)$ where $1 \leq r \leq N_R$ and $1 \leq l \leq n$, then there exist l_0, l_1, r_0, r_1 such that $l_0 < l < l_1$ and $p \in L_{i,r_0}(l_0) \cap L_{i,r_1}(l_1)$.

c) If $p \in L_{i,r_t}(l_t)$ for $t = 1, \ldots, N_i$, where $l_1 < l_2 < \cdots < l_{N_i}$, then there exist l'_t, r'_t such that $p \in L_{k,j}(n) \cap L^i_{r'_t,i}(l'_t)$ and $l_t < l'_t < l_{t+1}$ $t = 1, \ldots, N_i - 1$.

Proof of Proposition A1.6:

a) By lemma A1.5 r', l' exist. To show that they are unique, assume they are not, and use lemma A1.1 and the assumption that $p \in R_i$ to show that this contradicts the assumption of case a).

b) Since, by definition, $L_{k,j}(n) \cap L^i_{r,i}(l) \subset L_{k,j}(n) \cap L_{r,i}(l)$, lemma A1.4 shows that $p \in L_{k,j}(n) \cap L^i_{r,i}(l)$ implies that there exists an r_1 and an l_1 such that $l < l_1$ and $p \in L_{i,r_1}(l_1)$.

Using lemma A1.5 for the lobe $L^i_{r,i}(l)$ shows that there exists an r_0 and an l_0 such that $l_0 < l$ and $p \in L_{i,r_0}(l_0)$.

c) By lemma A1.1, $p \in L_{i,r_t}(l_t) \cap L_{i,r_{t+1}}(l_{t+1})$ for $t = 1, \ldots, N_i - 1$, which together with the assumption that $p \in R_i$ implies that $p \in L^i_{r'_t,i}(l'_t)$ where $l_t < l'_t < l_{t+1}$ $t = 1, \ldots, n-1$. Moreover, since $p \in L^i_{k,j}(n)$ implies that $p \in R_i$ and that $p \in L_{k,j}(n)$, we obtain that $p \in L_{k,j}(n) \cap L^i_{r'_t,i}(l'_t)$ for $l_t < l'_t < l_{t+1}$ $t = 1, \ldots, n-1$.

□.

We now show that equation (4.4) result in the right counting. We break up the proof to four cases:

a. $A \subset L^i_{k,j}(n)$ and $N_A = 1$.

b. $A \subset L^i_{k,j}(n)$ and $N_A > 1$.

c. $A \not\subset L^i_{k,j}(n)$ and $M_A = 0$.

d. $A \not\subset L^i_{k,j}(n)$ and $M_A > 0$.

Recall equation (4.4):

$$\mu(L^i_{k,j}(n)) = \underbrace{\sum_{s=1}^{N_R} \sum_{m=1}^{n} \mu(L_{k,j}(n) \cap L_{i,s}(m))}_{\mathbf{I}} - \underbrace{\sum_{s=1}^{N_R} \sum_{l=1}^{n-1} \mu(L_{k,j}(n) \cap L_{r,i}(l))}_{\mathbf{II}}$$

a. When $A \subset L^i_{k,j}(n)$ but $A \not\subset L_{k,j}(n) \cap L^i_{r,i}(l)$ for all $1 \le r \le N_R$ and all $1 \le l \le n$ then, by proposition A1.6 there exists a unique r' and a unique l' such that $A \subset L_{i,r'}(l')$, and therefore $\mu(A)$ is added exactly once through **I**. Note that $\mu(A)$ is not subtracted through **II**; since by assumption $A \subset R_i$, if A was contained in a set of **II** it would imply that $A \subset L_{k,j}(n) \cap L^i_{r,i}(l)$ contradicting the assumption of case a. Hence we proved that $\mu(A)$ is added exactly once to the lhs of (4.4) in case a.

b. If $A \subset L^i_{k,j}(n)$ and $A \subset L_{k,j}(n) \cap L^i_{r,i}(l)$ where $1 \le r \le N_R$ and $1 \le l \le n$, then $\mu(A)$ is added N_A times through **I** and subtracted $N_A - 1$ times through **II**. We show first that if $\mu(A)$ is added N_A times through **I** it is subtracted *at least* $N_A - 1$ times through **II** and then complete the proof by showing that if $\mu(A)$ is subtracted $N_A - 1$ times from **II** then it is added *at least* N_A times through **I**.

1) If $\mu(A)$ is added N_A times through **I**, then it belongs to N_A $L_{i,s}(m)$ lobes, and therefore, by part c) of proposition A1.6 A also belongs to $N_A - 1$ $L^i_{r,i}(l)$ lobes, and hence to $N_A - 1$ $L_{r,i}(l)$ lobes, which shows that $\mu(A)$ is subtracted at least $N_A - 1$ times through **II**.

2) If $\mu(A)$ is subtracted $N_A - 1$ times through **II**, then A belongs to the $N_A - 1$ sets $L_{k,j}(n) \cap L_{r_t,i}(l_t)$ where $t = 1, \ldots, N_A - 1$ and $l_1 < \cdots < l_{N_A-1}$. Since by assumption $A \subset R_i$, this implies that $A \subset L_{k,j}(n) \cap L^i_{r_t,i}(l_t)$, hence using part b) of proposition A1.6 we conclude that there exist $l'_0 < l_1$ and $l'_{N_A-1} > l_{N_A-1}$ such that $A \subset L_{k,j}(n) \cap L_{i,r'_t}(l'_t)$ for $t = 0,\ N_A - 1$. Using lemma A1.2 we find that there exist l'_t, $t = 1, \ldots N_A - 2$ such that $A \subset L_{k,j}(n) \cap L_{i,r'_t}(l'_t)$ and $l_t < l'_t < l'_{t+1}$. Altogether, we have shown that A is contained in at least N_A sets of **I**.

c. $A \not\subset L^i_{k,j}(n)$ and $M_A = 0$.

1) If $A \not\subset L_{k,j}(n)$ then trivially A is not contained in any of the sets of **I** or **II**.

2) If $A \subset L_{k,j}(n)$ but $A \not\subset L_{i,s}(m)$ for all $1 \leq s \leq N_R$ and $1 \leq m \leq n$ then A is trivially not contained in the sets of **I**, and by lemma A1.4 A cannot be contained in any of the **II** sets without contradicting the assumption that $A \not\subset L_{i,s}(m)$.

d. $A \not\subset L^i_{k,j}(n)$ and $M_A > 0$. We show that if A is contained in M_A sets of **I** then A is contained in at least M_A sets of **II** and we complete the proof by showing the converse.

1) If $A \in L_{k,j}(n) \cap L_{i,s_t}(l_t)$ where $t = 1, \ldots, M_A$ and $l_1 < \cdots < l_{M_A}$ then, by lemma A1.1 there exist l'_t, $t = 1, \ldots, M_A - 1$ such that $A \subset L_{k,j}(n) \cap L_{s'_t,i}(l'_t)$ and $l_t < l'_t < l_{t+1}$. Moreover, since we assume in this case that $A \not\subset R_i$ and that A leaves R_i at iteration l_1, A must be contained in a lobe which enters R_i before iteration l_1, namely there exists an $l'_0 < l_1$ such that $A \subset L_{k,j}(n) \cap L_{s'_t,i}(l'_0)$, and therefore A is contained in at least M_A sets of **II**.

2) If $A \in L_{k,j}(n) \cap L_{s_t,i}(l_t)$ where $t = 1, \ldots, M_A$ and $l_1 < \cdots < l_{M_A}$ then,

by lemma A1.2 there exist l'_t, $t = 1, \ldots, M_A - 1$ such that $A \subset L_{k,j}(n) \cap L_{i,s'_t}(l'_t)$ and $l_t < l'_t < l_{t+1}$. Moreover, by lemma A1.4, $A \subset L_{k,j}(n) \cap L_{s_{M_A},i}(l'_{M_A})$ implies that there exists an l'_{M_A} such that $A \subset L_{k,j}(n) \cap L_{i,s'M_A}(l'_{M_A})$ and $l'_{M_A} > l_{M_A}$. Hence, A is contained in at least M_A sets of $\mathbf{I}$.

□.

References

Abraham, R. and Shaw, C. 1982 *Dynamics: The Geometry of Behavior. Part Three: Global Behavior*, Aerial Press, Santa Cruz, California.

Bensimon, D. and Kadanoff, L. P. 1984 Extended Chaos and Disappearance of KAM Trajectories, *Physica*, **13D**, 82.

Channell, P. J. and Scovel, J. C. 1988 Symplectic Integration of Hamiltonian Systems, preprint.

Chirikov, B. V. 1979 A Universal Instability of Many-Dimensional Oscillator Systems, *Physics Reports*, **52**, No. 5, 263.

Easton, R. W. 1985 Trellises Formed by Stable and Unstable Manifolds in the Plane, *Transaction of the A.M.S.*, **294, 2**, 719-732.

Escande, D. F. 1987 Hamiltonian Chaos and Adiabaticity, Proceed. Int. Workshop, Kiev.

Franjione, J. G. and Ottino, J. M. 1987 Feasibility of Numerical Tracking of Material Lines and Surfaces in Chaotic Flows, *Phys. Fluids*, **30**, No. 12, 3641.

Guckenheimer, J. and Holmes, P. 1983 *Non-Linear Oscillations, Dynamical Systems and Bifurcations of Vector Fields*, Springer-Verlag, New York.

Kaper, T. 1988 Private Communication.

Karney, F. F. 1983 Long Time Correlations in the Stochastic Regime, *Physica*, **8D**, 360.

Lichtenberg, A. J. and Lieberman, M. A. 1983 *Regular and Stochastic Motion*, Springer-Verlag, New York.

Ling, F. H. 1986 A Numerical Study of The Applicability of Melnikov's Method, *Phys. Letters A*, Vol. 119,**9**, 447-452.

Mackay, R. S., Meiss, J. D. and Percival, I. C. 1984 Transport in Hamiltonian

Systems, *Physica*, **13D**, 55.

Mackay, R. S. and Meiss, J. D. 1986 Flux and Differences in Action for Continuous Time Hamiltonian Systems, *J. Phys. A.: Math Gen.*, **19**, 225.

Mackay, R. S., Meiss, J. D. and Percival, I. C. 1987 Resonances in Area Preserving Maps, *Physica*, **27D**, 1.

Meiss, J. D. and Ott, E. 1986 Markov Tree Model of Transport in Area Preserving Maps, *Physica*, **20D**, 387.

Poincaré, H. 1892 *Les Methods Nouvelles de la Mechanique Celeste*, Gauthier-Villars, Paris.

Rom-Kedar, V., Leonard, A. and Wiggins, S. 1988 An Analytical Study of Transport, Chaos and Mixing in an Unsteady Vortical Flow, preprint.

Wiggins, S. 1988 *Global Bifurcations and Chaos - Analytical Methods* to appear in "Springer Applied Mathematics Series".